Extension Of Stress-Based Finite Element Model Using Resilient Modulus Material Characterization To Develop A Theoretical Framework for Realistic Response Modeling of Flexible Pavements on Cohesive Subgrades

DISSERTATION

Presented in Partial Fulfillment of the Requirements for the Degree Doctor of Philosophy in the Graduate School of The Ohio State University

By

Kadri Parris, M.S., PMP

Graduate Program in Civil Engineering

The Ohio State University

2015

Dissertation Committee:

Dr. William E. Wolfe, Advisor

Dr. Tarunjit Butalia, Co-Advisor

Dr. Frank Croft

Dr. Fabian Tan

Abstract

Pavement design methodologies have over the past decades seen philosophical evolutions and eventually practical implementation of new postulates. As more contributions are made by pavement researchers to the State-of-the-Art in pavement design, there exist a chasm between pavement engineers and state-of-the-art pavement research in terms of incorporation into pavement design guidelines. In developing countries such as Guyana in South America, as well as several Departments of Transportation, municipalities and townships in the United States, pavement engineers still use the American Association of State Highway and Transportation Officials (AASHTO) Pavement Design Guide (1993). This empirical pavement design guide and its previous iterations were based primarily on data that was collected and processed from the then American Association of State Highway Officials (AASHO) Road Test conducted between 1958 and 1960. The limitations with continued use of this method are obvious since the data was gathered under specific environmental conditions, a specific subgrade type, and with specific materials as well as specific pavement cross-sections. The continued use of this guide does not account for advances in material technology, different types and volumes of vehicular traffic, changing climatic conditions and also can be costly in expanding road networks. To solve this dilemma pavement researchers started working toward a more mechanistic approach for design and through the work of National Cooperative Highway Research Program (NCHRP), culminated in the publishing of the Mechanistic-Empirical Pavement Design

Guide (MEPDG) in 2004. The finite element model used in the MEPDG is premised upon a displacement based theory. These theories are capable of making good predictions regarding global responses such as displacements and sometimes in-plane stresses but not the transverse stress distribution. To predict transverse stress distribution, stress based theories are more suitable for use in formulations. At The Ohio State University, Chyou (1989), Schoeppner (1991) and Butalia (1996) worked on different versions of the stress based model for composite laminates. This model was initially extended by Tu (2007) to good effect for analyzing the responses in pavement systems. In this research effort, this response model is being further extended to incorporate a material characterization model into the stiffness matrix for more accurate structural response predictions. The material characterization model (Kim 2004) allows the pavement designer to make predictions of Resilient Modulus, Mr, for cohesive subgrades without the need for conducting the test which can be both costly and complex. This approach renders a cost effective way of obtaining one of the most important parameters for employing a mechanistic approach which is also a major prohibition for many developing countries to move closer to the State-of-the-Art. This new synthesis allows for good predictions of global responses as well as transverse stress distribution which is critical for overcoming pavement layer debonding that can reduce pavement life significantly. Considering the results of the analysis compared to ABAQUS 3D Finite Element Models, this new synthesis forms the basis of a good pavement response model which can be used to further a more mechanistic approach for relatively small design agencies.

Dedication

Every good gift is from above, and comes down from the Father of lights, with whom is no variableness, neither shadow of turning. God has truly been faithful. I give all praise and thanks to my Lord and Savior Jesus Christ who makes all things possible. This document is dedicated to my incredibly loving and supportive wife Melissa, as well as our dear children Josiah and Hadassah. To my mother and father, Leila and Compton Parris who impressed upon me at an early age, the need to learn daily and to apply my knowledge for the greater good of others. To my brother Duane Parris and my sister Nkechi Jemmott for always encouraging me and being two of my biggest supporters. To my in-laws, relatives, church family and friends for all their prayer and support through the years.

Acknowledgments

I take the opportunity to express sincere gratitude to my advisor Dr. William E Wolfe for his mentorship, unwavering patience and steady guidance throughout the pursuit of this research effort. I also wish to thank my co-advisor Dr. Tarunjit Butalia for his support and encouragement. Special Thanks to my committee members Dr. Frank Croft and Dr. Fabian Tan for agreeing to serve on my committee and offering valuable feedback. My sincere gratitude to Dr. John Merrill and the leadership and staff of EEIC here at The Ohio State University for providing substantial support in the course of this academic pursuit.

Vita

2004…………………………………BEng. Civil Engineering University of Guyana, S.A.

2005-2008 ……………………………….Design/Senior Engineer, Ministry of Public Works and Communications, Guyana, S.A.

2008-2009……………………………......International Road Federation Fellow

2008-2009……………………………......Graduate School Matching Fellowship, The Ohio State University, Columbus Ohio

2010 ………………...MS Civil Engineering, The Ohio State University, Columbus Ohio.

2011 to present ....Graduate Teaching Associate, Engineering Education Innovation Center, First Year Engineering Program, The Ohio State University

Publications

- Parris, K., Tu, W., Wolfe, W., and Butalia, T.S., Stress-Based Displacement Model For Realistic Analysis of Pavements." International Road Federation World Meeting 2013, Riyadh, Saudi Arabia.

- Rodriguez, C., Parris, K., Wolfe, W., and Thumann, C., “Pavement Management for Honduras.” International Conference on Sustainable Infrastructure 2014: pp. 1-10.

Fields of Study

Major Field: Civil Engineering

Table of Contents

List of Tables

List of Figures

Chapter 1: Introduction

1.1 Background and Objectives

The design of pavements though ever evolving, remains an engineering undertaking that requires innovative techniques and new approaches in order to optimize the use of limited funding to expand and sustain road infrastructure in municipalities, cities, states and countries. This dilemma, though common in many areas of the world, is exacerbated in the case of many developing countries. There is oft times the lack of a clear road design philosophy, ultimately resulting in a pavement that is not functional for the entirety of its design life. The effects are consequential and continue, in part, to stymie efforts aimed at economic advancement.

In 2003, The Government of Guyana entered into an agreement with Texas Research and Development Incorporated (TRDI) to implement a routine maintenance program for Guyana's road network which is approximately 4000km in length with 16% of the network paved. A pilot project was conducted which targeted 409 km of paved roadway along sections of the main thoroughfares in the country and other heavily trafficked streets. After the initial success, the maintenance program was extended to the major roads of Guyana. As of 2008, in excess of Four Hundred and Eighty (480) Million Guyana Dollars or approximately Two Million Four Hundred Thousand United States Dollars has been spent on routine maintenance efforts, aimed at attempting to prolong the serviceability of underperforming pavements along the major thoroughfares in Guyana (IADB Report 2008). In the United States, the American Society of Civil Engineers issued its 2013 “Report Card” for roads, which indicates that 32% of America’s major roads are in poor or mediocre condition. As a direct consequence, the report goes on to state an estimate of approximately $324USD in additional expenses borne by each motorist for maintenance and operation of his/her vehicle. Also, deficient pavements are more common in urban areas with the indication that 47% of the urban interstate vehicle miles travelled (VMT) is traversed in unacceptable pavement conditions. These findings underscore the importance of advancing the body of knowledge regarding road pavement design and innovating to reach more effective and robust solutions. In both the developed and developing country contexts, there is a growing indication that traditional dependency on public funds to support the demand for infrastructure development is unsustainable. There is a growing chasm between funding available for both maintenance and expansion of road networks vis-à-vis the budgets required to execute these projects. Even with the advent or emerging prominence of innovative financing mechanisms such as public private partnerships (PPPs), in order to protect the investments made, pavements have to be designed using state of the practice methods. These methods need ongoing development through solid research in theory and practice.

In the past five (5) years, the Inter-American Development Bank (IDB) has made significant, ongoing investments in the transportation sector of Guyana. As depicted in Figure 1.1, this sector has received approximately 38% or 111 Million USD of the overall investment portfolio of the IDB in Guyana. Future plans acknowledge the important and inextricable link between transport infrastructure development and economic prosperity.

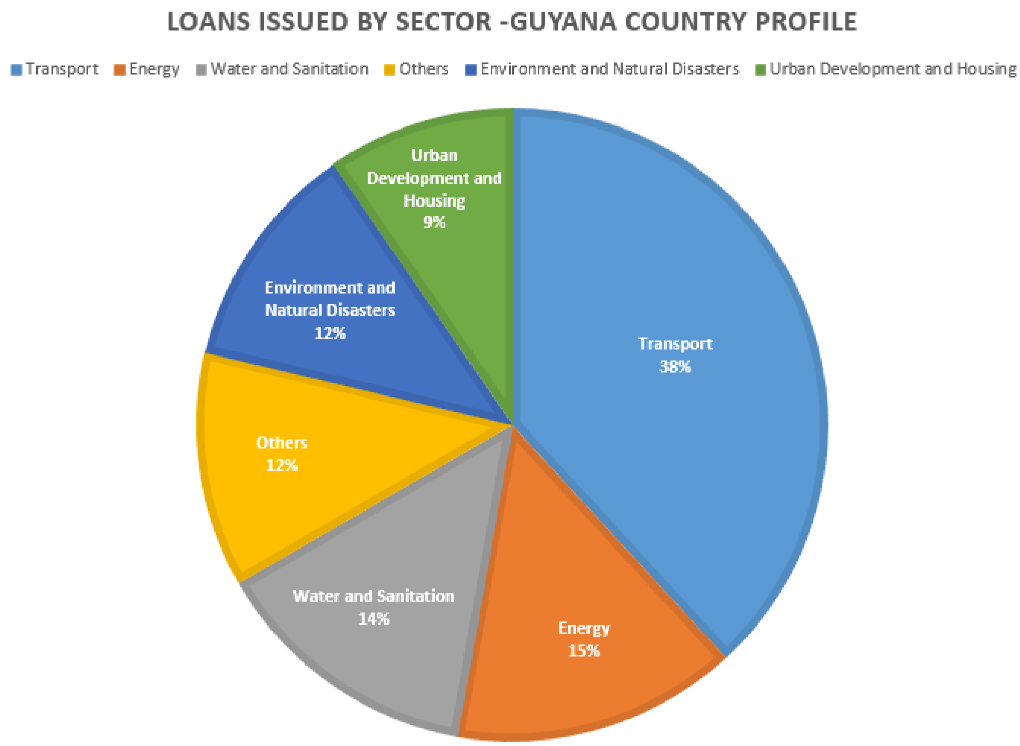

Figure 1.1 IDB Investment Portfolio by sector in Guyana.

According to the IDB website, the bank has affirmed its intention to "support restructuring of the transport sector to improve its efficiency with the shift from rehabilitating the road system to expand its capacity and the improvement of the urban transportation in a sustainable manner." Therefore, particularly in the third world setting with Guyana as a prime example, a more robust pavement design philosophy has to be adopted to ensure that investment in road infrastructure can be beneficial over its design life. Additionally, more efficient design approaches can result in substantial savings and thereby allow for more work to be undertaken with the same resources.

Many agencies tasked with road pavement design the world over are still using the American Association of State Highway and Transportation Officials (A.A.S.H.T.O) Interim Pavement Design Guide, which is primarily an empirical method. Over the past three decades, significant thought has been employed with increasing but gradual effect, to design pavements using a more mechanistic approach, based on actual stresses, strains and deflections in the pavement system. The release of the Mechanistic Empirical Pavement Design Guide (MEPDG) incorporates a multi-layer elastic theory as well as displacement based finite element methods. One deficiency of displacement-based models has been the inability to assess the transverse stress distribution of wheel load exerted repeatedly on pavements. The determination of this transverse normal and shear stress distribution is a critical step in modeling the practical use of pavements and being able to mitigate against a principal cause of premature failure in pavements, pavement layer debonding.

A Stress - Based Finite Element Model was developed for analyzing composite laminates at The Ohio State University Chyou (1989). This model was further improved by (Schoeppner 1991), Butalia (1996) and was first adopted by Tu (2007) as a mathematical framework for use with road pavements. This very model is now being extended for full scale pavement application with the real possibility of applying the results to realistic design of pavements. One of the key input parameters to the model is the elastic response of the roadbed soils or subgrades in a pavement, to repeated traffic loading. The Resilient Modulus (Mr) is a realistic measure of this elastic behavior. Unfortunately, the startup costs for the Mr testing equipment is difficult for most agencies to justify and further, to achieve repeatability of tests results require highly skilled technicians. At The Ohio State University, a material characterization model, primarily for cohesive soils, was developed by Kim (2004) for the prediction of Mr from a series of basic tests already typically conducted in soils laboratories. This model shows great promise in overcoming the need to directly measure this parameter via a dedicated laboratory test. The OSU Model which incorporates linear regression theory produces an explicit equation which is incorporated into the stiffness matrix of the Stress-Based Finite Element Model for more reliable results.

1.2 Presentation of the Research

The main objective of this research effort is to extend a stress-based finite element model, originally developed for composite laminates but adopted for pavements, thereby allowing for greater accuracy in predicting deflections and interfacial transverse stress distributions in pavements. In order to achieve this objective, a thorough review of the literature spanning the initial and somewhat primitive efforts to the state of the practice in mechanistic pavement design must first be conducted. This is presented in Chapter 2. The material characterization and the OSU Stress-Based model are both presented in Chapter 3 for completeness of presentation. The material characterization model for cohesive subgrades, has been investigated to determine whether in its general form, it is suitable for Mr predictions in cohesive soils from other depositional environments. This model is then incorporated into the stiffness matrix of the OSU Stress Based Finite Element Model. In Chapter 4, the new formulation is validated by comparison with the result of 3D Finite

Element Models using ABAQUS. The ability to employ this new synthesis for response modeling in the mechanistic approach, will demonstrate the practical usefulness of this new method in places like Guyana. The conclusions of this research effort as well as recommendations for future work are presented in Chapter 5.

Chapter 2: Review of the State of the Practice in Pavement Design

2.1 History of Pavement Design Philosophy

Pavement design philosophy and practice has changed over the years from largely empirical methods based on engineering experience to more mechanistic-empirical methods in recent times.

2.1.1 Carthaginian and Roman Road Design Philosophy

The early records of any formal philosophy on pavement design can be traced to the days of the Carthaginian Empire around 600 BC. They were widely considered the first to design and maintain road pavements. After the Roman Empire vanquished the Carthaginians, they built roads within the empire totaling an estimate of 87,000km, which is approximately the same length as the present day US Interstate Highway system. It is believed that the Romans adopted the practice of a military road system from the Carthaginians (Pavement Interactive 2008). An early road design used by the Romans in the UK, consisted of four layers of material (Hart and Collins, 1936) as shown in Table 2.1. The cross-section of one such Roman road design, near Radstock in the UK is shown in Figure 2.1. It was typical for Roman road designs to range from approximately 0.9 to 2.4 m in overall cross-sectional thickness. Accordingly, the Roman road construction was relatively expensive.

Layer #	Name	Description
Layer 1	Summa Crusta	smooth, polygonal blocks bedded in underlying soil
Layer 2	Nucleus	gravel and sand with lime cement
Layer 3	Rudus	rubble masonry and smaller stones set in lime mortar
Layer 4	Statumen	two or three courses of flat stones set in lime mortar

Table 2.1 Typical road constructed by the Romans after 146 BC

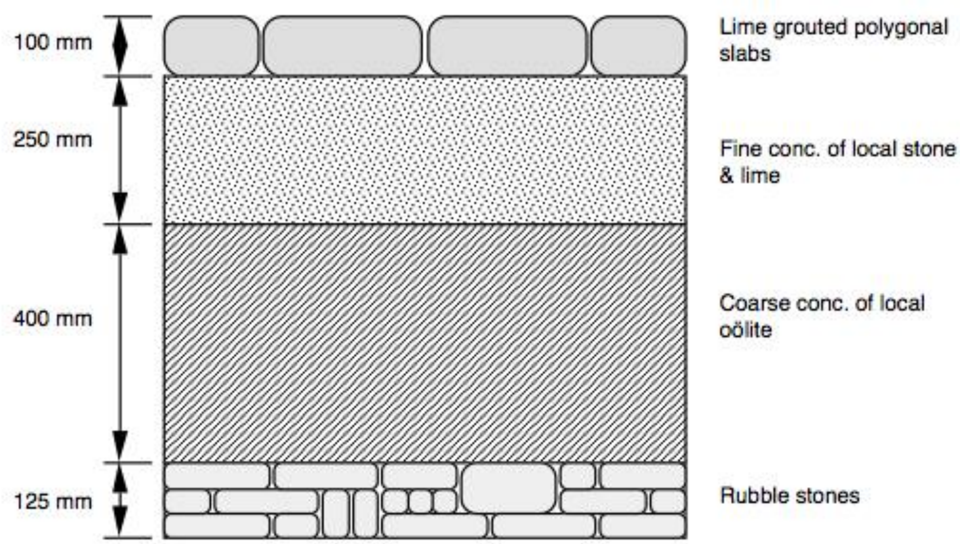

Figure 2.1 Cross-section of Roman designed road pavement near Radstock in the UK (Pavement Interactive, 2008).

Even in these early stages of road pavement design and construction, an understanding was developed regarding the need to effectively drain the road pavement since failing which, the strength of the pavement system could be compromised due to infiltration of water into the subgrade.

2.1.2. Trésaguet Road Design Philosophy

Pierre-Marie-Jérôme Trésaguet, a well-respected and practicing French engineer, is widely considered to be the first man to introduce a modern approach to pavement construction after the Roman influence on road building methodology (Oglesby 1975). Trésaguet is credited for advancing and successfully improving the construction and maintenance of stone roads. He is also believed to have made it possible for Napoleon to build the French highway system. As a result of his considerable experience gained in road pavement design, Trésaguet wrote a treatise on road design in the year 1775. The essence of his proposal and improvement on Roman efforts, were focused on better drainage, crowned subgrade as well as crowned foundation and reducing the thickness of the broken stone layer to approximately 0.25m. His treatise addressed designing roads with geographical constraints along the route, suggested reduction in the width of the carriageway, removing ditches on one side of the road and ensuring the slope was not greater than 7%. His main innovations involved gravelling techniques. In summary, his proposal involved a road with three layers of stone on the crowned subgrade (Oglesby 1975). Descriptions of the three (3) layers, top to bottom, are captured in Table 2.2.

Layer #	Description
Layer 1	angular, hand-broken aggregate of max size 25mm to a depth of 51mm.
Layer 2	angular, hand-broken aggregate of max size 76mm to a depth of 203mm.
Layer 3	angular, hand-broken aggregate of max size 76mm to a depth of 203mm.

Table 2.2 Typical road design by Trésaguet

Trésaguet's design philosophy was used primarily on main roads. It was slowly adopted only around Paris and Limousin because of the expensive nature of construction as well as prohibitive cost to maintain roads made of broken stone as opposed to paved highways (Conchon 2006). In the early 1800s, the Telford then Macadam design philosophies took root.

2.1.3. Telford Road Design Philosophy

Telford's school of thought, sought to build on the advances made by Trésaguet in the design of pavements and his particular preference was to do so on flat subgrades wherever possible. The reason for taking this position is that he felt it would reduce the number of horses required to haul cargo along the carriageway. The proposed overall pavement thickness of 350mm - 450mm was considerably less than previous attempts at pavement design and like Trésaguet, employed three layers of material above the subgrade. The distinct approach taken by Telford was to have the foundation course, above the subgrade, comprise large cubic shaped stones which were approximately 75mm minimum thickness, 125mm breadth and 175mm in height (Oglesby 1975). The two additional layers comprised smaller stones, approximately 65mm maximum size and collective width of 150-250mm. In some cases a further 40mm layer of gravel would be added as a surface course to complete the road design. Due to preference for building on flat subgrades, Telford attempted to achieve the crowned surface or crossfall slope by using stones of varying height. Figure 2.2 shows an example of a typical Telford road design.

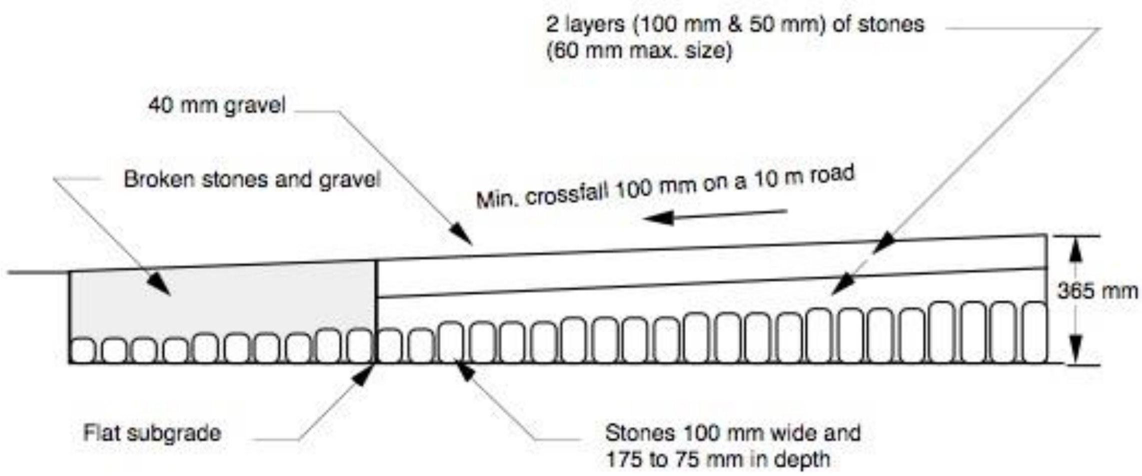

Figure 2.2 Example of a cross section of Telford Road Design (Pavement Interactive, 2008)

2.1.4. Macadam Road Design Philosophy

After Telford, Macadam further advanced road design philosophy from its initial stages of development and as a result the design methodology was named after him. In his approach, Macadam modified the Telford design by removing the foundation layer of relatively large stones and replaced it with small broken stones not exceeding 75mm. Macadam posited that the smaller stones were more suitable for interlock with each other due to angularity. In practice, unlike the Telford method, the subgrade was sloped and the small broken stone was in two layers for a total depth of 200mm. Additionally, a wearing course 50 mm thick, made of 25mm stones completed the cross-sectional profile of the Macadam road. An example of a typical Macadam road design is shown in Figure 2.3

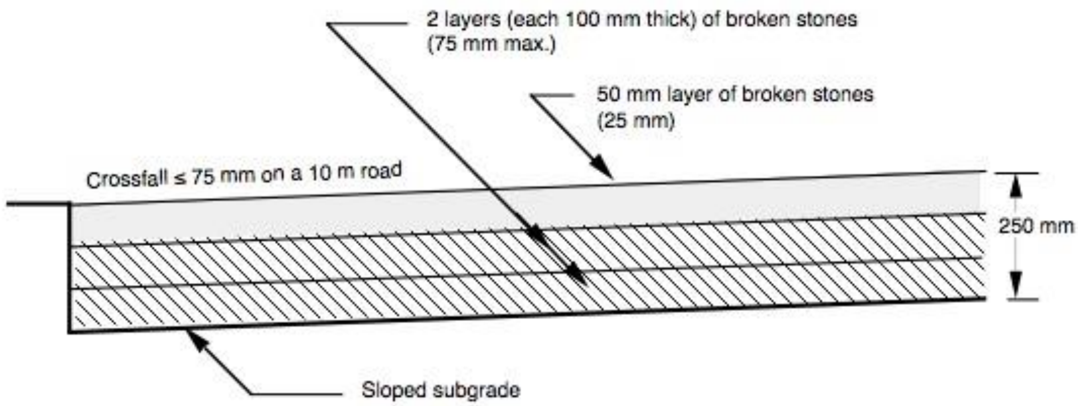

Figure 2.3 Example of a cross section of Macadam Road Design (Pavement Interactive, 2008).

There were primarily two types of Macadam road designs implemented known as the water-bound and tar-bound designs. Generally, Macadam surfaces refer to a road surface or base where crushed ledge stone was mechanically interlocked via rolling. In the original (water-bound) design, the bonding of constituent parts is done by working stone screenings and water into the existing void spaces (Oglesby 1975). This methodology was later improved by using bituminous material as the binder instead of water and this was part of the early introduction of the flexible or viscoelastic pavements. The original Macadam method existed for approximately 100 years as the highest known type of road surface. An example of its widespread use is evidenced in the fact that in the state of Massachusetts, U.S., Macadam surfaces were employed on approximately 95% of the state highways (Oglesby 1975). The practice of designing water bound Macadam roads was largely discontinued because of some inherent flaws in this philosophy. The overarching effect of the vacuum created under the moving vehicle and the thrust of its wheels resulted in the rapid removal of the binder. In essence, the road surface was reduced to a pile of rubble and was no longer capable of providing acceptable levels of service for the road user. In addition, the cost effectiveness of the Macadam design was deemed questionable, particularly in parts of the world where labor costs tend to be high.

2.2. The AASHO Road Test

The use of the aforementioned as well other methodologies employed for pavement design, underwent a considerable shift in philosophy in the early 1960s with the advent of the American Association of State Highway Officials (AASHO) road test program. The Interstate Highway System (IHS) in the United States is arguably the single greatest and most expensive public works project to date (Hallin et Al 2007). This system is unrivalled in many parts of the world and provides the infrastructural substratum for the relative economic prosperity of the United States. In many ways, the AASHO test program was authorized by IHS legislation enacted in June of 1956 and championed by President Eisenhower. In essence, the public highway system developed concomitantly with the motor vehicle industry. As motor vehicles underwent changes in weight, size, speed, capacity and sheer volume, it became evident that the early methods would not be adequate and accordingly, new and more advanced methodologies had to be developed. In the post-World War I and post-World War II eras, the ensuing years accounted for a sharp rise in vehicle registrations in the United States. During the period 1919-1929, vehicle registrations tripled and from 1945-1955 the number doubled (Highway Research Board 1961). Consistent with the earlier methods of road construction discussed in this chapter, highway engineers in the 1920s were aware that the structural integrity of the road pavement system was premised on the axle loads of vehicles. However, the volume of traffic was so low, it was assumed that the pavements which resisted natural forces were adequate for that traffic loading. Nevertheless, with the surge of vehicular traffic traversing the roadway, a more direct assessment of the relationship between pavement design and axle weights saw practitioners build on initial test efforts initiated throughout the early 1900s such as the Bates Experimental Road Test conducted by the Division of Highways of the Illinois Department of Public Works and Buildings between 1922 and 1923. The cost of the AASHO Road test was approximately Twenty Seven (27) Million USD dollars in 1960 and was located just Northwest of Ottawa, Illinois approximately 80 miles southwest of Chicago as shown in Figure 2.4.

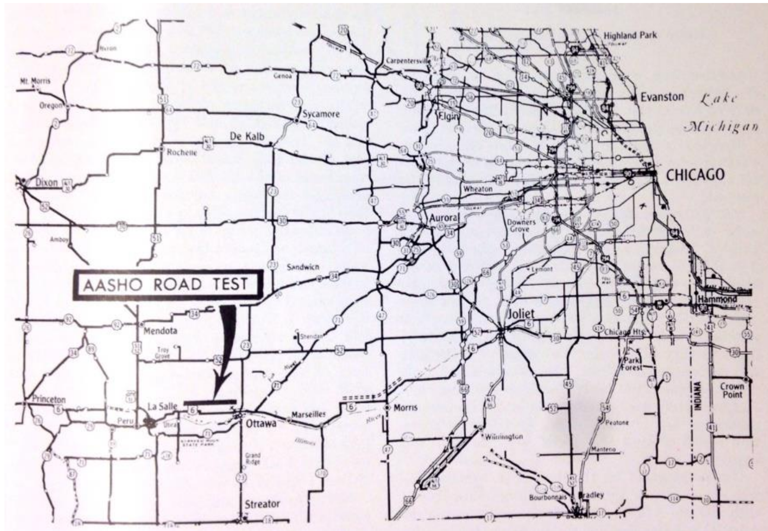

Figure 2.4 Location of the AASHO Test Site (Highway Research Board, 1961)

The tests were conducted from 1958 – 1960 and the compiled results were used to inform more broadly applicable scientific approaches to design. These results formed the basis of the design of most of the IHS post 1961 (Hallin et al 2007). In fact, all the pavement design guides issued by AASHTO until 1993 are incapable of easily adapting to significant improvements made in pavement engineering, design and materials (Timm et al, 2014). The Test site consisted of six (6) constructed loops of roadway with two minor loops (1 and 2) and four major loops (3 through 6). These loops were tested with several axle load configurations but only one axle load combination at a time so as to observe the performance of the roads as well as bridges. A map of the Road Test area as well as typical layout of each loop can be seen in Figures 2.5, 2.6 and 2.7.

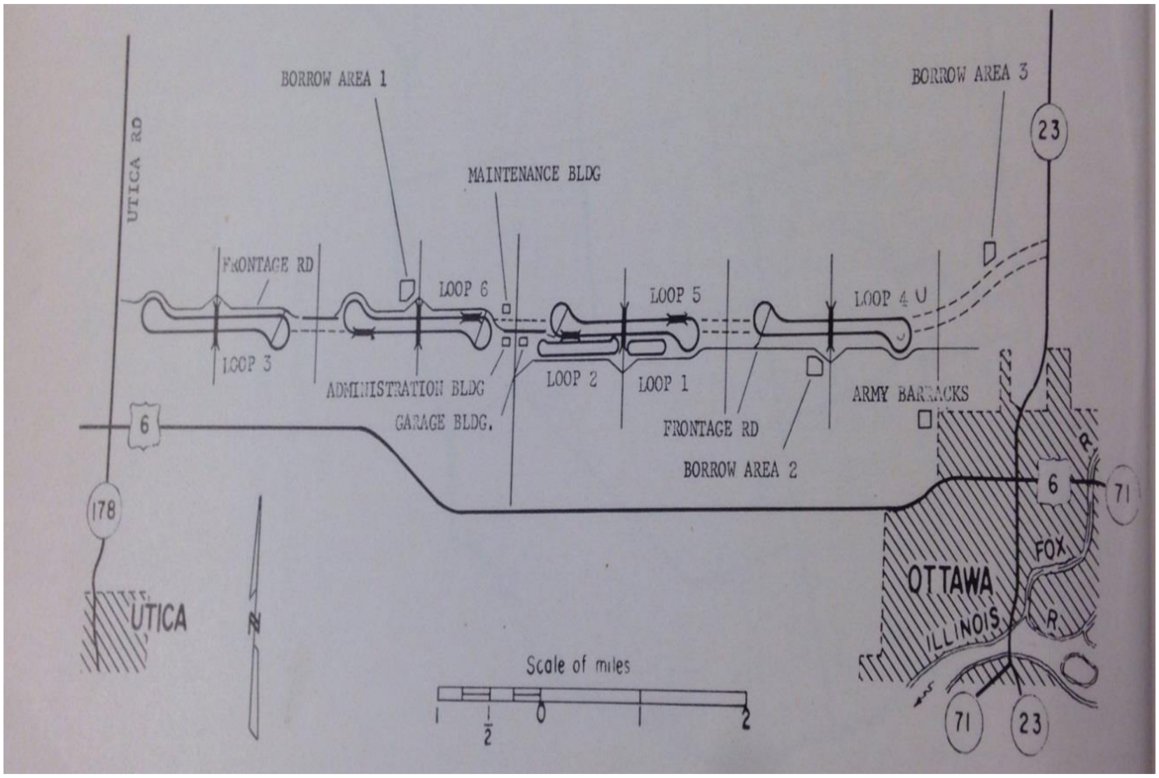

Figure 2.5 Map of AASHO Road Test (Highway Research Board, 1961)

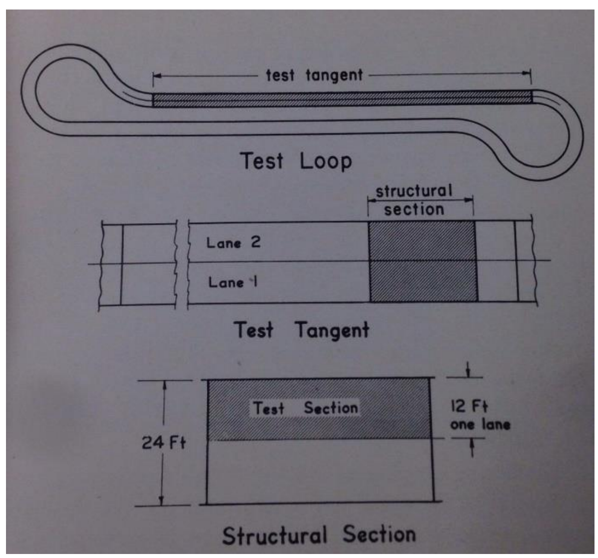

Figure 2.6 Typical layout of test loops (Highway Research Board, 1961).

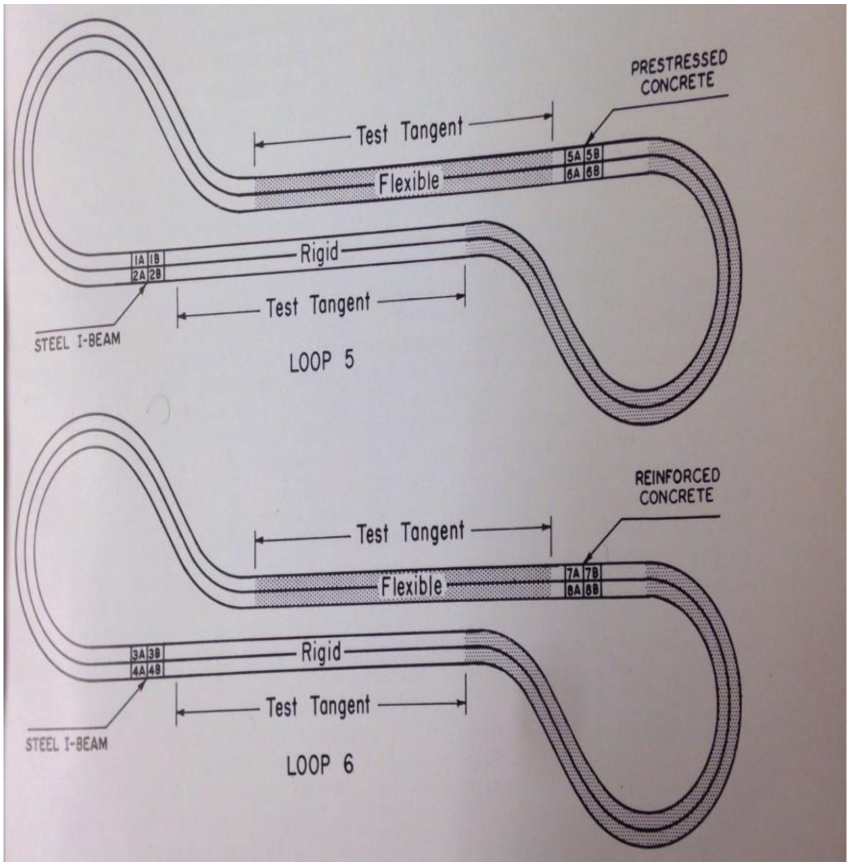

Figure 2.7 Bridge locations on Test Loops (Highway Research Board, 1961).

Each loop has two lane road segments or tangents which run parallel to each other with turnarounds at the end of the loops (Figures 2.6 and 2.7). Loop 1 was used primarily to collect data on environmental effects and was therefore not subject to traffic. Loops 2 through 6 were subjected to specific traffic loads. The test tangents were constructed as both flexible pavement and rigid pavements. Figures 2.8 and 2.9 show typical cross sections of flexible and rigid pavement design sections, used in the AASHO test.

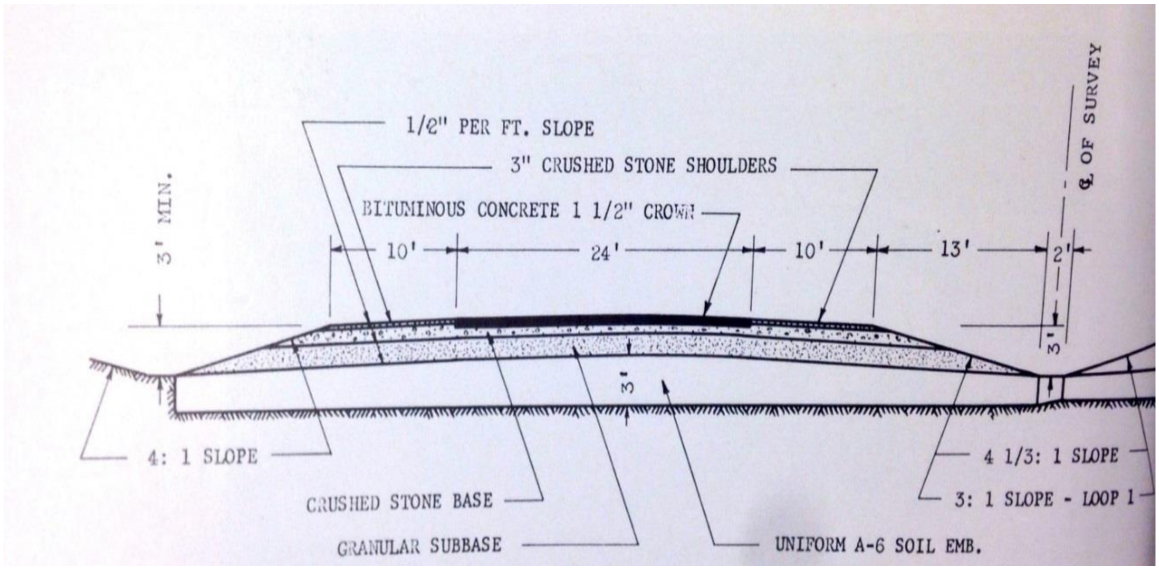

Figure 2.8 Typical Flexible Pavement Section used in AASHO Road Test (Highway Research Board, 1961)

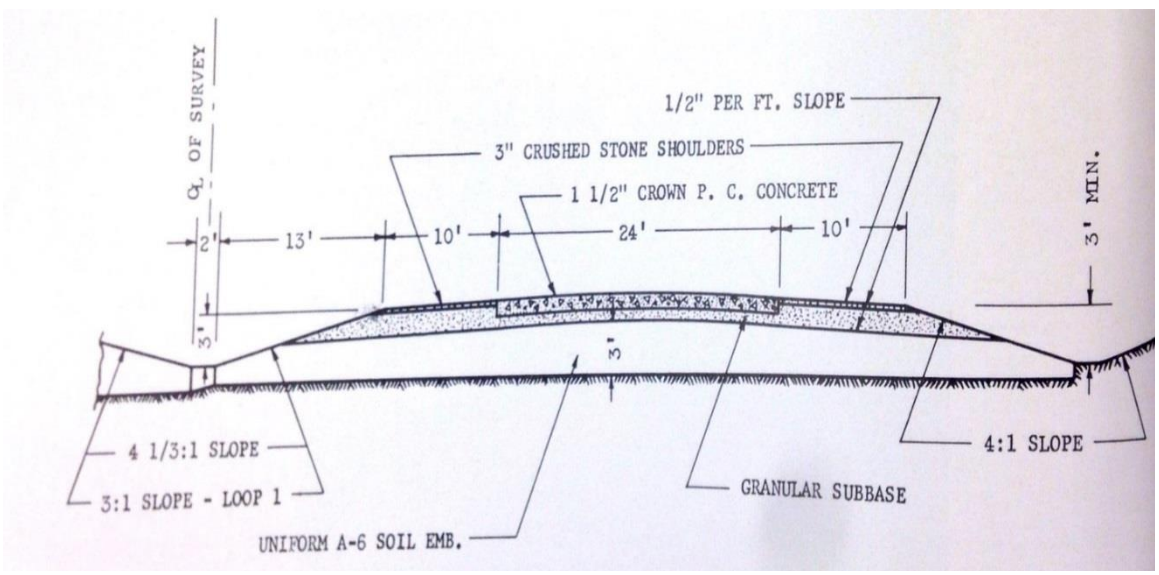

Figure 2.9 Typical Rigid Pavement Section used in AASHO Road Test (Highway Research Board, 1961)

2.3. Types of Pavements

Road pavements can be designed as flexible, rigid or semi-rigid pavements depending on the particular constraints a designer has to work with regarding cost, availability of material, existing site conditions.

2.3.1. Flexible Pavement

Flexible pavements are pavement systems that comprise a bituminous or asphaltic surface wearing course, a base course and a subbase course all sitting on a natural or stabilized pavement subgrade. The reason it is referred to as a flexible pavement is because the entire pavement system flexes as it transfers traffic load from the surface through the subsequent layers as seen in Figure 2.10. In cases where the load is large enough, the load can be transferred all the way through to the subgrade soil. Under sustained or repeated loads, the bituminous surface may deflect and not recover completely (Oglesby 1975).

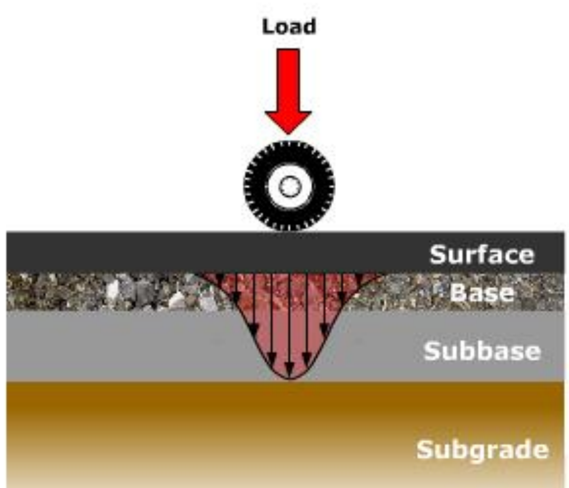

Figure 2.10 Flexible pavement under wheel loading (Muench, 2006)

2.3.2. Rigid Pavement

In contrast to flexible pavements, rigid pavements are so defined because Portland Cement Concrete (PCC) slabs have a very high modulus of elasticity when compared to the underlying base course and subgrade. This means that the slab is highly elastic and returns to its original configuration once loads have been removed. Accordingly, if the layers under the PCC slab do not recover as the slab does, this could lead to a separation between the base and the slab. If this happens sufficiently enough and large loads are applied to the slab at the surface it can fail in flexure (Oglesby 1975). Most of the load is subsumed by the PCC slab and as such is spread across a larger area of the slab as shown in Figure 2.11.

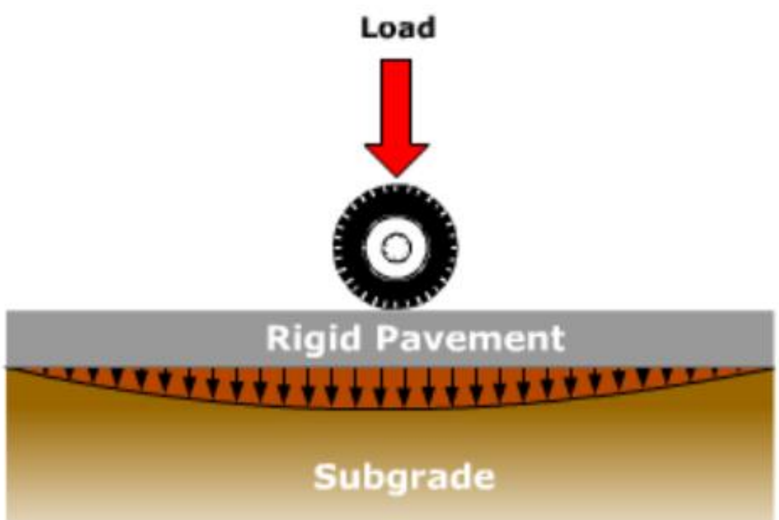

Figure 2.11 Rigid pavement under wheel loading (Muench, 2006)

2.3.2. Semi-Rigid Pavement

Semi-rigid or composite pavement systems are pavements where an asphaltic concrete surface is underlain by a PPC slab, base course, subbase on natural or stabilized subgrade. In this case the composite modulus is higher than that of a flexible pavement and the behavior under loading tends more to that of a rigid pavement.

2.4. Behavior of Flexible Pavement System Under load

Oglesby (1975) makes the analogy between a bridge and a road pavement system. The postulate is that in much the same manner as a bridge is required to support vehicular traffic by transferring the loads through successive members to the foundation beneath, the road pavement behaves in a similar fashion. As the vehicles traverse the carriageway the dynamic loads experienced at the pavement surface are transmitted through subsequent layers to the subgrade soil. The wheel loads that are exerted on the surface results in some deflection in the surface course and underlying layers of the pavement system. If the load exerted far exceeds the design load or the supporting layers do not carry the required stiffness (modulus), repeated applications can ultimately lead to failure of the road pavement. Oglesby (1975) presents three possible reasons for the deflection of the pavement under loading namely, elastic deformation, consolidation deformation and plastic deformation.

Elastic deformation occurs when the wheel loads temporarily deform the foundation material, compressing the air voids in the base and subgrade layers. In a truly theoretical sense, as it relates to elastic deflections, road pavement surfaces return to its original position after the load has passed as this ensures that there is no permanent deformation to the pavement surface under repeated loads. Generally, with small deflections there should be no damage done to the pavement system, but in cases where the subgrade soil can be described as highly resilient, heavy repeated wheel loads can cause fatigue failure or distresses to appear in the bituminous surface. Examples of this phenomenon includes distresses such as alligator or map cracking seen in Figure 2.12.

Figure 2.12 Alligator/Map cracking observed in a flexible pavement (Coastal Road Repair, 2015)

Consolidation deformation occurs when the wheel loads exerted on the road pavement system are sufficiently large enough to result in an expulsion of water and air from the voids in the subgrade soil and or the additional pavement layers, due to the buildup of pore pressures. This leads to some amount of consolidation in the pavement. The degree to which consolidation occurs due to one load can be infinitesimal but the deformation is permanent. Accordingly, as repetition of the load continues, consolidation intensifies. In the context of highway pavements, wheel paths are usually tracked with more regularity in the same general alignment and as such the result of excessive consolidation is usually manifested in rutting (Figure 2.13) which reduces the level of service on the highway.

Figure 2.13 Mix Design Rutting and Wheel path rutting in road pavements (Pavement Interactive, 2008)

Plastic Deformation occurs when roadway material is displaced due to a combination of the fluid and air pressure in the pores of the subgrade and other layers of the pavement system as well as the forces produced in the system by the wheel load applications. Oglesby (1975) indicates that deflections that are a direct result of plastic deformation is progressive under load repetition and constitutes one of the major causes of roadway failure. Figure 2.14 shows the usual occurrences of plastic deformation in road pavements. In each case, a shear failure occurs which is accompanied by movement in the susceptible layer. The figures show the planes of failure and demonstrates that the deeper the occurrence of plastic deformation, the longer the failure surface.

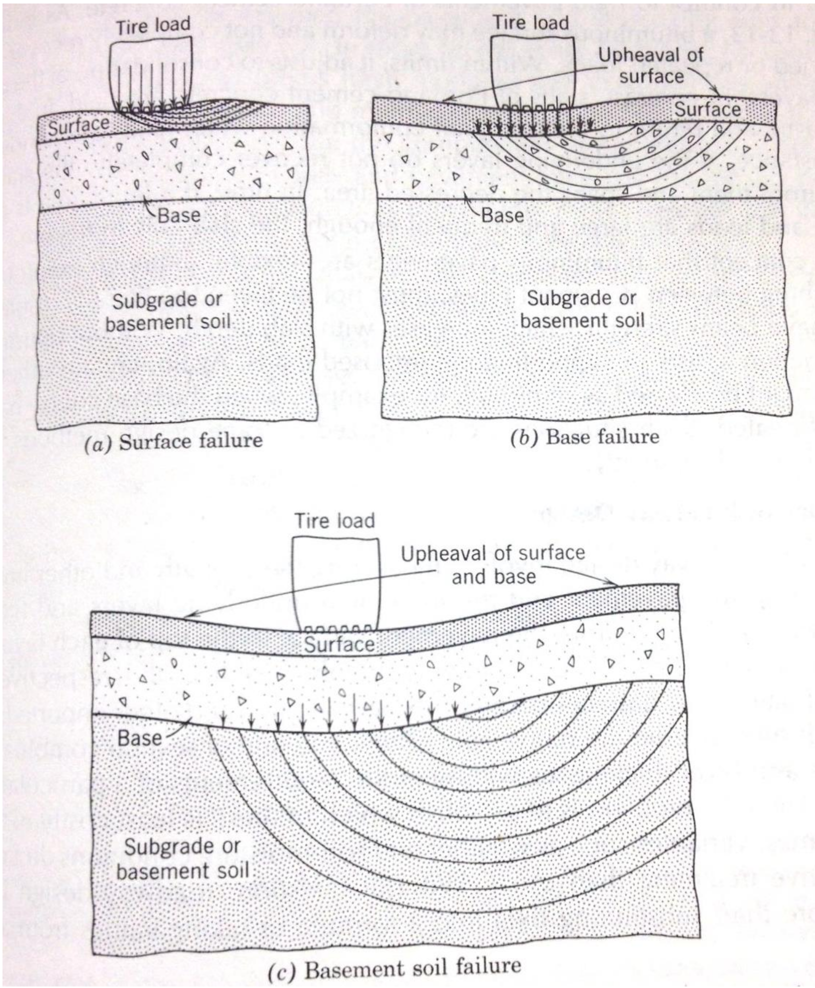

Figure 2.14 Failure surfaces in different layers of a flexible pavement system (Oglesby, 1975).

2.5. Predominant design practice

As previously mentioned, the design of most pavements are either flexible or rigid to a lesser extent. The main prohibitive factor against widespread use of rigid pavements is the overall cost vis-à-vis other options. According to the National Asphalt Paving Association

(NAPA), the United States has approximately 2.6 million miles of paved road and highways. Ninety three (93) percent of these pavements are covered with asphalt. The majority are full depth asphalt pavements and others are asphalt overlays on deteriorating rigid pavements. Even though there is an effort to use more mechanistic approaches to pavement design, the use of the 1993 AASHTO Pavement Design Guide is still the most common approach taken by practitioners. It is relatively easy to use and especially in developing countries like Guyana where state of the art practices are not readily entertained due to lack of human resources, systems and equipment, it is an option from which practitioners derive great comfort. Emergent from the AASHO Road Test, equation 2.1 was developed for flexible pavement design based on a calculated structural number.

$$logW_{18} = Z_R S_0 + 9.36 log(SN+1) - 0.20 + \frac{log\left[\frac{\Delta PSI}{4.2-1.5}\right]}{0.4 + \frac{1094}{(SN+1)^{5.19}}} + 2.32 log M_R - 8.07 \tag{2.1}$$

Where:

W_{18}= predicted number of 80 KN (18,000 lb) Equivalent Single Axle Loads

Z_R = standard normal deviate

So = combined standard error of the traffic prediction and performance prediction

SN = Structural Number (an index that is indicative of the total pavement thickness required)

ΔPSI = difference between the initial design serviceability index, po, and the design terminal serviceability index, pt

M_R = subgrade resilient modulus (in psi)

Alternatively, the 1993 AASHTO Pavement Design Guide provided the nomograph in Figure 2.15 which essentially allows the practitioner to determine the structural number without the algebraic computational tedium required to solve the above equation.

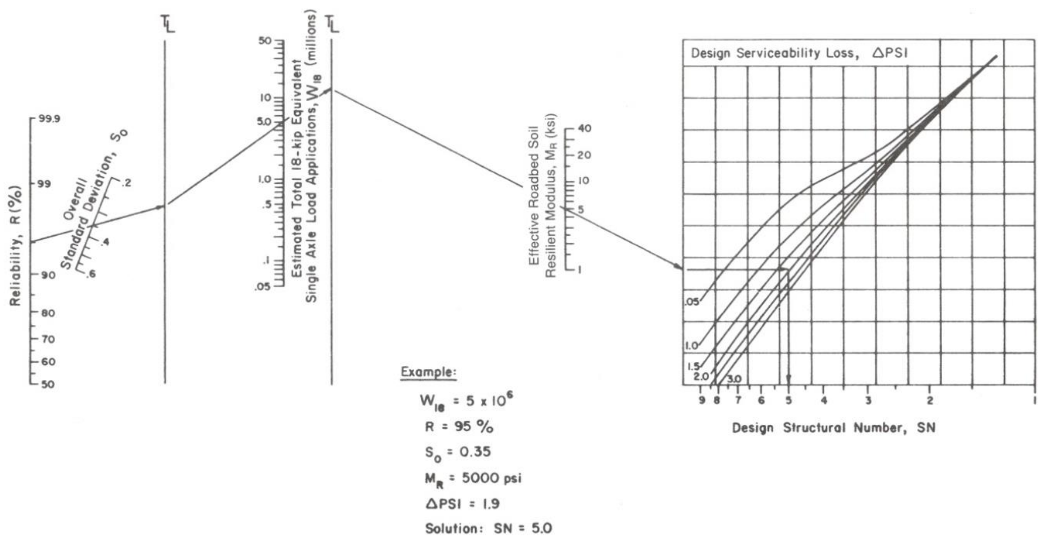

Figure 2.15 AASHTO Flexible Pavement Design Nomograph (AASHTO 1993)

Once the Structural Number (SN) has been determined for the flexible pavement system, the design is then based on a combination of material types and layer thicknesses which yield the appropriate design after following the appropriate iterative process as outlined in the design guide.

SN = a1D1 + a2D2m2 + a3D3m3+…+aiDimi (2.2)

Where

ai = ith layer coefficient

Di = ith layer thickness (inches)

mi = ith layer drainage coefficient

It is important to recall, that while relatively easy to use, there are inherent flaws in continuing to use this method today as well as in the future. The reason for the caution is the manner in which the experimental research was done. The road tests were conducted on one type of subgrade, namely soils under the classification AASHTO A-6 and having a group index of 9 to 13 (Highway Research Board 1961). In addition, the environmental conditions were specific to that of the test site between 1958 and 1960, there were specific road pavement materials used and the loading was applied in an accelerated two year period as opposed to 20 years, thereby making it impossible to simulate the environmental conditions over that period.

For all the foregoing reasons, any use of the AASHTO 1993 guide to design roads today will demand that the engineer makes a number of assumptions which ultimately leads to an unwise extrapolation of the data to compensate for factors not encountered in the actual AASHO Road Test. This can lead to the overdesign of road pavements costing stakeholders money that in many cases they can ill afford to spend. Since this recognition is not novel, it stands to reason that more mechanistic approaches to pavement design should be adopted.

2.6. The Mechanistic Approach to Pavement Design

As established in Chapter 1 and addressed in greater detail here in Chapter 2, the need existed for developing a methodology or road design philosophy which was cost effective and longer lasting than the 1993 AASHTO Design guides. Changes in traffic volumes, pavement materials, vehicle weights and Level of Service (LOS) to the road user were the driving factors. This need was addressed by National Cooperative Highway Research Program (NCHRP) via Project 1-37A which led to the creation of the Mechanistic Empirical Pavement Design Guide (MEPDG) in the early 2000s. The philosophy was to adopt a more mechanistic approach to pavement design where stresses, strains and deflections under wheel loads could be evaluated and consequently, the pavement is designed to withstand critical levels of the aforementioned parameters without failure.

In the Mechanistic approach, pavement response predictions of stresses, strains and deflections are determined by utilizing Multilayer Elastic Theory (MLET) or Finite Element Method (FEM). These predicted responses are then compared with pavement field performance via empirical models, hence the accurate determination of pavement responses are critical for producing a reliable design (Zhao et al 2012). The mechanistic design process can be captured as shown in Figure 2.16, informed by Schwartz and Carvalho (2007).

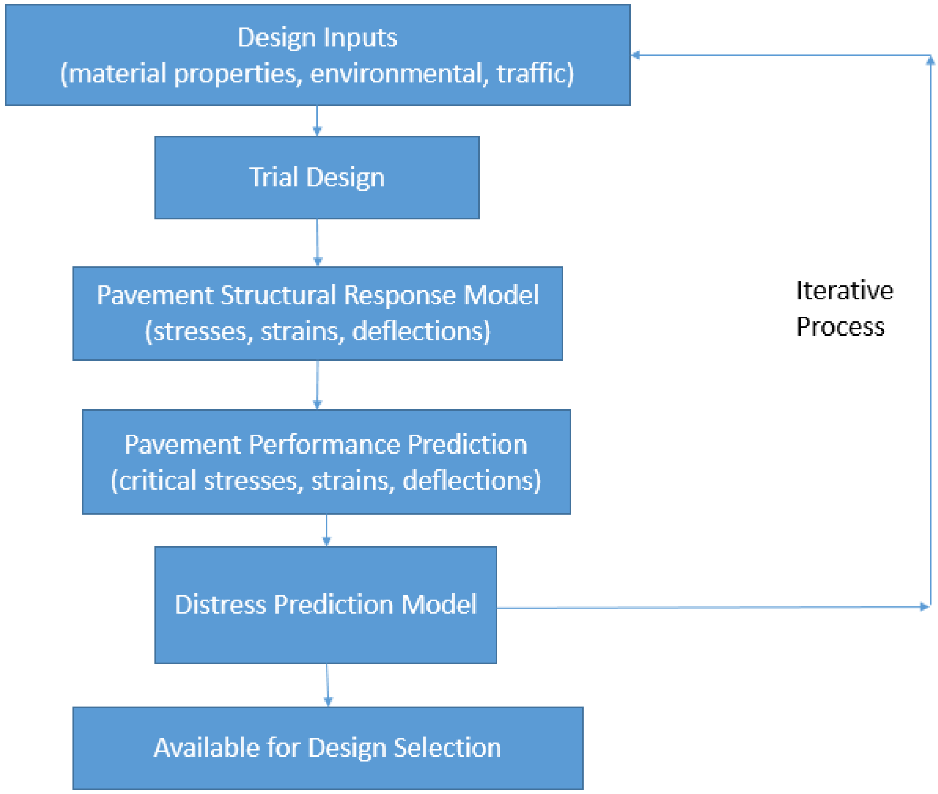

Figure 2.16 Chart showing the Mechanistic-Empirical Design Methodology

The main focus of this research effort addresses a key component in the mechanistic approach which is the Pavement Response Model where stresses, strains and deflections are predicted.

2.6.1. Multilayer Elastic Theory

The literature surrounding response modeling has continued to evolve over time even as different postulates on pavement design has evolved. According to Yoder et al (1975), there are three elements which must gain consideration if a design approach is to be considered as rational. These elements are:

- The theory used to predict the failure or distress parameter.
- The evaluation of pertinent material properties necessary for conducting the analysis of the failure theory.
- A well understood relationship between the determined parameter, its magnitude compared with known failure levels or desired performance.

Notwithstanding the fact that predicted responses in road pavements are not always accurate, there is still value in the estimates and the general thought processes that a research or practicing engineer needs to grapple with when conducting a design. Huang (2004) suggests that the most prudent way to consider a flexible pavement under wheel load for analysis, is to think of it as a homogenous half-space. This means that it has an infinitely large area and an infinite depth.

Yoder et al (1975) present the basic concept of the multilayered elastic system as shown in Figure 2.17. The assumptions made in producing an analytical solution to the state of stress or strain are as follows:

- The material properties are homogenous for each layer.
- Each layer is isotropic.
- Individual layers have finite thicknesses with the exception of the natural subgrade which is semi-infinite.
- Full friction is developed at the interface between layers
- Surface shearing forces are not present at the surface
- Elastic Modulus, E and Poisson's Ratio, μ are the two material properties needed for the stress solutions.

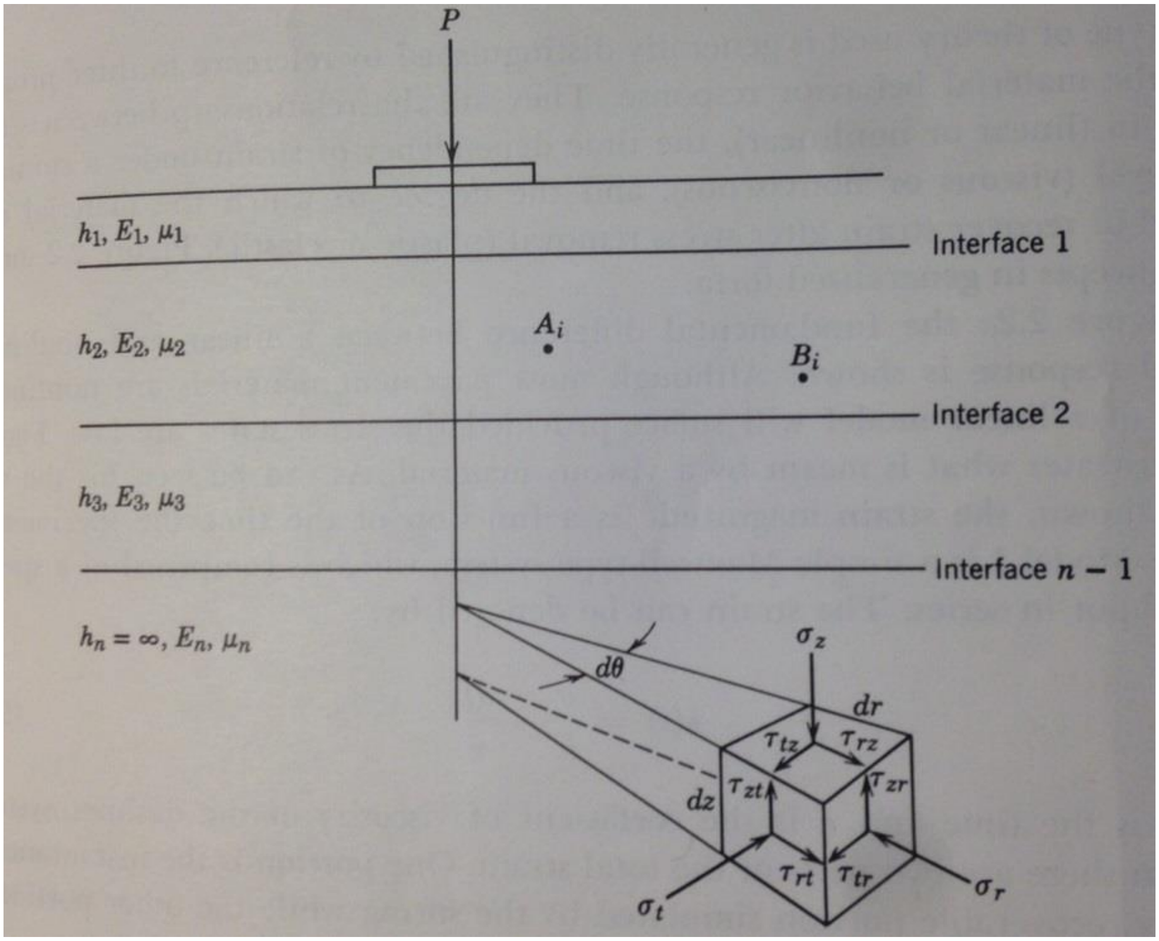

Figure 2.17 Generalized Multi-Layer Elastic Theory (Yoder et al, 1975)

The Layered theory was initially based on Bouissneq's equations which were developed for isotropic, homogenous and elastic media and was used to analyze the one-layer configuration. Burmister (1943) continued to develop the theory and extended it for a two-layered system. Jones and Peattie (1962) expanded the two-layer solution to a much wider range of parameters. Acum and Fox (1951) further extended to analyze a three-layer system and Schiffman (1962) extended the work to accommodate several layers. These methods were aimed at determining via closed form analysis, the structural responses (stresses, strains and deflections) in a pavement system. With advanced computing available and the tedious nature of the more complex pavement structures for analytical solutions, finite element models which tend to be more accurate as well as other simple programs such as EVERSTRESS, WESLEA and KENLAYER are still used to predict flexible pavements responses.

2.7. Challenges in State of the Practice

Despite the development of new mechanistic approaches to pavement design, there is still appreciable resistance to abandoning the empirical methods and embracing the inevitable changes. In many ways, practitioners have deemed these methodologies impractical for implementation due to the complexity of mechanistic approaches. The State of the Art in road pavement design since the 1990s has been consistently trending towards a more mechanistic approach but the gap is yet to be bridged between the pavement researchers and pavement engineers (Timm et al 2014). It is clear that there are many benefits to be derived from the State of the Art Solutions such as more efficient designs which save cost. In Chapter 3, the postulate of a new synthesis is presented to form the basis of a realistic and philosophical approach to mechanistic pavement modeling. This includes a material characterization model for cohesive subgrades as well as a Stress- Based FEM to model pavement response.

2.8. Pavement Layer Debonding

Pavement layer debonding can be described as the phenomenon where adhesion between adjacent layers in a pavement system is lost and may even result in eventual separation. Tschegg et al (1995) underscore the need for bonding between layers of a road pavement by using an analogy of a multilayer beam under loading. As seen in Figure 2.18, the deflection of several well bonded beams is nine times less than the deflection of a debonded beam. Excessive deflections can lead to pavement layer debonding which has been reported to reduce the life of the pavement by as much as 80% (Kruntcheva et al 2005). Accordingly, design and analysis models must have the capability of determining the transverse stress distribution. This is imperative for the realistic modeling of in-pavement behavior.

A stress based model developed at The Ohio State University shows great promise in being able to predict transverse stress distribution at the layer interfaces, thereby overcoming the shortcomings of the traditionally acceptable methods.

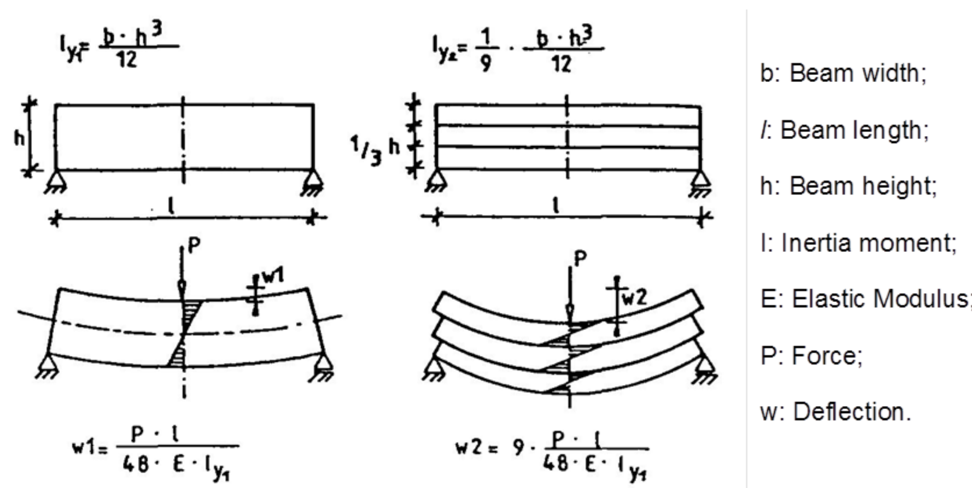

Figure 2.18 Beam deflection analogy showing the effect of debonding on the magnitude of deflection (Tschegg et al, 1995).

Chapter 3: Synthesis of Stress Based Finite Element and Material Characterization

3.1 Introduction

The unique synthesis of these two individual models has not been presented in literature up to now regarding flexible pavement design. This new approach is presented as an important tool in the development of a pavement design philosophy to be adopted by the pavement engineering community in Guyana and further afield. In this mechanistic approach to design, the transverse stress profile can be determined which is critical for the accurate analysis of flexible pavements under loading, to overcome the pavement layer debonding phenomenon, which is often responsible for premature failure of pavements.

3.2 Material Characterization Model to Determine Resilient Modulus, Mr

Resilient modulus is a measure of the elastic response of roadbed or supporting base, subbase and subgrade materials in a flexible pavement, to repeated traffic loading. In the OSU Stress Based Model extension proposed, the determination of the resilient modulus of the subgrade material is a key mechanical input parameter for the design of pavements. This material characterization is more realistic than the currently used California Bearing Ratio (CBR) test, which is then used in empirical formulae to estimate a value for Mr. Unlike the resilient modulus test, the CBR test does not possess a dynamic fatigue component.

Mr is numerically described as being equal to the ratio of deviator stress to recoverable strain after a large number of load cycles.

$$M_r = \frac{\sigma_d}{\varepsilon_r}; \qquad \sigma_d = (\sigma_1 - \sigma_3) \tag{3.1}$$

Where: M_r = resilient modulus,

σ_1 = major principal stress,

σ_3 = minor principal stress,

σ_d = repeated axial deviator stress,

ε_r = recoverable (resilient) axial strain.

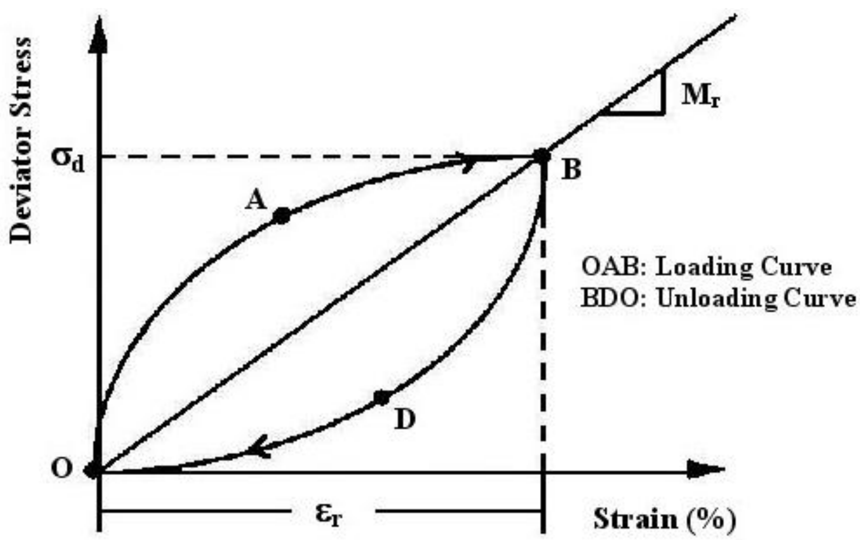

Figure 3.1 Graphical representation of the Measurement of Resilient Modulus (Kim and Drabkin, 1994)

Figure 3.1 shows how Mr is determined by examining the relationship between the deviator stress and the recoverable strain during loading and unloading of cohesive soils.

Direct measurement of Mr in a laboratory test, regardless of the chosen protocol, has proven to be expensive as it relates to the capital investment on equipment. Conducting this test and being able to achieve reliable and repeatable results requires highly skilled personnel. It is usually determined by cyclic repeated load triaxial tests with constant confining pressure and deviator stress cycled between hydrostatic state and positive deviator stress.

3.2.1 Mr Model for Cohesive Subgrades

Kim (2004) presented a new constitutive model for prediction of resilient modulus, Mr, for cohesive subgrade soils. This model was based primarily on a regression analysis incorporating the octahedral stresses and several material constants.

This model significantly reduces the need to conduct the cyclic triaxial test and the main input parameters for the model, based on conventional laboratory tests, are as follows:

- percent of soil particles passing through a #200 sieve (P#200)
- plasticity index (PI),
- liquid limit (LL),
- Unconfined compressive strength (q_u)
- optimum moisture content by weight (w_{opt}),
- actual moisture content by weight (w_c)
- degree of saturation (S_r),

- confining stress (σ_3),
- deviator stress (σ_d)

The derivation and presentation of the model is developed by Kim (2004) but is restated here for completeness and relevance to the new synthesis.

$$\frac{M_r}{P_a} = k_1 \left[\frac{\frac{\sigma_{oct}}{P_a}}{\left(\frac{\tau_{oct}}{P_a} \right)^2} \right]^{k_2} \tag{3.2}$$

$$= k_1 \left[\frac{P_a \cdot \sigma_{oct}}{\tau_{oct}{}^2} \right]^{k_2} \tag{3.3}$$

$$= k_1 \left[\frac{9P_a}{2} \left(\frac{1}{3\sigma_d} + \frac{\sigma_3}{\sigma_d^2} \right) \right]^{k_2} \tag{3.4}$$

Where: M_r: Resilient Modulus (kPa)

P_a: Atmosphere Pressure (101 kPa)

σ_{oct}: Octahedral Normal Stress ([σ_1+2 σ_3]/3)

τ_{oct} : Octahedral Shear Stress ({$2^{0.5}$[σ_1-σ_3]}/3)

σ_1 : Major Principal Stress ($\sigma_d + \sigma_3$)

σ_d : Deviator Stress (kPa)

σ_3 : Minor Principal Stress or Confining stress (kPa)

k_1, k_2: model constants

Model Constants

$$k_1 = a_1 \sigma_3^{\ a_2} + a_3 \left(\frac{S}{100}\right)^{a_4} + a_5 q_u + a_6 PI + a_7 (LL - w) + a_8 (w_{opt} - w) + a_9 (\%passing\#200 - a_{10}) \tag{3.5}$$

$$k_2 = b_1 \sigma_3^{\ b_2} + b_3 \left(\frac{S}{100}\right)^{b_4} + b_5 q_u^{\ b_6} + b_7 PI + b_8 LL \tag{3.6}$$

Where $a_1 = a_{11} + a_{12}\left(\frac{w_{opt} - w}{w_{opt}}\right)$ (3.7)

$$b_1 = b_{11} + b_{12}\left(w - w_{opt}\right) \tag{3.8}$$

w_{opt}: Optimum Moisture Content (%)

w: Moisture Content (%)

σ_3: Confining stress (kPa)

S: degree of saturation (%)

q_u: Unconfined compressive strength (kPa)

PI: Plasticity Index

LL: Liquid limit

%passing#200: percent soil particles finer than 0.075mm (%)

This model was compared to similar established models to predict Mr Values using basic soil laboratory tests. These models include the USDA Model (Carmichael & Stuart, 1986), Hyperbolic Model (Drumm, et. al., 1990), GDOT Model (Santha, 1994), TDOT Model (Pezo & Hudson, 1994), UCS Model (Lee, et al., 1995) and the ODOT Model (ODOT, 1999). The Kim (2004) model was proven to provide more accurate predictions for cohesive soils. It has also proven capable of predicting Mr for chemically stabilized cohesive soils.

In the validation of this Mr model, Kim observed predictions for general cohesive soils as well as predictions for specific cohesive soils (AASHTO Classifications - A-4, A-6 and A-7-6). The resulting postulate was that the use of soil specific regressions coefficients in the model gave better predictions of Mr with a higher degree of correlation than the general regression coefficients.

3.2.2 Extension of Mr Model for Cohesive Subgrades

Samples of cohesive soils were obtained from Guyana so as to determine whether the model could be extended beyond the geographical boundaries of the United States as provided by the Kim study. The samples were obtained from the Stratsphey and Cane View areas on the East Coast of Demerara and Greater Georgetown respectively. In the case of Stratsphey, progressive failure in the pavement was observed a few years after construction of the railway embankment road, and the Cane View sample was representative of a route designated for the construction of a second road linkage between Timehri and Georgetown. The attempt to verify the model’s capability of making relatively accurate predictions of Mr, for the A-7-5 soils was of particular interest since cohesive soils of this classification are unavailable in the current data set. The model parameters for the Guyana soils, obtained from routinely performed laboratory tests are summarized in Table 3.1.

	Location	
Model Parameters	**Stratsphey, ECD**	**Cane View, Greater Georgetown**
Liquid Limit (%)	64.5	57.8
Plasticity Index (%)	28.2	27.9
Optimum Moisture Content (%)	25.2	22.5
Moisture Content (%)	25	15.3
Confining Stress (KPa) *	41.4	41.4
Deviator Stress (KPa) *	14.37	14.37
Degree of Saturation	54	45
Unconfined Compressive Strength (KPa)	254.41	225.46
% passing the # 200 sieve	97.64	87.58
Soil Classification (AASHTO)	**A-7-5**	**A-7-5**

Table 3.1 Model parameters obtained from basic soil laboratory tests

* Denotes parameters used in the model but obtained from the T-294-94 protocol

In order to verify the practicality and reliability of the model, the regression coefficients of the general model were used to make Mr predictions for the Stratsphey and Cane View samples. The regression coefficients of the general Kim model are shown in Table 3.2.

The analysis yielded predicted values of Mr for both sites, including those obtained from specimens 2% wet of optimum and 2% dry of optimum for Stratsphey. In effect, 75 additional points were obtained for the database. When tested at optimum moisture content, the measured Mr values were in the range of 21.52MPa to 112.28 MPa for Stratsphey and in the case of Cane View between 19.45 MPa and 93 MPa. Since they are both A-7-5 soils, the expected published value should be in the range of 55- 120 MPa (NCHRP 1-37A, 2004). It was also noted that in tropical climates such as Mexico (Instituto Mexicano del Transporte 2001), the published data for A-7-5 soils were also in the range of 14.07-

70.37MPa. The model predictions were between 21.52 and 206.34MPa for all conditions with Stratsphey specimens while Cane View fell in the range of 19.45-366.98 MPa.

k_1		k_2	
Coefficient	Value	Coefficient	Value
a_{11}	7.588	b_{11}	0.00361
a_{12}	48.471	b_{12}	0.0011
a_2	0.6588	b_2	0.51
a_3	-128.76	b_3	0.213
a_4	7.3	b_4	14.7
a_5	0.875	b_5	1.4923
a_6	4.01	b_6	-0.596519
a_7	6.84	b_7	-0.000109
a_8	18.9	b_8	-0.000204
a_9	0		
a_{10}	0		

Table 3.2 Coefficients of the Material Characterization Model (Kim 2004)

Measured Mr Values of Guyana Soils A-7-5 (MPa)				
Stratsphey			Cane View Avenue	
2% Wet of OMC	OMC	2% Dry of OMC	OMC	2% Dry of OMC
19.45	31.59	51.36	21.52	42.01
40.28	63.22	89.12	39.88	85.40
49.15	74.37	106.18	47.89	96.98
42.77	60.22	91.02	43.20	79.14
42.11	54.83	86.47	42.40	80.12
30.75	56.52	70.66	40.62	74.51
42.95	67.91	98.04	52.25	91.28
78.46	136.96	186.81	94.25	169.06
86.93	149.92	215.68	98.38	198.95
55.79	83.30	125.08	61.64	113.65
93.00	191.76	366.98	112.28	334.95
81.79	144.55	250.00	107.44	206.34
78.41	127.92	184.21	100.35	182.08
74.68	134.76	189.89	92.72	169.30
74.62	133.17	180.21	88.52	164.82

Table 3.3 Measured resilient modulus (Mr) values for Guyana A-7-5 soils at optimum moisture content (OMC) as well as wet and dry of optimum.

The results of the Mr testing were obtained using AASHTO Testing Protocol T-294-94 and are captured in Table 3.3. There are some factors, which researchers have been able to establish in the literature, that contribute in varying degrees to the values of Mr. Included among others are effects of confining stress, deviator stress and moisture content.

Seed et al (1962) as well as Rada et al (1981) show that as the applied confining stress increases, the resilient modulus also increases. However, Robnett and Thompson (1973) posited that confining stress did not have a significant impact on Mr when considering fine grained soils. The deviator stress has a significant impact on the Mr of cohesive soils (Titti et al 2006). For that matter, the conventional wisdom is that resilient modulus of cohesive soils is a function of deviator stress. As deviator stress is increased at constant confining stress, the value of Mr decreases for fine grained soils. It is worth noting that in the case of granular soils, it is not uncommon for the opposite to occur. This is usually attributed to strain hardening due to reorientation of the individual particles in granular soil into a more dense state. According to Visser et al (1983), studies done on soils in Brazil were compared unto cohesive soils from the United States and as opposed to Brazilian soils, it was the US soils that proved moisture had a significant effect on Resilient Modulus testing results.

A closer examination of the complete dataset obtained from tests on the Guyana soils in this study (Table A8 and A9 in Appendix A), reveal rather interesting behavior that is worth further investigation. In fact, as confining stress was held constant as per the AASHTO T-294-94 protocol and deviator stress increased, the value of measured Mr actually increased which as mentioned before runs counter to what is expected based on the literature. Accordingly, these results make it somewhat impractical to attempt a direct comparison based on specific stress states but what is clear is that the predicted values do fall within the range of acceptable values in the literature. In addition, as moisture content increased, the measured Mr decreased.

In summary, one of the challenges for practicing engineers is to be able to confidently choose a value of Mr for design since Mr varies based on the different stress states and is not a constant value. Approximating the state of stress in-situ may be possible but very difficult to ascertain. Additionally, it is clear that different Mr values can be obtained for the same classification of soil when they originate from different depositional environments. The foregoing further underscores the challenge of attempting to repeat these tests successfully and more so encourage engineering practitioners to attempt this in order to arrive at appropriate values. The need for a characterization model becomes critical and with the predicted values falling within the published range makes this characterization model promising for further development regarding cohesive subgrades.

3.3 Stress Based FEM for Pavement Response Model

The OSU Stress Based Model used in this research was developed by Chyou (1989), extended by Schoeppner (1991) and further extended by Butalia (1996). Tu (2007) extended this research work for use in response modeling of pavements subject to dynamic surface loading.

3.3.1 Stress Based Discrete Layer Pavement Model

Pavement layer debonding in road pavements is similar to that of delamination in composite laminates. Schoeppner (1991) postulated a stress based theory describing the dynamic behavior of laminated plates, to predict stress and displacement response due to dynamic disturbances. He proffered that existing dynamic theories based on a prescribed through the thickness displacement distribution, were capable of predicting global responses but not accurately predicting stress behavior. Schoeppner (1991) showed that a stress based theory proved to be better at predicting transverse stress distributions at layer interfaces and continuous displacements than displacement based theories. The problem of pavement layer debonding is similar to the delamination of composite laminates. The finite element formulation of Schoeppner's stress based theory, capable of accurately modeling the dynamic stresses and displacement behavior of laminates while accounting for delaminations, made it ideal for future applications for detecting and predicting damage. This model was extended for laminated composites by Butalia (1996) and subsequently by Tu (2007) for pavements.

Butalia's extension to Schoeppner's model included the effect of variable mass density for a plate under dynamic loading. Chai et al (1980) indicate that when laminates encounter low velocity dynamic loading, delamination may occur. This is critical mode of failure which must be predicted. Butalia (1996) stated that delamination in composite laminates is governed by transverse shear stresses (σ_{13}, σ_{23}) as well as transverse normal stresses (σ_{33}) in the vicinity of lamina interfaces Abrate (1991). The accurate determination of the stresses at the lamina interfaces allows for the prediction of damage development and failure, thereby making it critical to have a theoretical framework capable of realistic estimates.

In summary, displacement based theories are known to provide accurate predictions of in-plane stresses and displacements but not the transverse stress distribution. Conversely, stress-based theories have provided a more robust way of predicting transverse stresses at the layer interfaces.

Tu (2007) successfully extended this model, originally developed for composite laminates, to road pavements. Composite laminates and road pavements are both layered systems and this is a critical underpinning of the rationale for the cross application, coupled with the similarity of failure modes delamination and pavement layer debonding respectively. However, the individual layer dimensions are orders of magnitude greater for pavement systems than they are for composite laminates. Accordingly, using the theoretical formulation presented by Schoeppner (1991) and Butalia (1996), but employing a numerical integration scheme and time step for numerical stability of the model more appropriate for asphalt and/or concrete pavements and soil systems, Tu (2007) was able to use the stress based model in pavement response applications (Parris et al 2013). The model as presented by Tu does not incorporate a material characterization model. Therefore, in order to allow for greater accuracy in pavement response modeling using this formulation, it is necessary to include a material characterization model which accurately predicts Resilient Modulus. In this dissertation a new synthesis is presented with the Kim (2004) material model in conjunction with the stress based finite element formulation, to complete the pavement response model and improve the accuracy of its predictive capability.

To facilitate a clear presentation, the derivation of the stress based approach is presented in the sections below and is an abridged version of the complete works of Schoeppner (1991) and Butalia (1996). It is also found in the presentation of Tu (2007) which was based entirely on the work of Schoeppner (1991) and Butalia (1996).

The variation on the Tu Model is the incorporation of the material characterization Mr model into the stiffness matrix of the stress based discrete layer model.

3.3.2 Lamina Stresses

Equilibrium equations, constitutive law and kinematic relations were used in order to derive the equations of motion for a lamina with variable mass density (Butalia 1996). For an assumed linear in-plane stress distribution, integrating the equilibrium equations allows for the derivation of transverse stresses. The result is a quadratic and cubic distribution of transverse shear and normal stresses respectively through the lamina thickness. No displacement assumptions are made over the lamina thickness.

3.3.3 Equilibrium Equations

Consider a rectangular lamina with thickness h, bounded by $x_1 = \pm a,\ x_2 = \pm b,$ and $x_3 = \pm \frac{h}{2}$ as shown in Figure 3.2. The equilibrium equations for this lamina can be written as:

$$\sigma_{ij,j} + f_i - \dot{p}_i = 0 \tag{3.9}$$

Below are the in-plane and transverse equations of equilibrium taken separately:

$$\sigma_{\alpha\beta,\beta} + \sigma_{\alpha 3,3} + f_\alpha - \dot{p}_\alpha = 0 \tag{3.10}$$

$$\sigma_{\alpha 3,\alpha} + \sigma_{33,3} + f_3 - \dot{p}_3 = 0 \tag{3.11}$$

Where

σ_{ij} is the symmetric Cauchy stress tensor

f_i is the body force per unit volume

$\dot{p}_i$ is the momentum density of the medium.

The momentum density term can be written in terms of medium mass density, ρ, and the displacement, u_i, as:

$$\dot{p}_i = \frac{\partial(\rho\dot{u})}{\partial t} = \dot{\rho}\dot{u}_i + \rho\ddot{u}_i \tag{3.12}$$

Where $\dot{\rho}$ represents the time dependent change of mass density which can be expressed in terms of the rate of change of volumetric strains as (Hiremath, 1987):

$$\dot{p}_i = -\rho\dot{\varepsilon}_{jj} = -\rho\dot{u}_{j,j} \tag{3.13}$$

Substituting Equation 3.13 into Equation 3.12 leads to

$$\dot{p}_i = -\rho\dot{u}_{j,j}\ddot{u}_i = \rho\left(\ddot{u}_i - \dot{u}_{j,j}\dot{u}_i\right) \tag{3.14}$$

The nonlinear term $\dot{u}_{j,j}\dot{u}$ results from the compressibility of the material.

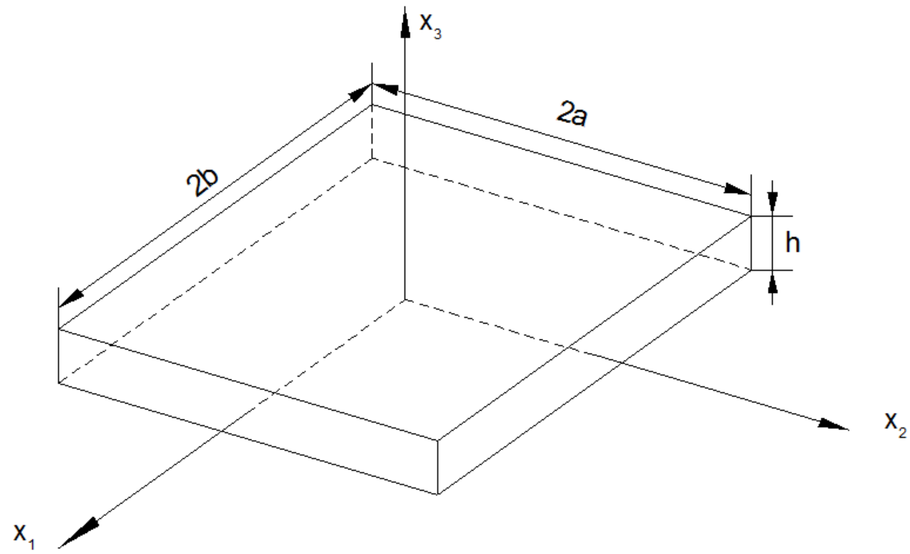

Figure 3.2 Lamina Geometry and Coordination System

The superposed dots represent differentiation with respect to time.

3.3.4 Constitutive Equations

Since the material types in this study are assumed to be linearly elastic, the generalized Hooke's Law is satisfied. The generalized Hooke's Law may be written as:

$$\sigma_{ij} = E_{ijkl}\varepsilon_{kl} \qquad (3.15)$$

Or conversely

$$\varepsilon_{ij} = S_{ijkl}\sigma_{kl} \qquad (3.16)$$

Where E_{ijkl} and S_{ijkl} are the components of the rate independent isothermal elasticity and compliance tensors respectively.

For a monoclinic material (essentially there is only one plane of symmetry about the plane $x_3 = 0$), the constitutive equations may be expanded as shown below.

$$\sigma_{\alpha\beta} = E_{\alpha\beta\gamma\delta}\varepsilon_{\gamma\delta} + E_{\alpha\beta 33}\varepsilon_{33}$$

$$\sigma_{\alpha 3} = \sigma_{3\alpha} = 2E_{\alpha 3\beta 3}\varepsilon_{\beta 3}$$

$$\sigma_{33} = E_{33\gamma\delta}\varepsilon_{\gamma\delta} + E_{3333}\varepsilon_{33} \tag{3.17}$$

Or conversely as

$$\varepsilon_{\alpha\beta} = S_{\alpha\beta\gamma\delta}\sigma_{\gamma\delta} + S_{\alpha\beta 33}\sigma_{33}$$

$$\varepsilon_{\alpha 3} = \varepsilon_{3\alpha} = 2S_{\alpha 3\beta 3}\sigma_{\beta 3}$$

$$\varepsilon_{33} = S_{33\gamma\delta}\sigma_{\gamma\delta} + S_{3333}\sigma_{33} \tag{3.18}$$

3.3.5 Kinematics

For small displacement, the Green-Lagrange strain tensor reduces to the infinitesimal strain tensor in Cartesian component form

$$\varepsilon_{ij} = u_{(i,j)} = \frac{1}{2}\left(u_{i,j} + u_{j,i}\right) \tag{3.19}$$

Through integrating Equation 3.19 along the lamina axes and substituting Equation 3.18, we get the displacement components:

$$u_1(x_1, x_2, x_3, t) = u_1(-a, x_2, x_3, t) + \int_{-a}^{x_1}\left[S_{11\alpha\beta}\sigma_{\alpha\beta} + S_{1133}\sigma_{33}\right]d\eta_1$$

$$u_2(x_1, x_2, x_3, t) = u_2(x_1, -b, x_3, t) + \int_{-b}^{x_{21}}\left[S_{22\alpha\beta}\sigma_{\alpha\beta} + S_{2233}\sigma_{33}\right]d\eta_2$$

$$u_3(x_1, x_2, x_3, t) = u_3\left(x_1, x_2, -\frac{h}{2}, t\right) + \int_{-\frac{h}{2}}^{x_3}\left[S_{33\alpha\beta}\sigma_{\alpha\beta} + S_{3333}\sigma_{33}\right]d\eta_3 \tag{3.20}$$

3.3.6 Equations of Motion

The three-dimensional spatial problem is reduced to two dimensions by integrating over the thickness of the lamina. Substituting Equations 3.14 and 3.20 into Equations 3.10 and 3.11 and incorporating constitutive equations (Equation 3.18) gives:

$$\sigma_{\alpha\beta,\beta} + \sigma_{\alpha 3,3} + f_\alpha - \rho[\ddot{u}_\alpha - \dot{u}_\alpha S_{kk\gamma\delta}\dot{\sigma}_{\gamma\delta} - \dot{u}_\alpha S_{kk33\dot{\sigma}_{33}}] = 0 \tag{3.21}$$

$$\sigma_{\alpha 3,\alpha} + \sigma_{33,3} + f_3 - \rho[\ddot{u}_3 - \dot{u}_3 S_{kk\gamma\delta}\dot{\sigma}_{\gamma\delta} - \dot{u}_3 S_{kk33\dot{\sigma}_{33}}] = 0 \tag{3.22}$$

Where

$$\ddot{u}_1(x_1, x_2, x_3, t) = \ddot{u}_1(-a, x_2, x_3, t) + \int_{-a}^{x1} [S_{11\alpha\beta}\ddot{\sigma}_{\alpha\beta} + S_{1133}\ddot{\sigma}_{33}]d\eta_1 \tag{3.23}$$

$$\ddot{u}_2(x_1, x_2, x_3, t) = \ddot{u}_2(x_1, -b, x_3, t) + \int_{-b}^{x2} [S_{22\alpha\beta}\ddot{\sigma}_{\alpha\beta} + S_{2233}\ddot{\sigma}_{33}]d\eta_2 \tag{3.24}$$

$$\ddot{u}_3(x_1, x_2, x_3, t) = \ddot{u}_3(x_1, x_2, -\frac{h}{2}, t) + \int_{-\frac{h}{2}}^{x3} [S_{33\alpha\beta}\ddot{\sigma}_{\alpha\beta} + S_{3333}\ddot{\sigma}_{33}]d\eta_3 \tag{3.25}$$

Similar expressions are written for velocity terms by integrating Equations 3.21 and 3.22 and the first moment of Equation 3.21 over the thickness of the lamina as shown below:

$$N_{\alpha\beta,\beta} + \left(\sigma^{+}_{\alpha 3} - \sigma^{-}_{\alpha 3}\right) + F_\alpha - \int_{-\frac{h}{2}}^{\frac{h}{2}} \rho[\ddot{u}_\alpha - \dot{u}_\alpha S_{kk\gamma\delta}\dot{\sigma}_{\gamma\delta} - \dot{u}_\alpha S_{kk33}\dot{\sigma}_{33}]dx_3 = 0 \tag{3.26}$$

$$V_{\alpha,\beta} + \left(\sigma^{+}_{33} - \sigma^{-}_{33}\right) + F_3 - \int_{-\frac{h}{2}}^{\frac{h}{2}} \rho[\ddot{u}_3 - \dot{u}_3 S_{kk\gamma\delta}\dot{\sigma}_{\gamma\delta} - \dot{u}_3 S_{kk33}\dot{\sigma}_{33}]dx_3 = 0 \tag{3.27}$$

$$M_{\alpha\beta,\beta} + \frac{h}{2}\left(\sigma_{\alpha 3}^{+} + \sigma_{\alpha 3}^{-}\right) - V_{\alpha} - \int_{-\frac{h}{2}}^{\frac{h}{2}} \rho[\ddot{u}_{\alpha} - \dot{u}_{\alpha} S_{kk\gamma\delta}\dot{\sigma}_{\gamma\delta} - \dot{u}_{\alpha} S_{kk33}\dot{\sigma}_{33}] x_3 dx_3 = 0 \qquad (3.28)$$

Where $N_{\alpha\beta,\beta}$, the in-plane stress resultant, $\int_{-\frac{h}{2}}^{\frac{h}{2}} \sigma_{\alpha\beta} dx_3$;

$M_{\alpha\beta,\beta}$, the in-plane moment resultant, $\int_{-\frac{h}{2}}^{\frac{h}{2}} \sigma_{\alpha\beta} x_3 dx_3$;

$V_{\alpha,\beta}$, the transverse shear stress resultant, $\int_{-\frac{h}{2}}^{\frac{h}{2}} \sigma_{\alpha 3} dx_3$;

ρ, the mass density, $\frac{\rho_0}{1+\varepsilon_{jj}} \cong \rho_0\left(1-\varepsilon_{jj}\right)$ for small strains $\left(\varepsilon_{ij} << 1\right)$.

The “+” and “–” superscripts denote the value of the variable at top ($x_3 = \frac{h}{2}$) and bottom ($x_3 = -\frac{h}{2}$) surface of the lamina.

The body force per unit volume is assumed to be constant over the thickness of the lamina.

$$F_i \equiv \int_{-\frac{h}{2}}^{\frac{h}{2}} f_i dx_3 = hf_i \qquad (3.29)$$

Defining in-plane weighted displacements as

$$\left(\tilde{u}_i, \bar{u}_i\right) \equiv \int_{\frac{h}{2}}^{-\frac{h}{2}} \left(1, \frac{2x_3}{h}\right) \frac{2}{h} u_i dx_3 \qquad (3.30)$$

Hence equations 3.26 to 3.28 take the form of the generalized equations of motion for a single lamina as follows:

$$N_{\alpha\beta,\beta} + \left(\sigma_{\alpha 3}^{+} - \sigma_{\alpha 3}^{-}\right) + F_{\alpha} + P_{\alpha} - \frac{\rho_0 h}{2}\ddot{\tilde{u}}_{\alpha} = 0 \qquad (3.31)$$

$$V_{\alpha,\alpha} + \left(\sigma_{33}^{+} - \sigma_{33}^{-}\right) + F_{3} + P_{3} - \frac{\rho_0 h}{2}\ddot{\tilde{u}}_{3} = 0 \qquad (3.32)$$

$$M_{\alpha\beta,\beta} + \frac{h}{2}\left(\sigma_{\alpha 3}^{+} + \sigma_{\alpha 3}^{-}\right) - V_{\alpha} + R_{\alpha} - \frac{\rho_0 h^2}{4}\ddot{\bar{u}}_{\alpha} = 0 \qquad (3.33)$$

Where $P_{\alpha} = \rho_0 \int_{-\frac{h}{2}}^{\frac{h}{2}} \varepsilon_{jj}\ddot{u}_{\alpha} dx_3 + \rho_0 \int_{-\frac{h}{2}}^{\frac{h}{2}} \left(1 - \varepsilon_{jj}\right)\dot{u}_{\alpha}\left(S_{kk\gamma\delta}\dot{\sigma}_{\gamma\delta} + S_{kk33}\dot{\sigma}_{33}\right)dx_3$

$$P_{3} = \rho_0 \int_{-\frac{h}{2}}^{\frac{h}{2}} \varepsilon_{jj}\ddot{u}_{3} dx_3 + \rho_0 \int_{-\frac{h}{2}}^{\frac{h}{2}} \left(1 - \varepsilon_{jj}\right)\dot{u}_{3}\left(S_{kk\gamma\delta}\dot{\sigma}_{\gamma\delta} + S_{kk33}\dot{\sigma}_{33}\right)dx_3$$

$$R_{\alpha} = \rho_0 \int_{-\frac{h}{2}}^{\frac{h}{2}} \varepsilon_{jj}\ddot{u}_{\alpha} x_3 dx_3 + \rho_0 \int_{-\frac{h}{2}}^{\frac{h}{2}} \left(1 - \varepsilon_{jj}\right)\dot{u}_{\alpha}\left(S_{kk\gamma\delta}\dot{\sigma}_{\gamma\delta} + S_{kk33}\dot{\sigma}_{33}\right)x_3 dx_3 \qquad (3.34)$$

P_i and R_{α} are the nonlinear pseudo-body force terms attributed to the compressibility of the monoclinic material.

3.3.7 Consistent Stress Field Derivation

In the present stress theory used in the finite element formulation, the in-plane stress distribution is assumed to be linear across the thickness of each lamina as,

$\sigma_{\alpha\beta} = A_{\alpha\beta} + B_{\alpha\beta} x_3$. Equation 3.35 gives the in plane stresses in terms of in-plane stress resultants as:

$$\sigma_{\alpha\beta} = \frac{N_{\alpha\beta}}{h} + \frac{12M_{\alpha\beta}}{h^3} x_3 \tag{3.35}$$

Integrating Equation 3.10 through the thickness of the lamina and substituting the momentum density term (Equation 3.14) gives

$$\sigma_{\alpha 3} = \sigma^{-}_{\alpha 3} - \int_{-\frac{h}{2}}^{x_3} \sigma_{\alpha\beta,\beta} d\eta_3 - \int_{-\frac{h}{2}}^{x_3} f_\alpha d\eta_3 + \rho_0 \int_{-\frac{h}{2}}^{x_3} \ddot{u}_\alpha d\eta_3$$

$$- \rho_0 \int_{-\frac{h}{2}}^{x_3} \varepsilon_{jj} \ddot{u}_\alpha d\eta_3 - \rho_0 \int_{-\frac{h}{2}}^{x_3} (1 - \varepsilon_{jj}) \dot{\varepsilon}_{jj} \dot{u}_\alpha d\eta_3 \tag{3.36}$$

The distribution of transverse shear stress is obtained by substituting Equation 3.35 into Equation 3.36 and using Equations 3.31 and 3.33 as

$$\sigma_{\alpha 3} = (\sigma^{+}_{\alpha 3} - \sigma^{-}_{\alpha 3}) \frac{x_3}{h} + \frac{(\sigma^{+}_{\alpha 3} + \sigma^{-}_{\alpha 3})}{4} \left(\frac{12x_3^2}{h^2} - 1 \right) + \frac{3}{2h} V_\alpha \left(1 - \frac{4x_3^2}{h^2} \right) - \frac{\rho_0}{2} [\ddot{\tilde{u}}_\alpha \left(x_3 + \frac{h}{2} \right)$$

$$+ \ddot{\bar{u}}_\alpha \left(\frac{3x_3^2}{h} - \frac{3h}{4} \right)] + \rho_0 \int_{-\frac{h}{2}}^{x_3} \ddot{u}_\alpha d\eta_3 - \rho_0 \int_{-\frac{h}{2}}^{x_3} \varepsilon_{jj} \ddot{u}_\alpha d\eta_3 - \rho_0 \int_{-\frac{h}{2}}^{x_3} (1 - \varepsilon_{jj}) \dot{\varepsilon}_{jj} \dot{u}_\alpha d\eta_3 + \frac{1}{h} \int_{-\frac{h}{2}}^{x_3} P_\alpha d\eta_3$$

$$+ \frac{12}{h^3} \int_{-\frac{h}{2}}^{x_3} R_\alpha \eta_3 d\eta_3 \tag{3.37}$$

Similarly, the transverse normal stress is obtained by integrating Equation 3.11 over the thickness of the lamina and substituting momentum density term (Equation 3.14) as

$$\sigma_{33} = \sigma^{-}_{33} - \int_{-\frac{h}{2}}^{x_3} \sigma_{\alpha 3,\alpha} d\eta_3 - \int_{-\frac{h}{2}}^{x_3} f_3 d\eta_3 + \rho_0 \int_{-\frac{h}{2}}^{x_3} \ddot{u}_3 d\eta_3 - \rho_0 \int_{-\frac{h}{2}}^{x_3} \varepsilon_{jj} \ddot{u}_3 d\eta_3$$

$$-\rho_0\int_{-\frac{h}{2}}^{x_3}(1-\varepsilon_{jj})\dot{\varepsilon}_{jj}\dot{u}_3 d\eta_3 \tag{3.38}$$

The expanded form of Equations 3.37 and 3.38 can be simplified by neglecting terms with order higher than $O(h^1)$. This leads to a cubic distribution of transverse normal stress as

$$\sigma_{33}=\frac{(\sigma_{33}^{+}+\sigma_{33}^{-})}{4}\left(\frac{12x_3^2}{h^2}-1\right)+\frac{(\sigma_{33}^{+}-\sigma_{33}^{-})}{4}\left(\frac{40x_3^3}{h^3}-\frac{6x_3}{h}\right)+\frac{3N_{33}}{2h}\left(1-\frac{4x_3^2}{h^2}\right)$$

$$+\frac{15M_{33}}{h^2}\left(\frac{2x_3}{h}-\frac{8x_3^3}{h^3}\right) \tag{3.39}$$

And quadratic distribution of transverse shear stresses as

$$\sigma_{13}=(\sigma_{13}^{+}-\sigma_{13}^{-})\frac{x_3}{h}+\frac{(\sigma_{13}^{+}+\sigma_{13}^{-})}{4}\left(\frac{12x_3^2}{h^2}-1\right)+\frac{3V_1}{2h}\left(1-\frac{4x_3^2}{h^2}\right)$$

$$+\frac{\rho_0}{h}\int_{-a}^{x_1}S_{1133}\left\{\left[\frac{h}{4}(\ddot{\sigma}_{33}^{+}+\ddot{\sigma}_{33}^{-})-\frac{1}{2}\ddot{N}_{33}\right]\left[\frac{4x_3^3}{h^2}-x_3\right]\right.$$

$$\left.+\left[\frac{h^2}{12}(\ddot{\sigma}_{33}^{+}-\ddot{\sigma}_{33}^{-})-\ddot{M}_{33}\right]\left[\frac{30x_3^4}{h^4}-\frac{9x_3^2}{h^2}+\frac{3}{8}\right]\right\}d\eta_1$$

$$-\frac{\rho_0}{h}\left(x_3+\frac{h}{2}\right)\int_{-\frac{h}{2}}^{\frac{h}{2}}\ddot{u}_1(-a,x_2,x_3,t)dx_3$$

$$-\frac{\rho_0}{h}\left(\frac{6x_3^2}{h^2}-\frac{3}{2}\right)\int_{-\frac{h}{2}}^{\frac{h}{2}}\ddot{u}_1(-a,x_2,x_3,t)x_3dx_3+\rho_0\int_{-\frac{h}{2}}^{x_3}\ddot{u}_1(-a,x_2,\eta_3,t)d\eta_3$$

$$+\frac{1}{h}\int_{-\frac{h}{2}}^{x_3}P_1d\eta_3+\frac{12}{h^3}\int_{-\frac{h}{2}}^{x_3}R_1\eta_3d\eta_3-\rho_0\int_{-\frac{h}{2}}^{x_3}\varepsilon_{jj}\ddot{u}_1d\eta_3$$

$$-\rho_0 \int_{-\frac{h}{2}}^{x_3} (1-\varepsilon_{jj}) \dot{\varepsilon}_{jj} \dot{u}_1 d\eta_3 \tag{3.40}$$

And

$$\sigma_{23} = \left(\sigma_{23}^{+} - \sigma_{23}^{-}\right)\frac{x_3}{h} + \frac{\left(\sigma_{23}^{+} + \sigma_{23}^{-}\right)}{4}\left(\frac{12x_3^2}{h^2} - 1\right) + \frac{3V_2}{2h}\left(1 - \frac{4x_3^2}{h^2}\right)$$

$$+ \frac{\rho_0}{h}\int_{-b}^{x_2} S_{2233}\left\{\left[\frac{h}{4}\left(\ddot{\sigma}_{33}^{+} + \ddot{\sigma}_{33}^{-}\right) - \frac{1}{2}\ddot{N}_{33}\right]\left[\frac{4x_3^3}{h^2} - x_3\right]\right.$$

$$\left. + \left[\frac{h^2}{12}\left(\ddot{\sigma}_{33}^{+} - \ddot{\sigma}_{33}^{-}\right) - \ddot{M}_{33}\right]\left[\frac{30x_3^4}{h^4} - \frac{9x_3^2}{h^2} + \frac{3}{8}\right]\right\} d\eta_2$$

$$- \frac{\rho_0}{h}\left(x_3 + \frac{h}{2}\right)\int_{-\frac{h}{2}}^{\frac{h}{2}} \ddot{u}_2\left(x_2, -b, x_3, t\right) dx_3$$

$$- \frac{\rho_0}{h}\left(\frac{6x_3^2}{h^2} - \frac{3}{2}\right)\int_{-\frac{h}{2}}^{\frac{h}{2}} \ddot{u}_2\left(x_1, -b, x_3, t\right) x_3 dx_3 + \rho_0 \int_{-\frac{h}{2}}^{x_3} \ddot{u}_2\left(x_1, -b, \eta_3, t\right) d\eta_3$$

$$+ \frac{1}{h}\int_{-\frac{h}{2}}^{x_3} P_2 d\eta_3 + \frac{12}{h^3}\int_{-\frac{h}{2}}^{x_3} R_2 \eta_3 d\eta_3 - \rho_0 \int_{-\frac{h}{2}}^{x_3} \varepsilon_{jj} \ddot{u}_2 d\eta_3$$

$$-\rho_0 \int_{-\frac{h}{2}}^{x_3} (1-\varepsilon_{jj}) \dot{\varepsilon}_{jj} \dot{u}_2 d\eta_3 \tag{3.41}$$

3.3.8 Governing Field Equations

The generalized variational technique presented by Sandhu and Salam (1975) is used in the derivation of the governing field equations for the stress based formulation. In general, the governing equations of a solid mechanics problem can be derived using either a vector approach (e.g., Newton's Second Law of motion) or a variational approach (e.g., the principle of virtual displacements). The vector approach provides an easy and direct way to derive the governing equations but becomes cumbersome for complicated systems. In the contrast, the variational approach yields not only the governing equations but also the associated boundary conditions (Reddy, 2004; Bathe, 1996).

3.3.9 Constitutive Equations

The following ten constitutive equations are obtained for the field variables $N_{\alpha\beta}, M_{\alpha\beta}, V_{\alpha}$, N_{33}, and M_{33}:

$$\tilde{u}_{(\alpha,\beta)} = \frac{2}{h}\left[S_{\alpha\beta\gamma\delta}N_{\gamma\delta} + S_{\alpha\beta33}N_{33}\right] \tag{3.42}$$

$$\bar{u}_{(\alpha,\beta)} = \frac{4}{h^2}\left[S_{\alpha\beta\gamma\delta}M_{\gamma\delta} + S_{\alpha\beta33}M_{33}\right] \tag{3.43}$$

$$\begin{aligned}\tilde{u}_{3,\alpha} - \hat{u}_{3,\alpha} - \frac{4}{h}\bar{u}_{\alpha} &= \frac{8}{15}S_{\alpha3\beta3}\left(\sigma^{+}_{\beta3} + \sigma^{-}_{\beta3}\right) - \frac{32}{5h}S_{\alpha3\beta3}V_{\beta} \\ &\quad - \frac{\rho_0}{h}\frac{16}{35}S_{\alpha3\beta3}S_{\underline{\beta\beta}33}\int_{-a,-b}^{x_\beta}\left[\frac{h^2}{12}\left(\ddot{\sigma}^{+}_{33} - \ddot{\sigma}^{-}_{33}\right) - \ddot{M}_{33}\right]d\eta_\beta \\ &\quad + \frac{\rho_0}{h}\frac{4h^2}{3}S_{\alpha3\beta3}\ddot{\tilde{v}}_{\beta} - \frac{\rho_0}{h}\frac{8h^2}{5}S_{\alpha3\beta3}\ddot{\tilde{v}}_{\beta} \\ &\quad + \frac{\rho_0}{h}\frac{16}{3}S_{\alpha3\beta3}\int_{-\frac{h}{2}}^{\frac{h}{2}}\left(\frac{6x_3^2}{h^2} - \frac{3}{2}\right)\int_{-\frac{h}{2}}^{x_3}\ddot{v}_{\beta}\,d\eta_3\,dx_3 - \frac{8}{3}\psi_3\end{aligned} \tag{3.44}$$

$$6\bar{u}_3 = 2S_{33\alpha\beta}N_{\alpha\beta} + \frac{12}{5}S_{3333}N_{33} - \frac{h}{5}S_{3333}\left(\sigma_{33}^{+} + \sigma_{33}^{-}\right) - \frac{\rho_0}{h}\frac{h^3}{8}S_{\alpha\alpha 33}\left(\ddot{\bar{\bar{u}}}_3 - \ddot{\bar{u}}_3\right)$$

$$-\frac{\rho_0}{h}\frac{h^3}{175}S_{3333}\left(S_{\alpha\alpha 33} - S_{3333}\right)\left[\frac{h}{4}\left(\ddot{\sigma}_{33}^{+} + \ddot{\sigma}_{33}^{-}\right) - \frac{1}{2}\ddot{N}_{33}\right]$$

$$-\frac{\rho_0}{h}2h^2 S_{\alpha\underline{\alpha}33}\int_{-a,-b}^{x_\alpha}\left[-\frac{1}{8}\left(3\ddot{\hat{u}}_\alpha - \ddot{\tilde{u}}_\alpha\right) + \frac{h}{30}S_{\alpha 3\beta 3}\left(\ddot{\sigma}_{\beta 3}^{+} - \ddot{\sigma}_{\beta 3}^{-}\right)\right]d\eta_\alpha$$

$$+\frac{\rho_0}{h}\frac{h^3}{8}S_{1133}\left[\ddot{\bar{\bar{u}}}_3\left(-a, x_2, x_3, t\right) - \ddot{\bar{u}}_3\left(-a, x_2, x_3, t\right)\right]$$

$$+\frac{\rho_0}{h}\frac{h^3}{8}S_{2233}\left[\ddot{\bar{\bar{u}}}_3\left(x_1, -b, x_3, t\right) - \ddot{\bar{u}}_3\left(x_1, -b, x_3, t\right)\right] \tag{3.45}$$

$$3\hat{u}_3 - \hat{u}_3 = \frac{4}{5h}S_{33\alpha\beta}M_{\alpha\beta} + \frac{8}{7h}S_{3333}M_{33} - \frac{h}{35}S_{3333}\left(\sigma_{33}^{+} - \sigma_{33}^{-}\right)$$

$$-\frac{\rho_0}{h}\frac{h^3}{32}S_{\alpha\alpha 33}\left(\ddot{\hat{\hat{u}}}_3 - \ddot{\hat{u}}_3\right) - \frac{\rho_0}{h}\frac{h^3}{160}S_{\alpha\alpha 33}\left(\ddot{\tilde{u}}_3 - \ddot{\hat{u}}_3\right)$$

$$-\frac{\rho_0}{h}\frac{h^2}{735}S_{3333}\left(S_{\alpha\alpha 33} - S_{3333}\right)\left[\frac{h^2}{12}\left(\ddot{\sigma}_{33}^{+} - \ddot{\sigma}_{33}^{-}\right) - \ddot{M}_{33}\right]$$

$$-\frac{\rho_0}{h}\frac{h^2}{15}S_{\alpha\underline{\alpha}33}\int\left[-\frac{3}{4}\left(5\ddot{\bar{\bar{u}}}_\alpha - 3\ddot{\bar{u}}_\alpha\right) + \frac{3h}{35}S_{\alpha 3\beta 3}\left(\ddot{\sigma}_{\beta 3}^{+} + \ddot{\sigma}_{\beta 3}^{-}\right) - \frac{6}{35}S_{\alpha 3\beta 3}\ddot{V}_\beta\right]d\eta_\alpha$$

$$+\frac{\rho_0}{h}\frac{h^3}{80}S_{1133}\left[\frac{5}{2}\ddot{\hat{\hat{u}}}_3\left(-a, x_2, x_3, t\right) - 3\ddot{\hat{u}}_3\left(-a, x_2, x_3, t\right) + \frac{1}{2}\ddot{\tilde{u}}_3\left(-a, x_2, x_3, t\right)\right]$$

$$+\frac{\rho_0}{h}\frac{h^3}{80}S_{2233}\left[\frac{5}{2}\ddot{\hat{\hat{u}}}_3\left(x_1, -b, x_3, t\right) - 3\ddot{\hat{u}}_3\left(x_1, -b, x_3, t\right) + \frac{1}{2}\ddot{\tilde{u}}_3\left(x_1, -b, x_3, t\right)\right] \tag{3.46}$$

Where

$$\psi_\alpha = -\frac{1}{h} S_{\alpha 3\beta 3} \int_{-\frac{h}{2}}^{\frac{h}{2}} \left(\frac{12x_3^2}{h^3} - \frac{3}{h} \right) \int_{-\frac{h}{2}}^{\frac{h}{2}} P_\beta d\eta_3 dx_3 - \frac{12}{h^3} S_{\alpha 3\beta 3} \int_{-\frac{h}{2}}^{\frac{h}{2}} \left(\frac{12x_3^2}{h^3} - \frac{3}{h} \right) \int_{-\frac{h}{2}}^{\frac{h}{2}} R_\beta \eta_3 d\eta_3 dx_3$$

$$\rho_0 S_{\alpha 3\beta 3} \int_{-\frac{h}{2}}^{\frac{h}{2}} \left(\frac{12x_3^2}{h^3} - \frac{3}{h} \right) \int_{-\frac{h}{2}}^{x_3} \left[\varepsilon_{jj} \ddot{u}_\beta + (1 - \varepsilon_{jj}) \dot{\varepsilon}_{jj} \dot{u}_\beta \right] d\eta_3 dx_3 \tag{3.47}$$

3.3.10 Equations of Motion

For arbitrary admissible variations of the weighted displacement quantities, generalized equations of motion are obtained:

$$N_{\alpha\beta,\beta} + \left(\sigma_{\alpha 3}^{+} - \sigma_{\alpha 3}^{-} \right) - \rho_0 \int_{-a,-b}^{x_\alpha} \left(S_{\alpha\underline{\alpha}\gamma\delta} \ddot{N}_{\gamma\delta} + S_{\alpha\underline{\alpha}33} \ddot{N}_{33} \right) d\eta_\alpha - \rho_0 \frac{h}{2} \ddot{\tilde{v}}_\alpha + F_\alpha$$

$$+ \rho_0 \int_{-\frac{h}{2}}^{\frac{h}{2}} \left[\varepsilon_{jj} \ddot{u}_\alpha + (1 - \varepsilon_{jj}) \dot{\varepsilon}_{jj} \dot{u}_\alpha \right] dx_3 = 0 \tag{3.48}$$

$$M_{\alpha\beta,\beta} + \left(\sigma_{\alpha 3}^{+} + \sigma_{\alpha 3}^{-} \right) - V_\alpha - \rho_0 \int_{-a,-b}^{x_\alpha} \left(S_{\alpha\underline{\alpha}\gamma\delta} \ddot{M}_{\gamma\delta} + S_{\alpha\underline{\alpha}33} \ddot{M}_{33} \right) d\eta_\alpha - \frac{\rho_0 h^2}{4} \ddot{\bar{v}}_\alpha$$

$$+ \rho_0 \int_{-\frac{h}{2}}^{\frac{h}{2}} \left[\varepsilon_{jj} \ddot{u}_\alpha + (1 - \varepsilon_{jj}) \dot{\varepsilon}_{jj} \dot{u}_\alpha \right] x_3 dx_3 = 0 \tag{3.49}$$

$$V_{\alpha,\alpha} - \frac{h}{6} \left(\sigma_{\alpha 3}^{+} + \sigma_{\alpha 3}^{-} \right) - \left(\sigma_{\alpha 3}^{+} - \sigma_{\alpha 3}^{-} \right) + \frac{20}{h^2} M_{33} + \frac{2}{3} F_3 - \frac{2\rho_0 h}{3} \ddot{u}_3^{-}$$

$$- \rho_0 S_{33\gamma\delta} \left[\frac{h}{3} \ddot{N}_{\gamma\delta} - \ddot{M}_{\gamma\delta} \right] - \rho_0 S_{3333} \left[\frac{h}{3} \ddot{N}_{33} - \ddot{M}_{33} \right]$$

$$+\frac{\rho_0}{h}\left(S_{\xi\xi 33}-S_{3333}\right)\left[\frac{h^2}{12}\left(\ddot{\sigma}_{33}^{+}-\ddot{\sigma}_{33}^{-}\right)-\ddot{M}_{33}\right]$$

$$+\frac{3\rho_0}{3}\int_{-\frac{h}{2}}^{\frac{h}{2}}\left[\varepsilon_{jj}\ddot{u}_\alpha+\left(1-\varepsilon_{jj}\right)\dot{\varepsilon}_{jj}\dot{u}_\alpha\right]dx_3=0 \tag{3.50}$$

$$N_{33}-\frac{h^2}{12}\left(\sigma_{\alpha 3,\alpha}^{+}-\sigma_{\alpha 3,\alpha}^{-}\right)-\frac{h}{2}\left(\sigma_{33}^{+}+\sigma_{33}^{-}\right)+\frac{\rho_0 h^2}{12}S_{33\gamma\delta}\ddot{N}_{\gamma\delta}+\frac{\rho_0 h^2}{12}S_{3333}\ddot{N}_{33}$$

$$+\frac{\rho_0 h^2}{12}\left(S_{\xi\xi 33}-S_{3333}\right)\left[\frac{h}{4}\left(\ddot{\sigma}_{33}^{+}+\ddot{\sigma}_{33}^{-}\right)-\frac{1}{2}\ddot{N}_{33}\right]=0 \tag{3.51}$$

$$\frac{60}{h^2}M_{33}-\frac{h}{2}\left(\sigma_{\alpha 3,\alpha}^{+}+\sigma_{\alpha 3,\alpha}^{-}\right)+V_{\alpha,\alpha}-5\left(\sigma_{33}^{+}-\sigma_{33}^{-}\right)+\rho_0 S_{33\gamma\delta}\ddot{M}_{\gamma\delta}+\rho_0 S_{3333}\ddot{M}_{33}$$

$$+\frac{3\rho_0}{2}\left(S_{\alpha\alpha 33}-S_{3333}\right)\left[\frac{h^2}{12}\left(\ddot{\sigma}_{33}^{+}-\ddot{\sigma}_{33}^{-}\right)-\ddot{M}_{33}\right]=0 \tag{3.52}$$

$$\frac{h}{4}\left(\ddot{\sigma}_{33}^{+}+\ddot{\sigma}_{33}^{-}\right)-\frac{1}{2}\ddot{N}_{33}=0 \tag{3.53}$$

$$\frac{h^2}{12}\left(\ddot{\sigma}_{33}^{+}-\ddot{\sigma}_{33}^{-}\right)-\ddot{M}_{33}=0 \tag{3.54}$$

3.3.11 Interface Displacement Equations

For arbitrary admissible variations of the transverse stress components on the top and bottom boundaries of the plate, six interface displacement equations are obtained:

$$u_\alpha^{+}=-h\left(\frac{3}{8}\hat{u}_{3,\alpha}-\frac{1}{8}\tilde{u}_{3,\alpha}-\frac{3}{2h}\bar{u}_\alpha\right)-\left(\frac{h}{4}\bar{u}_{3,\alpha}-\frac{1}{2}\tilde{u}_\alpha\right)+4S_{\alpha 3\beta 3}\left[\frac{\left(4\sigma_{\beta 3}^{+}-\sigma_{\beta 3}^{-}\right)h}{30}-\frac{V_\beta}{10}\right]$$

$$-\frac{\rho_0}{h}\frac{2h^2}{15}S_{\alpha3\beta3}S_{\underline{\beta\beta}33}\int_{-a,-b}^{x_\beta}\left[\frac{h}{4}\left(\ddot{\sigma}_{33}^{+}+\ddot{\sigma}_{33}^{-}\right)-\frac{1}{2}\ddot{N}_{33}\right]d\eta_\beta$$

$$-\frac{\rho_0}{h}\frac{6h}{35}S_{\alpha3\beta3}S_{\underline{\beta\beta}33}\int_{-a,-b}^{x_\beta}\left[\frac{h^2}{12}\left(\ddot{\sigma}_{33}^{+}-\ddot{\sigma}_{33}^{-}\right)-\ddot{M}_{33}\right]d\eta_\beta$$

$$-\frac{\rho_0}{h}\frac{h^3}{6}S_{\alpha3\beta3}\ddot{\tilde{v}}_\beta-\frac{\rho_0}{h}\frac{h^3}{10}S_{\alpha3\beta3}\ddot{\tilde{v}}_\beta$$

$$-\frac{\rho_0}{h}S_{\alpha3\beta3}\int_{-\frac{h}{2}}^{\frac{h}{2}}\left(-\frac{12x_3^2}{h}-4x_3+h\right)\int_{-\frac{h}{2}}^{x_3}\ddot{v}_\beta d\eta_3 dx_3+2K_\alpha \tag{3.55}$$

$$u_\alpha^{-}=h\left(\frac{3}{8}\hat{u}_{3,\alpha}-\frac{1}{8}\tilde{u}_{3,\alpha}-\frac{3}{2h}\bar{u}_\alpha\right)-\left(\frac{h}{4}\bar{u}_{3,\alpha}-\frac{1}{2}\tilde{u}_\alpha\right)-4S_{\alpha3\beta3}\left[\frac{\left(4\sigma_{\beta3}^{-}-\sigma_{\beta3}^{+}\right)h}{30}-\frac{V_\beta}{10}\right]$$

$$-\frac{\rho_0}{h}\frac{2h^2}{15}S_{\alpha3\beta3}S_{\underline{\beta\beta}33}\int_{-a,-b}^{x_\beta}\left[\frac{h}{4}\left(\ddot{\sigma}_{33}^{+}+\ddot{\sigma}_{33}^{-}\right)-\frac{1}{2}\ddot{N}_{33}\right]d\eta_\beta$$

$$-\frac{\rho_0}{h}\frac{6h}{35}S_{\alpha3\beta3}S_{\underline{\beta\beta}33}\int_{-a,-b}^{x_\beta}\left[\frac{h^2}{12}\left(\ddot{\sigma}_{33}^{+}-\ddot{\sigma}_{33}^{-}\right)-\ddot{M}_{33}\right]d\eta_\beta$$

$$-\frac{\rho_0}{h}\frac{h^3}{6}S_{\alpha3\beta3}\ddot{\tilde{v}}_\beta+\frac{\rho_0}{h}\frac{h^3}{10}S_{\alpha3\beta3}\ddot{\tilde{v}}_\beta$$

$$-\frac{\rho_0}{h}S_{\alpha3\beta3}\int_{-\frac{h}{2}}^{\frac{h}{2}}\left(-\frac{12x_3^2}{h}-4x_3-h\right)\int_{-\frac{h}{2}}^{x_3}\ddot{v}_\beta d\eta_3 dx_3-2L_\alpha \tag{3.56}$$

$$u_3^{+}=\frac{3}{4}\left(5\hat{u}_3-\tilde{u}_3\right)+\frac{3}{2}\bar{u}_3-\frac{1}{70h}S_{3333}\left[\left(6\sigma_{33}^{+}+\sigma_{33}^{-}\right)h^2-7hN_{33}-30M_{33}\right]$$

$$+\frac{\rho_0}{h}S_{\xi\xi33}\left[\frac{5h^3}{128}\left(\ddot{\hat{\hat{u}}}_3-\ddot{\hat{u}}_3\right)+\frac{h^3}{32}\left(\ddot{\bar{\bar{u}}}_3-\ddot{\bar{u}}_3\right)+\frac{h^3}{128}\left(\ddot{\tilde{u}}_3-\ddot{\hat{u}}_3\right)\right]$$

$$+\frac{\rho_0}{h}\frac{h^3}{700}S_{3333}\left(S_{\xi\xi 33}-S_{3333}\right)\left[\frac{h}{4}\left(\ddot{\sigma}_{33}^{+}+\ddot{\sigma}_{33}^{-}\right)-\frac{1}{2}\ddot{N}_{33}\right]$$

$$+\frac{\rho_0}{h}\frac{h^2}{588}S_{3333}\left(S_{\xi\xi 33}-S_{3333}\right)\left[\frac{h^2}{12}\left(\ddot{\sigma}_{33}^{+}-\ddot{\sigma}_{33}^{-}\right)-\ddot{M}_{33}\right]$$

$$-\frac{\rho_0}{h}\frac{h^2}{16}S_{\alpha\underline{\alpha}33}\int_{-a,-b}^{x_\alpha}\left[\left(5\ddot{\bar{\bar{u}}}_\alpha-3\ddot{\bar{u}}_\alpha\right)+\left(3\ddot{\hat{u}}_\alpha-\ddot{\tilde{u}}_\alpha\right)\right.$$

$$\left.-\frac{8h}{105}S_{\alpha 3\beta 3}\left(5\ddot{\sigma}_{\beta 3}^{+}-2\ddot{\sigma}_{\beta 3}^{-}\right)+\frac{8}{35}S_{\alpha 3\beta 3}\ddot{V}_\beta\right]d\eta_\alpha$$

$$+\frac{\rho_0}{h}S_{1133}\left[-\frac{5h^3}{128}\ddot{\hat{\hat{u}}}_3\left(-a,x_2,x_3,t\right)-\frac{h^3}{32}\ddot{\bar{\bar{u}}}_3\left(-a,x_2,x_3,t\right)+\frac{3h^3}{64}\ddot{\hat{u}}_3\left(-a,x_2,x_3,t\right)\right.$$

$$\left.+\frac{h^3}{32}\ddot{\bar{u}}_3\left(-a,x_2,x_3,t\right)-\frac{h^3}{128}\ddot{\tilde{u}}_3\left(-a,x_2,x_3,t\right)\right]$$

$$+\frac{\rho_0}{h}S_{2233}\left[-\frac{5h^3}{128}\ddot{\hat{\hat{u}}}_3\left(x_1,-b,x_3,t\right)-\frac{h^3}{32}\ddot{\bar{\bar{u}}}_3\left(x_1,-b,x_3,t\right)+\frac{3h^3}{64}\ddot{\hat{u}}_3\left(x_1,-b,x_3,t\right)\right.$$

$$\left.+\frac{h^3}{32}\ddot{\bar{u}}_3\left(x_1,-b,x_3,t\right)-\frac{h^3}{128}\ddot{\tilde{u}}_3\left(x_1,-b,x_3,t\right)\right] \qquad (3.57)$$

$$u_3^{-}=\frac{3}{4}\left(5\hat{u}_3-\tilde{u}_3\right)-\frac{3}{2}\bar{u}_3-\frac{1}{70h}S_{3333}\left[\left(6\sigma_{33}^{+}+\sigma_{33}^{-}\right)h^2-7hN_{33}-30M_{33}\right]$$

$$+\frac{\rho_0}{h}S_{\xi\xi 33}\left[\frac{5h^3}{128}\left(\ddot{\hat{\hat{u}}}_3-\ddot{\hat{u}}_3\right)-\frac{h^3}{32}\left(\ddot{\bar{\bar{u}}}_3-\ddot{\bar{u}}_3\right)+\frac{h^3}{128}\left(\ddot{\tilde{u}}_3-\ddot{\hat{u}}_3\right)\right]$$

$$-\frac{\rho_0}{h}\frac{h^3}{700}S_{3333}\left(S_{\xi\xi 33}-S_{3333}\right)\left[\frac{h}{4}\left(\ddot{\sigma}_{33}^{+}+\ddot{\sigma}_{33}^{-}\right)-\frac{1}{2}\ddot{N}_{33}\right]$$

$$+\frac{\rho_0}{h}\frac{h^2}{588}S_{3333}\left(S_{\xi\xi 33}-S_{3333}\right)\left[\frac{h^2}{12}\left(\ddot{\sigma}_{33}^{+}-\ddot{\sigma}_{33}^{-}\right)-\ddot{M}_{33}\right]$$

$$+\frac{\rho_0}{h}\frac{h^2}{16}S_{\alpha\underline{\alpha}33}\int_{-a,-b}^{x_\alpha}\Big[-\left(5\ddot{\bar{\bar{u}}}_\alpha-3\ddot{\bar{u}}_\alpha\right)+\left(3\ddot{\hat{u}}_\alpha-\ddot{\tilde{u}}_\alpha\right)$$

$$-\frac{8h}{105}S_{\alpha 3\beta 3}\left(5\ddot{\sigma}^{+}_{\beta 3}-2\ddot{\sigma}^{-}_{\beta 3}\right)-\frac{8}{35}S_{\alpha 3\beta 3}\ddot{V}_\beta\Big]d\eta_\alpha$$

$$-\frac{\rho_0}{h}S_{1133}\Big[\frac{5h^3}{128}\ddot{\hat{\hat{u}}}_3(-a,x_2,x_3,t)-\frac{h^3}{32}\ddot{\bar{\bar{u}}}_3(-a,x_2,x_3,t)-\frac{3h^3}{64}\ddot{\hat{u}}_3(-a,x_2,x_3,t)$$

$$+\frac{h^3}{32}\ddot{\bar{u}}_3(-a,x_2,x_3,t)+\frac{h^3}{128}\ddot{\tilde{u}}_3(-a,x_2,x_3,t)$$

$$-\frac{\rho_0}{h}S_{2233}\Big[\frac{5h^3}{128}\ddot{\hat{\hat{u}}}_3(x_1,-b,x_3,t)-\frac{h^3}{32}\ddot{\bar{\bar{u}}}_3(x_1,-b,x_3,t)-\frac{3h^3}{64}\ddot{\hat{u}}_3(x_1,-b,x_3,t)$$

$$+\frac{h^3}{32}\ddot{\bar{u}}_3(x_1,-b,x_3,t)+\frac{h^3}{128}\ddot{\tilde{u}}_3(x_1,-b,x_3,t) \tag{3.58}$$

Where

$$K_\alpha=-\frac{1}{h}S_{\alpha 3\beta 3}\int_{-\frac{h}{2}}^{\frac{h}{2}}\left(-\frac{6x_3^2}{h^2}-\frac{2x_3}{h}+\frac{1}{2}\right)\int_{-\frac{h}{2}}^{x_3}P_\beta\, d\eta_3\, dx_3$$

$$-\frac{12}{h^3}S_{\alpha 3\beta 3}\int_{-\frac{h}{2}}^{\frac{h}{2}}\left(-\frac{6x_3^2}{h^2}-\frac{2x_3}{h}+\frac{1}{2}\right)\int_{-\frac{h}{2}}^{x_3}R_\beta\eta_3\, d\eta_3\, dx_3$$

$$+\rho_0 S_{\alpha 3\beta 3}\int_{-\frac{h}{2}}^{\frac{h}{2}}\left(-\frac{6x_3^2}{h^2}-\frac{2x_3}{h}+\frac{1}{2}\right)\int_{-\frac{h}{2}}^{x_3}\left[\varepsilon_{jj}\ddot{u}_\beta+(1-\varepsilon_{jj})\dot{\varepsilon}_{jj}\dot{u}_\beta\right]d\eta_3\, dx_3 \tag{3.59}$$

$$L_\alpha=\frac{1}{h}S_{\alpha 3\beta 3}\int_{-\frac{h}{2}}^{\frac{h}{2}}\left(\frac{6x_3^2}{h^2}-\frac{2x_3}{h}-\frac{1}{2}\right)\int_{-\frac{h}{2}}^{x_3}P_\beta\, d\eta_3\, dx_3$$

$$-\frac{12}{h^3}S_{\alpha 3\beta 3}\int_{-\frac{h}{2}}^{\frac{h}{2}}\left(\frac{6x_3^2}{h^2}-\frac{2x_3}{h}-\frac{1}{2}\right)\int_{-\frac{h}{2}}^{x_3}R_\beta \eta_3 d\eta_3 dx_3$$

$$-\rho_0 S_{\alpha 3\beta 3}\int_{-\frac{h}{2}}^{\frac{h}{2}}\left(\frac{6x_3^2}{h^2}-\frac{2x_3}{h}-\frac{1}{2}\right)\int_{-\frac{h}{2}}^{x_3}\left[\varepsilon_{jj}\ddot{u}_\beta+\left(1-\varepsilon_{jj}\right)\dot{\varepsilon}_{jj}\dot{u}_\beta\right]d\eta_3 dx_3 \tag{3.60}$$

3.3.12 Operator Form of Governing Equations

The governing equations (Equations 3.52 to 3.58) are derived for a single lamina. To derive the equations for an N-layer laminate, the following generalized displacements are defined:

$$\left(\tilde{g},\bar{g},\hat{g},\bar{\bar{g}},\hat{\hat{g}}\right)\equiv\int_{-\frac{h_k}{2}}^{\frac{h_k}{2}}g\left(1,\frac{2x_3}{h},\frac{4x_3^2}{h^2},\frac{8x_3^3}{h^3},\frac{16x_3^4}{h^4}\right)\frac{2}{h}dx_3 \tag{3.61}$$

$$\bar{v}_\rho^{(k)}\equiv\frac{\tilde{u}_\rho^{(k)}}{2} \tag{3.62}$$

$$\bar{\phi}_\rho^{(k)}\equiv\frac{3\bar{u}_\rho^{(k)}}{h_k} \tag{3.63}$$

$$\bar{v}_3^{(k)}\equiv\frac{3}{4}\left(\tilde{u}_3-\hat{u}_3\right)^{(k)} \tag{3.64}$$

$$\bar{\phi}_3^{(k)}\equiv\left(5\hat{u}_3-\tilde{u}_3\right)^{(k)} \tag{3.65}$$

Where k = 1 and k = N represent the top and bottom laminae (Figure 3.2).

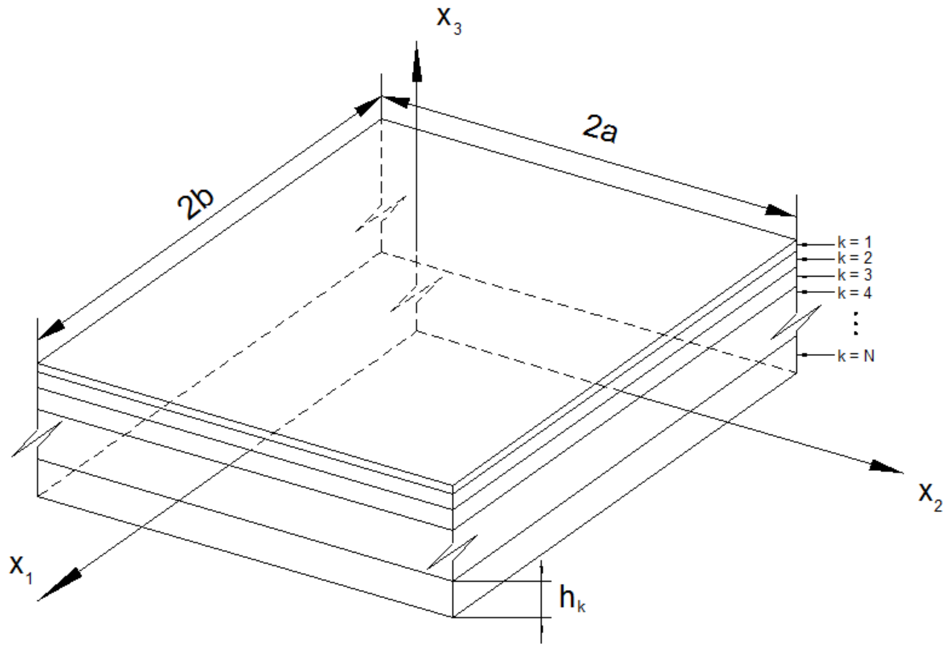

Figure 3.3 Coordinate System for a N-layer Laminate (Tu 2007)

The governing equations, Equation 3.52 to Equation 3.58, for the *k*-th lamina, after being rewritten into self-adjoint form and eliminating the time derivatives using Gurtin's bilinear mapping (1963, 1964), can be expressed in an operator form as:

$$[A]^{(k)}\{u\}^{(k)} + [B]^{(k)}\{\sigma\}^{-(k)} + [C]^{(k)}\{\sigma\}^{+(k)} + [D_u]^{(k)}\{F\}^{(k)}$$
$$+[H]^{(k)} + \{E_u\}^{(k)} + \{Z_u\}^{(k)} = 0 \qquad (3.66)$$

Where

$[A]^{(k)}$, $[B]^{(k)}$, $[C]^{(k)}$ and $[D_u]^{(k)}$: the field operator matrices for the *k*-th layer(k = 1,2,…N);

$[u]^{(k)}$ and $\{\sigma\}^{\pm(k)}$: field variable vectors;

$[F]^{(k)}$: generalized body force vector;

$[H]^{(k)}$: pseudo body force vector;

$[E]^{(k)}$: in-plane boundary term vector;

$[Z_u]^{(k)}$: explicit initial conditions vector from Gurtin's convolution bilinear mapping.

The vectors of (20N + 3) field variables are defined as

$$\{[u]^{(k)}\}^T = [\bar{v}_\gamma^{(k)} \quad \bar{\phi}_\gamma^{(k)} \quad \bar{v}_3^{(k)} \quad \bar{\phi}_3^{(k)} \quad \bar{u}_3^{(k)} \quad N_{\alpha\beta}^{(k)} \quad N_{33}^{(k)} \quad M_{\alpha\beta}^{(k)} \quad M_{33}^{(k)} \quad V_\gamma^{(k)}] \tag{3.67}$$

$$[\{\sigma\}^{\pm(k)}]^T = [\sigma_{\gamma 3}^{\pm(k)} \quad \sigma_{33}^{\pm(k)}] \tag{3.68}$$

The interface continuity equations for the *k*-th layer can be expressed as

$$\begin{aligned}
&[\Lambda]^{(k)}\{\sigma\}^{-(k-1)} + [\overline{B}]^{(k)}\{u\}^{(k)} + [\Xi]^{(k)}\{\sigma\}^{-(k)} + [\overline{C}]^{(k+1)}\{u\}^{(k+1)} \\
&+ [\overline{\Lambda}]^{(k+1)}[\sigma]^{-(k+1)} + \{D_s\}^{(k)}\{F\}^{(k)} + [\overline{D}_s]^{(k+1)}\{F\}^{(k+1)} \\
&+ \{\overline{H}\}^{(k)} + \{\overline{\overline{H}}\}^{(k+1)} + \{E_s\}^{(k)} + \{Z_s\}^{(k)} = 0
\end{aligned} \tag{3.69}$$

The governing function for the self-adjoint form of the initial boundary value problem was derived using the generalized variational formulation presented by Sandhu and Salam (1975). The number of field variables was reduced from 20N+3 (Equations 3.66 to 3.69) to 10N+3 by the following specializations:

- Eliminating the derivatives on generalized stresses;
- Enforcing stress boundary conditions at free edges;
- Eliminating the self-adjoint terms of the interface continuity equations;
- Neglecting the acceleration terms associated with interface transverse shear stress continuity conditions;

- Neglecting the body forces (pseudo-body force accounted for);
- No jump discontinuities in the interior of the laminate.

The reduced field variables are

$$\left\{[u]^{(k)}\right\}^T = \left[\bar{v}_\alpha^{(k)} \quad \bar{\phi}_\alpha^{(k)} \quad \bar{v}_3^{(k)} \quad \bar{\phi}_3^{(k)} \quad \bar{u}_3^{(k)}\right] \tag{3.70}$$

$$\left[\{\sigma\}^{\pm(k)}\right]^T = \left[\sigma_{\alpha 3}^{\pm(k)} \quad \sigma_{33}^{\pm(k)}\right] \tag{3.71}$$

3.3.13 Finite Element Method – Spatial Discretization

In the implementation of the finite element method, the domain of interest R, is divided into a number of elements R_e, such that

$$\bar{R} = \lim_{m \to \infty} \sum_{e=1}^{m} R_e \tag{3.72}$$

Where e = 1,2,3,…,m with m representing the number of elements

The elements do not overlap and are connected to each other through nodal points. For any element "e", an unknown field variable $\bar{v}_\alpha$ can be approximated in matrix form as

$$\bar{v}_\alpha = [\psi]_e^T \{a_v\}_e \tag{3.73}$$

Where

$[\psi]_e$ represents the set of base functions;

$\{a_v\}_e$ represents the column vector of unknown coefficients.

The value of any arbitrary point in the element can be approximated as

$$\bar{v}_\alpha = [\psi_{v\alpha}]_e^T \{\bar{v}_\alpha\}_e \tag{3.74}$$

Where

$[\psi_{v\alpha}]_e^T$ is the set of interpolation function, $[\psi]_e^T\left[[\psi]_e^{i\,T}\right]^{-1} = [\psi]_e^T[\psi]^{-1}$.

For the k-th layer,

$$\bar{v}_{\alpha}^{(k)} = [\psi_{v\alpha}]_e^T\{\bar{v}_{\alpha}\}_e^{(k)} \tag{3.75}$$

Similarly, for the other unknown field variables in Equations 3.55 and 3.56 can be approximated as

$$\bar{\phi}_{\alpha}^{(k)} = [\psi_{v\alpha}]_e^T\{\bar{\phi}_{\alpha}\}_e^{(k)} \tag{3.76}$$

$$\bar{v}_{3}^{(k)} = [\psi_{v3}]_e^T\{\bar{v}_{3}\}_e^{(k)} \tag{3.77}$$

$$\bar{\phi}_{3}^{(k)} = [\psi_{\phi 3}]_e^T\{\bar{\phi}_{3}\}_e^{(k)} \tag{3.78}$$

$$\bar{u}_{3}^{(k)} = [\psi_{u3}]_e^T\{\bar{u}_{3}\}_e^{(k)} \tag{3.79}$$

$$\sigma_{\gamma 3}^{-(k)} = [\psi_{\gamma 3}]_e^T\{\sigma_{\gamma 3}\}_e^{-(k)} \tag{3.80}$$

$$\sigma_{33}^{-(k)} = [\psi_{33}]_e^T\{\sigma_{33}\}_e^{-(k)} \tag{3.81}$$

Substituting Equations 3.75 to 3.81 into the specialized governing equation, the matrix form of the governing function for each element can be written as

$$\Omega_e = -\{U\}_e^T[M]_e\{U\}_e - t*\{U\}_e^T[K]_e\{U\}_e + 2\{U\}_e^T\left(\{R_0\}_e + t*\{R\}_e - t*\{\bar{R}\}_e\right) \tag{3.82}$$

Where $[M]_e$ is the element mass matrix;

$[K]_e$ is the element stiffness matrix;

$[U]_e$ is the vector of field variables at nodal points of an element “e”

$[R_0]_e$ is the equivalent nodal load vector due to initial conditions

$\left[R\right]_e$ is the applied load vector

$\left[\overline{R}\right]_e$ is the vector of pseudo body forces

" $*$ " is the convolution integral.

Using equation 3.82, the governing function for the global system can be written as:

$$\Omega_5 = \sum_{e=1}^{m} \Omega_e = -\{U\}^T [M]\{U\} - t * \{U\}^T [K]\{U\} + 2\{U\}^T \left(\{R_0\} + t * \{R\} - t * \{\overline{R}\}\right) \tag{3.83}$$

Taking the differential of Equation 3.83 with respect to $\{U\}$ and setting it to zero produces:

$$[M]\{U\} + t * [K]\{U\} = \{R_0\} + t * \{R\} - t * \{\overline{R}\} \tag{3.84}$$

Where $[M]$ is the global mass matrix

$[K]$ is the global stiffness matrix

$\{U\}$ represents the nodal value field variable vector

$[R_0]$ denotes the equivalent nodal load vector due to initial conditions

$[R]$ is the applied load vector

$[\overline{R}]$ is the pseudo body force vector

Differentiating Equation 3.84 time with respect to twice finally gives:

$$[M]\{\ddot{U}\} + [K]\{U\} = \{R\} - \{\overline{R}\} \tag{3.85}$$

Based on the specialization of the governing equation, it has been assumed that the field variables $\overline{v}_\alpha^{(k)}$, $\overline{\phi}_\alpha^{(k)}$, $\overline{v}_3^{(k)}$, $\overline{\phi}_3^{(k)}$, $\overline{u}_3^{(k)}$, and $\sigma_{i3}^{-(k)}$ are continuous across inter-element boundaries. For rectangular elements, bilinear interpolation is needed for $\overline{v}_\alpha^{(k)}$, $\overline{\phi}_\alpha^{(k)}$, $\overline{v}_3^{(k)}$,

$\bar{\phi}_3^{(k)}$, $\bar{u}_3^{(k)}$, and $\sigma_{33}^{-(k)}$ while the transverse shear stress $\sigma_{\alpha 3}^{-(k)}$ requires higher order of interpolation.

The Heterosis element first introduced by Hughes and Cohen (1974) was selected to apply the stress-based theory in the finite element model. The Heterosis element (Figure 3.4) includes a synthesis of the selectively integrated nine-node Lagrange element and eight-node serendipity element. Hughes (1987) showed that Heterosis element has the advantage over both nine-node Lagrange element and eight-node serendipity element for combining their attributes but avoiding their shortcomings. Nine-node Lagrangian interpolation was used for the in-plane generalized displacements, $\bar{v}_\alpha^{(k)}$, $\bar{\phi}_\alpha^{(k)}$, and transverse shear stresses $\sigma_{\alpha 3}^{-(k)}$. The generalized transverse displacements, $\bar{v}_3^{(k)}$, $\bar{\phi}_3^{(k)}$, $\bar{u}_3^{(k)}$, and the transverse normal stress, $\sigma_{33}^{-(k)}$ were approximated by 8-node iso-parametric quadratic interpolation scheme.

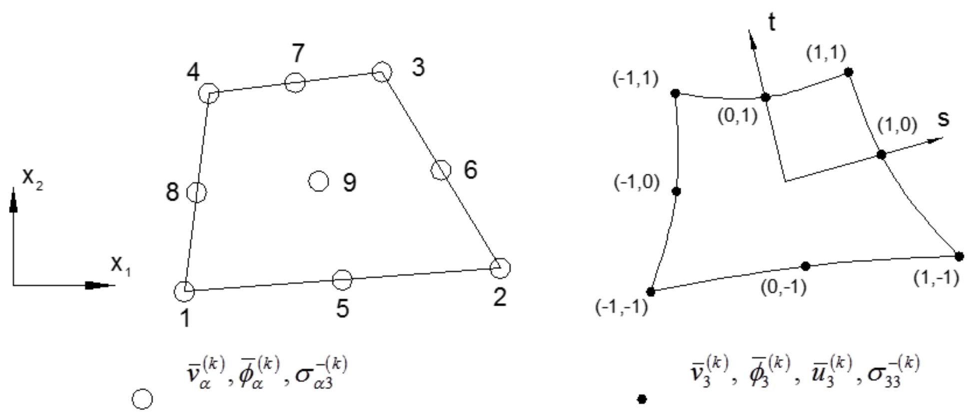

Figure 3.4 Heterosis Element (Tu 2007)

3.3.14 Temporal Discretization

After spatial discretization, the governing equations have been reduced to a system of ordinary differential equations in the time domain (Equation 3.85). To complete the solution process and solve this linear dynamic problem numerically, the equations must be integrated. The direct integration methods which are widely used in computational structural dynamics (Dokainish and Subbaraj, 1989; Subbaraj and Dokainish, 1989) can be subdivided into explicit and implicit methods. Explicit time integration methods demand less storage than implicit methods but generally require small time steps to ensure numerical stability. Implicit methods usually require considerably more computational effort per time step than the explicit methods but the time steps may be larger and many implicit methods are unconditionally stable for linear analysis.

Wilson's $\beta-\gamma-\theta$ step-forward implicit integration method (Ghaboussi and Wilson, 1972; Hiremath et al., 1988) was used to solve the differential matrix equations for the dynamic stress-based theory.

The nodal value field variable vector and its first order derivative with respect to time at time $(t_n+\theta t)$, can be expressed in terms of $\{U\}$, $\{\dot{U}\}$, and $\{\ddot{U}\}$ at time t_n as:

$$\{U\}_{n+\theta}=\{U\}_{\theta}+\theta\Delta t\{\dot{U}\}_{n}+\left(\frac{1}{2}-\beta\right)(\theta\Delta t)^{2}\{\ddot{U}\}_{n}+\beta(\theta\Delta t)^{2}\{\ddot{U}\}_{n+\theta} \tag{3.86}$$

$$\{\dot{U}\}_{n+\theta}=\{\dot{U}\}_{\theta}+(1-\gamma)(\theta\Delta t)\{\ddot{U}\}_{n}+(\gamma\theta\Delta t)\{\ddot{U}\}_{n+\theta} \tag{3.87}$$

Where β, γ, and θ are integration constants.

Substituting Equations 3.71 and 3.72 into Equation 3.70 yields

$$\left[K^*\right]\{U\}_{n+\theta} = \left\{R^*\right\}_{n+\theta} - \left\{\overline{R}^*\right\}_{n+\theta} \tag{3.88}$$

Where

$$\left[K^*\right] = [K] + \frac{1}{\beta(\theta\Delta t)^2}[M] \tag{3.89}$$

$$\left[R^*\right]_{n+\theta} - \left[\overline{R}^*\right]_{n+\theta} = [R]_{n+\theta} - \left[\overline{R}\right]_{n+\theta} + \frac{1}{\beta(\theta\Delta t)^2}[M]\{a\}_{n+\theta} \tag{3.90}$$

$$\{a\}_{n+\theta} = \{U\}_n + (\theta\Delta t)\{\dot{U}\}_n + \left(\frac{1}{2} - \beta\right)(\theta\Delta t)^2\{\ddot{U}\}_n \tag{3.91}$$

Assuming cubic variation of nodal field variables over the time step (t_n, t_{n+1}) in terms of nodal field variables, its first and second derivatives with respect to time at time t_n, the values of these vectors at time $(t_n + \Delta t)$ are:

$$\{U\}_{n+1} = \frac{1}{\theta^3}\{U\}_{n+\theta} + \left(1 - \frac{1}{\theta^3}\right)\{U\}_n + \left(1 - \frac{1}{\theta^2}\right)\Delta t\{\dot{U}\}_n + \frac{1}{2}\left(1 - \frac{1}{\theta}\right)(\Delta t)^2\{\ddot{U}\}_n \tag{3.92}$$

$$\{\dot{U}\}_{n+1} = \frac{\gamma}{\beta\theta^3\Delta t}\left(\{U\}_{n+\theta} - \{U\}_n\right) + \left(1 - \frac{\gamma}{\beta\theta^2}\right)\{\dot{U}\}_n + \left(1 - \frac{\gamma}{2\beta\theta^2}\right)\{\ddot{U}\}_n \tag{3.93}$$

$$\{\ddot{U}\}_{n+1} = \frac{1}{\beta\theta^3\Delta t^2}\left(\{U\}_{n+\theta} - \{U\}_n\right) - \frac{1}{\beta\theta^2\Delta t}\{\dot{U}\}_n + \left(1 - \frac{1}{2\beta\theta}\right)\{\ddot{U}\}_n \tag{3.94}$$

The equations are solved iteratively. For each time step, the field variable and its derivatives $\{U\}$, $\{\dot{U}\}$, and $\{\ddot{U}\}$ are first calculated by neglecting the pseudo-body force term $\{\overline{R}\}$. An updated $\{\overline{R}\}$ is then calculated from the values of $\{U\}$, $\{\dot{U}\}$, and $\{\ddot{U}\}$ obtained.

The updated $\{\overline{R}\}$ is used to calculate the updated $\{U\}$, $\{\dot{U}\}$, and $\{\ddot{U}\}$ values. This iterative process is repeated until the required level of convergence is achieved

3.3.15 Model Extension – Synthesis

Following the derivation of Chyou (1989), Schoeppner (1991) and Butalia (1996) for the stress based theory and the subsequent adaptation for framework of a pavement response model postulated by Tu (2007), the Resilient Modulus model (Kim 2004) is incorporated into the stiffness matrix of the stress based finite element model as an appropriate material characterization for more accurate pavement responses. This is done by providing the nine (9) input parameters for the material characterization model and passing the determined Mr value through the Stiffness matrix subroutine.

In summary, two suitable but separate formulations for pavement response modeling have been adopted and fused into a new synthesis to provide a means by which a shift in philosophy can be adopted by developing countries such as Guyana in order to embrace a more mechanistic approach to pavement design. In the next chapter, the combination of these two models will be used to confirm the viability of this response model.

Chapter 4: Experimental Verification of the Stress Based Model and the New Synthesis

4.1 Experimental Verification of the OSU Stress-Based pavement response model

Wolfe et al (2006) conducted full scale pavement testing to investigate the suitability of coal combustion products as pavement construction materials. Instrumented flexible and rigid pavement sections (3 each) were designed constructed and monitored under accelerated loading and controlled environmental conditions at the Ohio Accelerated Pavement Loading Facility (APLF). The pavement deflections and transverse normal stress at the interface between sub-base and subgrade layers with calculated response of the stress based model were compared. The results presented in Fig 4.1 and 4.2 show good agreement between the measurements and the predictions of the stress based model. As can be seen in figure 4.1, the prediction of deflection using the OSU Stress Based Model was greater than the measured results by approximately 15 percent. Figure 4.2 shows that the vertical compressive stress at the interface between sub-base and subgrade layers in the pavement, found using the stress based model over-predicted the measured stresses by approximately 30 percent. These discrepancies, though relatively small, may be due to simplifying assumptions made in the formulation of the stress based model, assumptions for material properties and limitations of the instrumentation employed for measuring.

The OSU Stress Based model underwent further verification by comparing the measured versus predicted responses of pavement with the OSU Full Depth Reclamation Project (FDR 2010). Two deficient road pavements in Ohio were rehabilitated and stress and displacement data were collected over a period of several months. Conditions measured shortly after the repairs were completed were used as inputs in the stress based model. The OSU Stress Based model over-predicted the transverse normal stress measured at the interface between the sub-base and subgrade by almost 60% as shown in Figure 4.3 (Tu 2007). The most likely reason for this difference between the measured and predicted responses is the input parameters for the rehabilitated sections were not well known and had to be assumed.

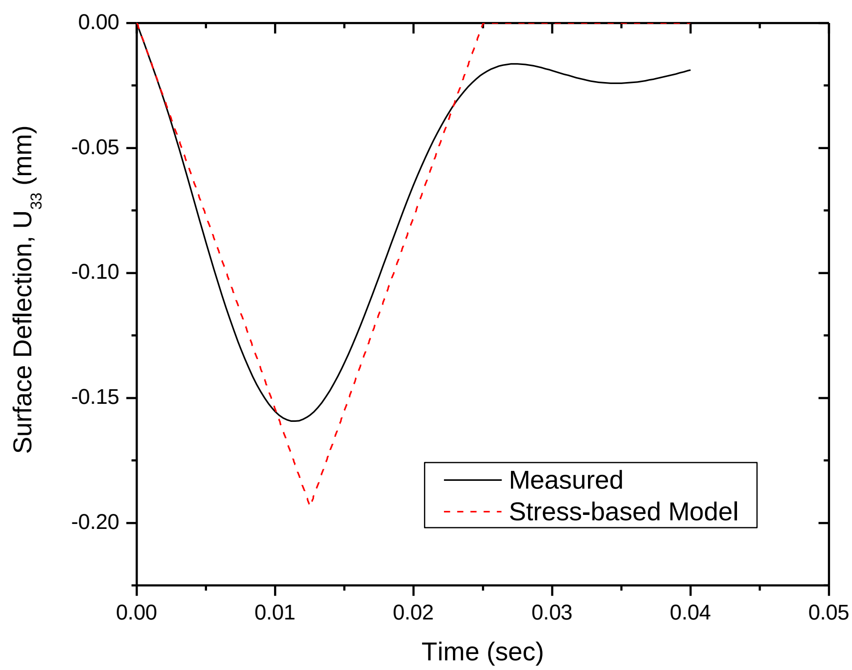

Figure 4.1 Comparison of Calculated and Measured Surface Deflection from the initial FWD Test of APLF AC Control Section (Tu, 2007).

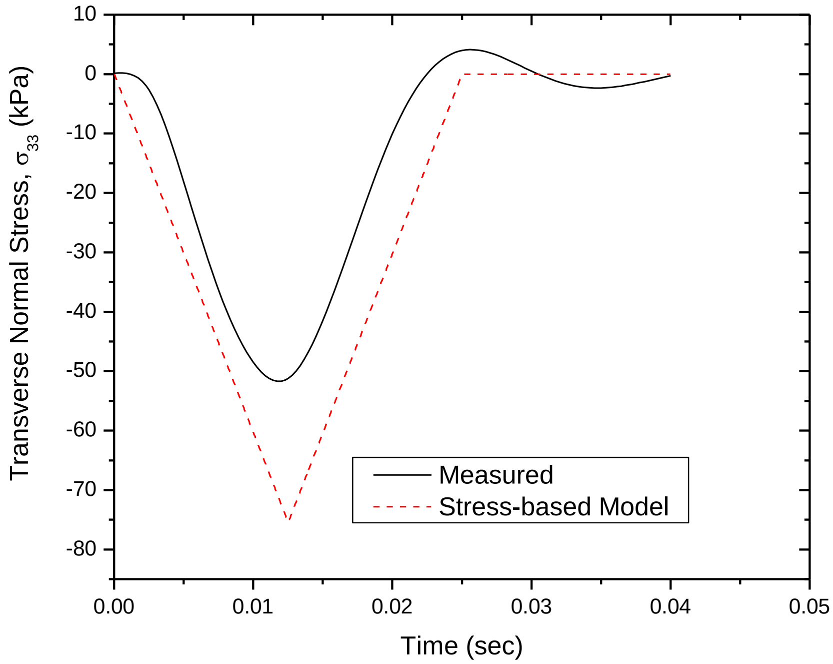

Figure 4.2 Comparison of Calculated and Measured Transverse Normal Stress from the Initial FWD Test of APLF AC Control Section (Tu, 2007).

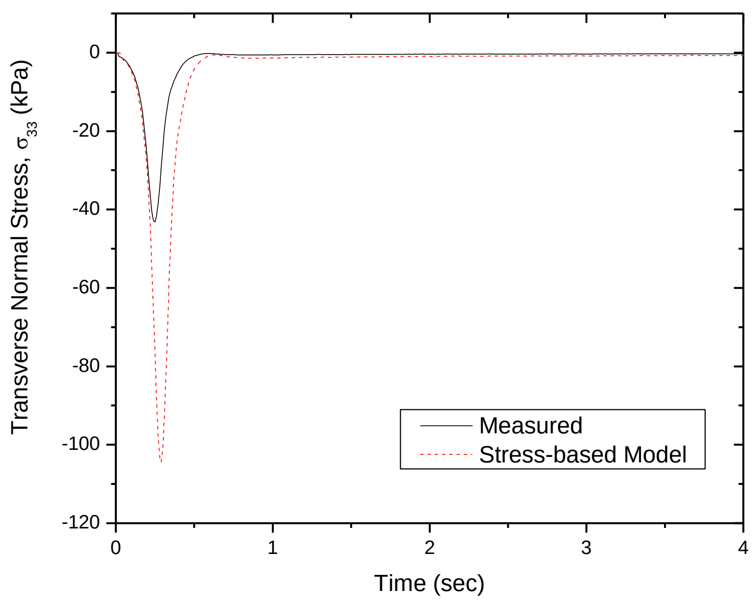

Figure 4.3 Comparison of predictions of the Stress- based model and the measured transverse normal stress for FDR DEL Section #6 under Truck Wheel Loads (Tu, 2007)

4.2 Verification of the New Synthesis

Under Loan Contract: LO2454-BL/GY between the Government of Guyana, on behalf of the people and the Inter-American Development Bank, a project is being funded to extend the East Bank Demerara four lane highway from Providence to Diamond. This project includes the construction of new pavement sections as well as the rehabilitation of existing sections. The cross sections of the tabled design, with the appropriate chainage is shown in Figure 4.4 and makes use of some of the locally sourced pavement material. The pavement layer components that constitute the system include, cohesive subgrades, white sand subbase, natural and cement stabilized sand clay (loam) base material and asphalt concrete binder and surface courses.

In order to assess the new synthesis, a typical geometry from the cross sections of this East Bank thoroughfare (Figure 4.5) was analyzed using the stress based formulation and making a comparison with results for a static 3D Finite Element Abaqus Model. The analysis governed the structural responses of the pavement based on loading in the pavement system. The results are presented for the propinquity of global responses such as displacement and transverse stress distribution at the layer interfaces through the thickness of the pavement. The analysis was conducted using typical values for the road building materials including the cohesive subgrade as well as with the input of the Characterization

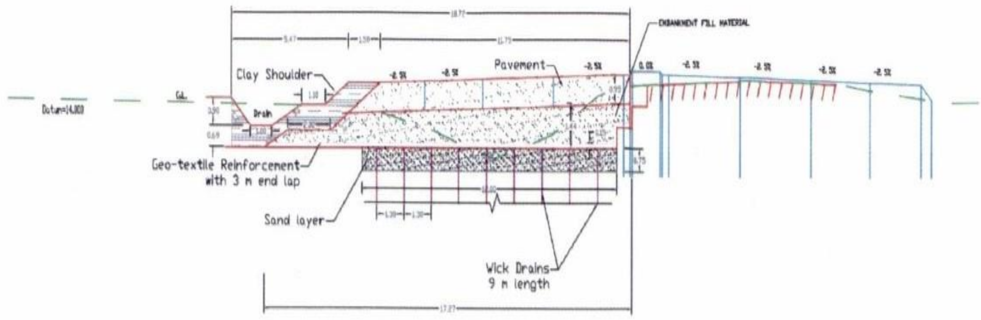

TYPICAL DESIGN SECTION BETWEEN CH 700.000 TO CH 1500.000

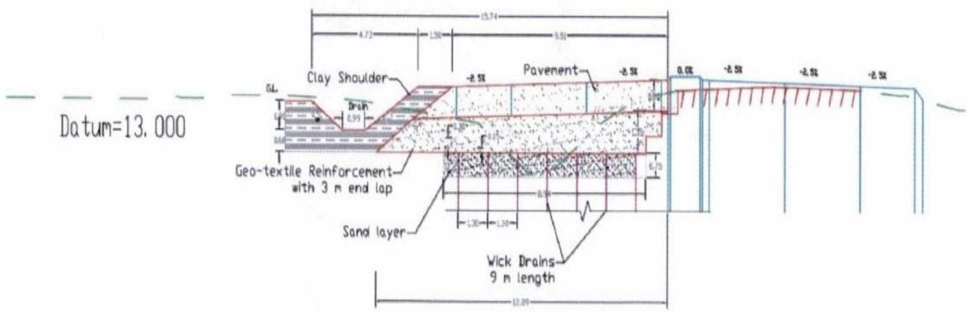

TYPICAL DESIGN SECTION BETWEEN CH 1500.000 TO CH 2600.000

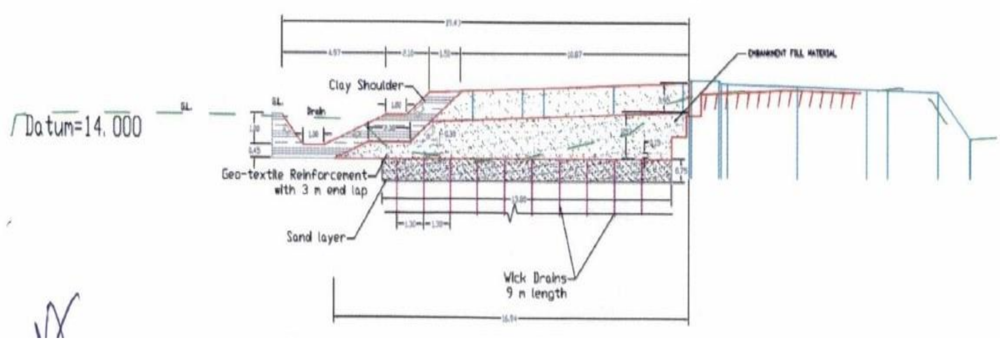

Figure 4.4 Typical pavement cross sections for East Bank Demerara Public Road (LO2454-BL/GY, 2011)

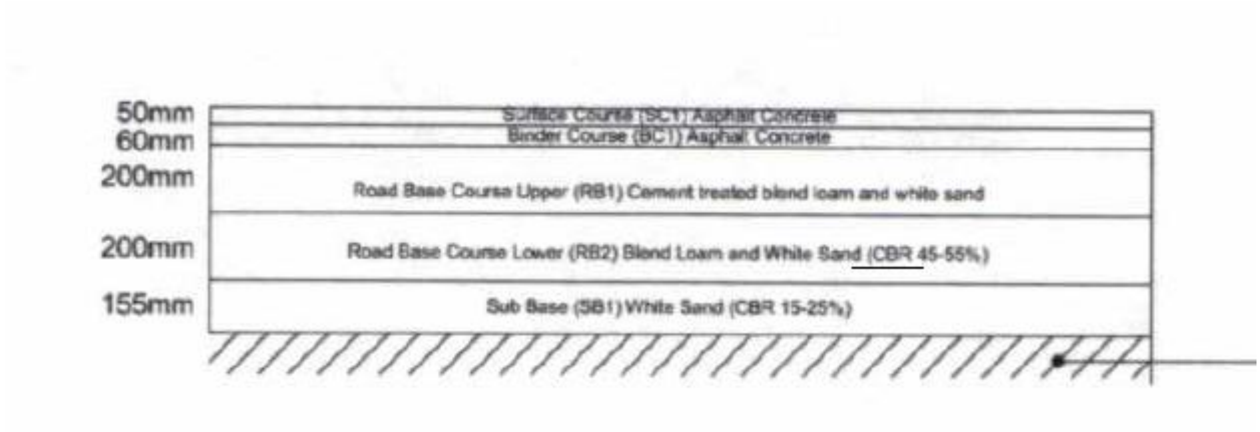

Figure 4.5 Typical Geometry of the pavement section (LO2454-BL/GY, 2011)

Model for cohesive subgrades in the stress based formulation. The nine (9) input parameters were entered for the Cane View Sample and the material model returned a Mr value of 83.68 MPa since the deposition is similar to that of the East Bank Public Road.

Layer #	**Layer**	**Material**	**Young's Elastic Modulus(E or Mr), GPa**	**Poisson Ratio**	**Thickness, mm**
1	Surface Course	Asphalt Concrete	20.684	0.25	50
2	Binder Course	Asphalt Concrete	13.789	0.25	60
3	Road Base Upper	Stabilized Sand Clay (Loam)	2.068	0.3	200
4	Road Base Lower	Sand Clay (Loam)	1.378	0.3	200
5	Sub Base	White Sand	0.413	0.35	155
6	Stabilized Subgrade	Cement Stabilized	0.345	0.4	200
7	Natural Subgrade	A-7-5 (Mr Model)	**0.084**	0.45	200

Table 4.1 Summary of pavement layers considered for analysis.

Layer descriptions and properties are summarized in the Table 4.1 which are based on typical values found in the literature for those material types. The primary objective is to test the pavement responses within this theoretical framework. Further, Table 4.2 provides a simplification of the pavement system configuration for ease of analysis. The values for pavement layers were based on typical values and are summarized in Table 4.3. This was done to reduce computational costs associated with having complicated meshing in the ABAQUS Model as well as several layers.

Layer #	**Layer**	**Material**	**Young's Elastic Modulus(E or Mr), GPa**	**Poisson Ratio**	**Thickness, mm**
1	Surface /Binder Course	Asphalt Concrete	20.684	0.25	110
2	Road Base Upper	Stabilized Sand Clay (Loam)	2.068	0.3	400
3	Sub Base	White Sand	0.413	0.4	355
4	Natural Subgrade	A-7-5	**0.084**	0.45	200

Table 4.2 Summary of parameters for response modeling.

The results of the stress based model were compared with a Static 3D Finite Element Abaqus Model to determine whether the predictions were reasonable. An appropriate meshing scheme at a reasonable computational cost was chosen for this analysis with a uniformly distributed load of 770 KPa, created by contact with a 6 inch radius tire contact. The finite element model along with the meshing and deflection graph are presented in Figures 4.6-4.8.

Material		Young's Elastic Modulus (E or M_r), psi	Poisson's Ratio (μ or ν)
Asphalt concrete (uncracked)	32 F 70 F 140 F	2,000,000 – 5,000,000 300,000 – 500,000 20,000 – 50,000	0.25 – 0.30 0.30 – 0.35 0.35 – 0.40
Portland cement concrete (uncracked)		3,000,000 – 5,000,000	0.15
Extensively cracked surfaces		Similar to granular base course materials	Similar to granular base course materials
Crushed stone base (clean, well-drained)		20,000 – 80,000	0.35
Crushed gravel base (clean, well-drained)		20,000 – 80,000	0.35
Uncrushed gravel base Clean, well-drained Clean, poorly-drained		 10,000 – 60,000 3,000 – 15,000	 0.35 0.40
Cement stabilized base Uncracked Badly cracked		 500,000 – 2,000,000 40,000 – 200,000	 0.20 0.30
Cement stabilized subgrade		50,000 – 500,000	0.20
Lime stabilized subgrade		20,000 – 150,000	0.20
Gravelly and/or sandy soil subgrade (drained)		10,000 – 60,000	0.40
Silty soil subgrade (drained)		5,000 – 20,000	0.42
Clayey soil subgrade (drained)		3,000 – 12,000	0.42
Dirty, wet, and/or poorly-drained materials		1,500 – 6,000	0.45 – 0.50
Intact Bedrock Note: Values greater than 500,000 have negligible influence on surface deflections.		250,000 – 1,000,000	0.20

Table 4.3 Typical values of Young's Elastic Modulus and Poisson's Ratio for pavement materials (Cornell 2015).

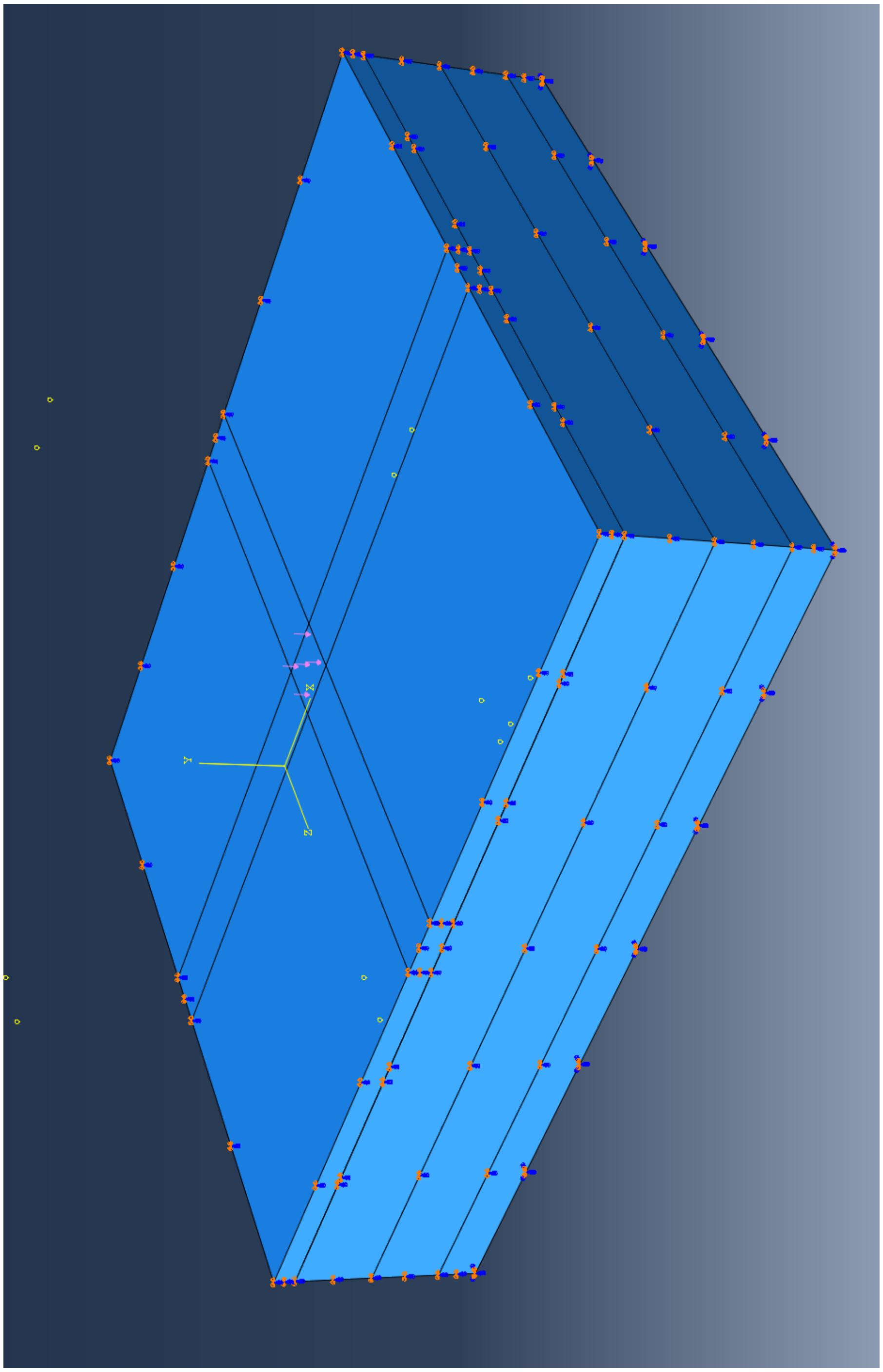

Figure 4.6 Finite Element Model of the flexible pavement system for response modeling.

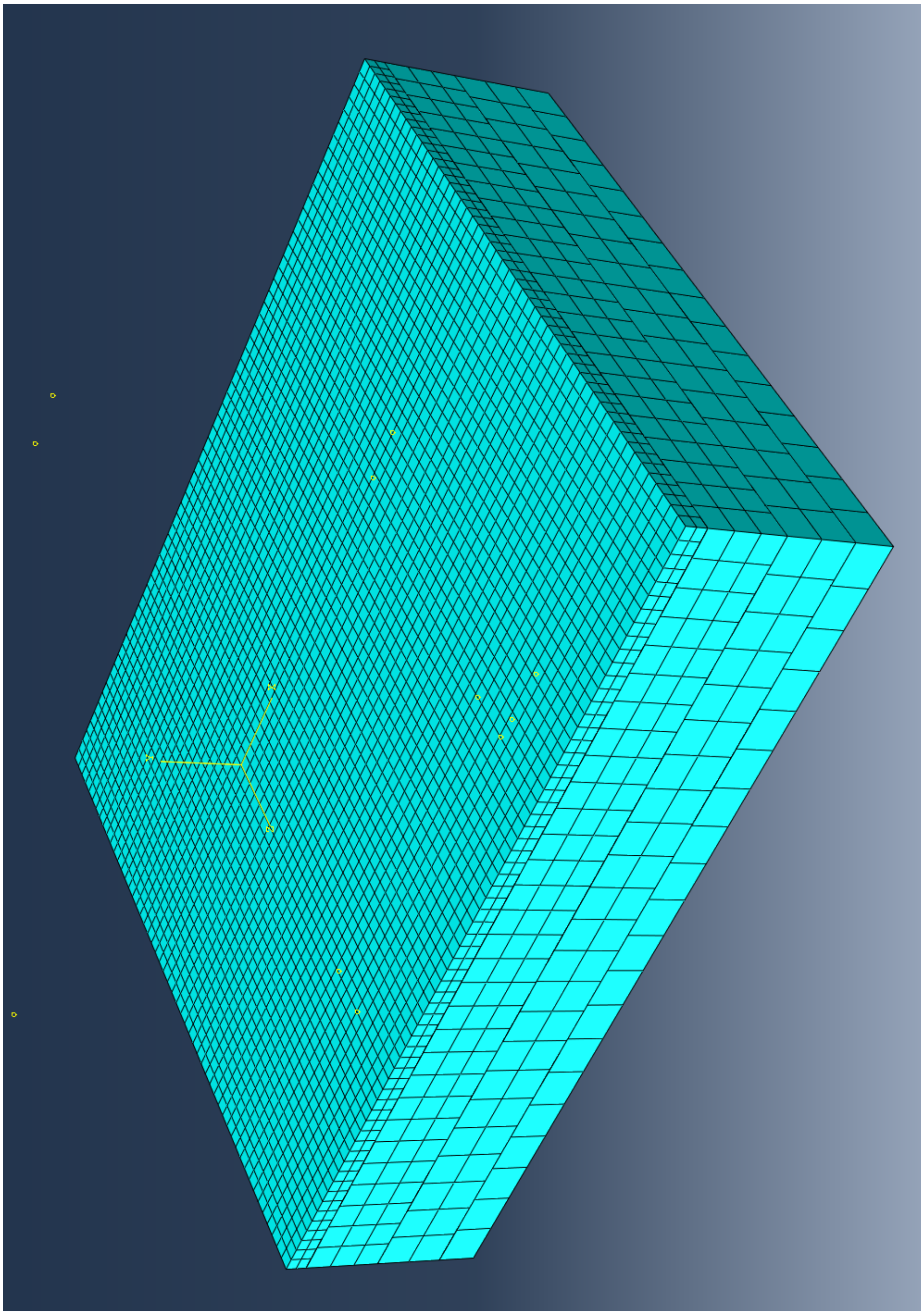

Figure 4.7 Meshing of the Finite Element ABAQUS Model.

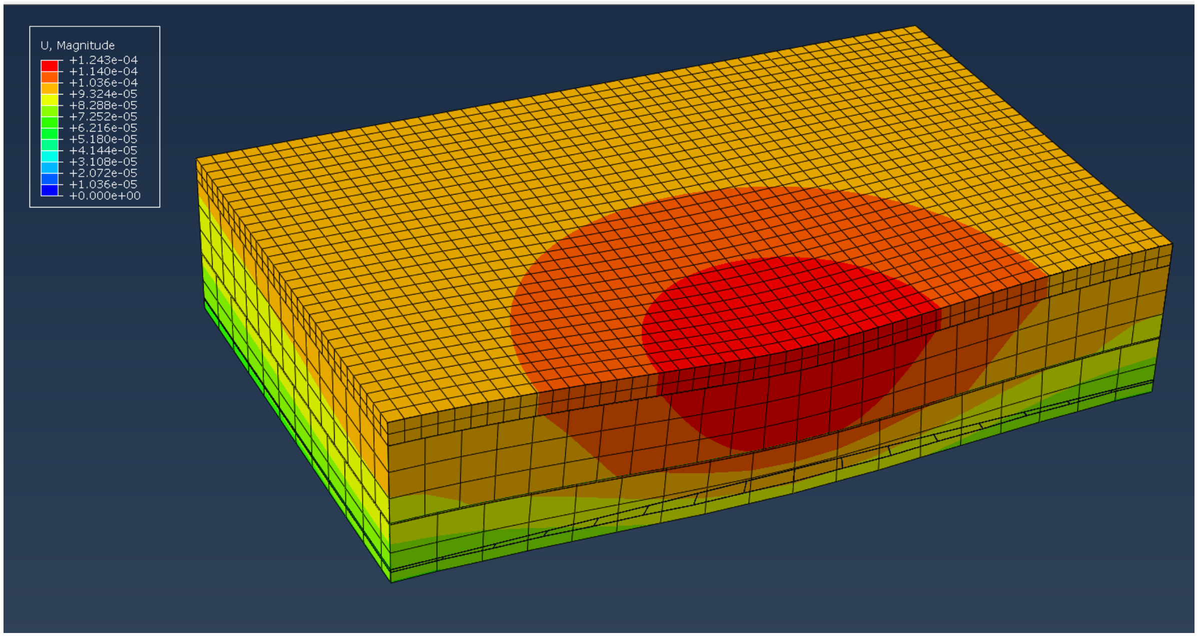

Figure 4.8 Cross-sectional contour plot showing deflection at the surface of pavement under load.

The deflection at the pavement surface under center of the wheel load was predicted by the Abaqus model to be 1.243 E-04 meters. This is less than the prediction made by the stress based model. The initial analysis without the material characterization was done to observe the predictions for deflection and transverse stress distribution without the effect of a robust material model. Subsequently, the analysis was done using the material characterization and the responses were compared. As can be seen in Figure 4.9, the OSU Stress Based model over predicts the displacement by approximately 30%. However, Figure 4.10 shows that when the material characterization model was used, the predictions improved with the deflection predicted by the OSU Stress Based model being closer to the ABAQUS finite element predictions. In the case of the normal transverse stresses at the layer interfaces, the stress based model proves capable of providing more realistic predictions for the load applied. Considering that the load applied was 770 KPa, the prediction by the ABAQUS model is an order of magnitude higher that the Stress based model predictions. In fact, the OSU Stress Based Model predicts the transverse normal stress at every interface between layers starting with the full load experienced at the surface and propagated through the pavement to the top of the seventh layer. The distribution is captured in Figure 4.11.

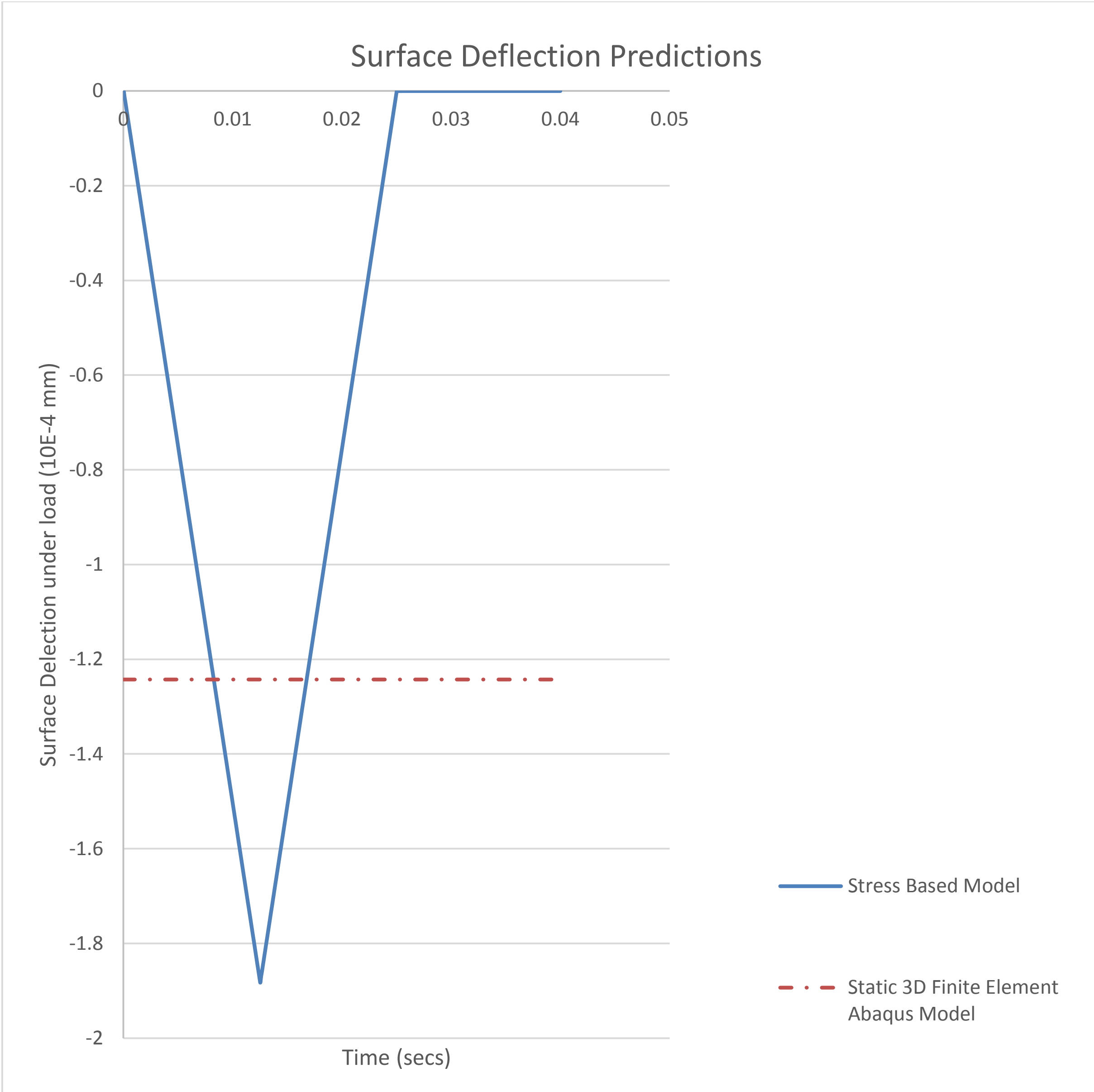

Figure 4.9 Surface deflections under load predicted by OSU Stress Based Model (without the Mr Model) and ABAQUS Model.

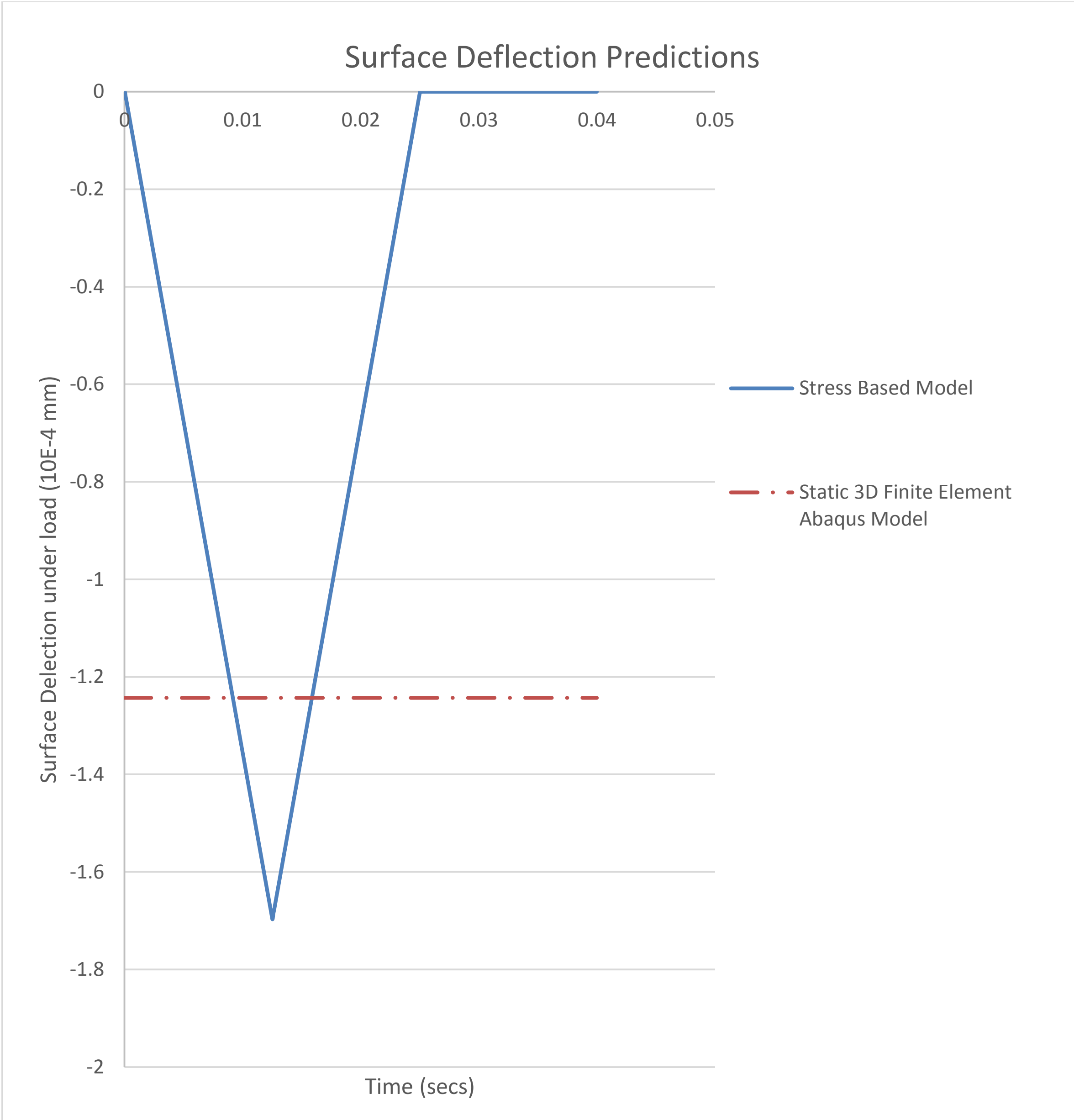

Figure 4.10 Surface deflections under load predicted by OSU Stress Based Model with Material Characterization Synthesis and ABAQUS Model.

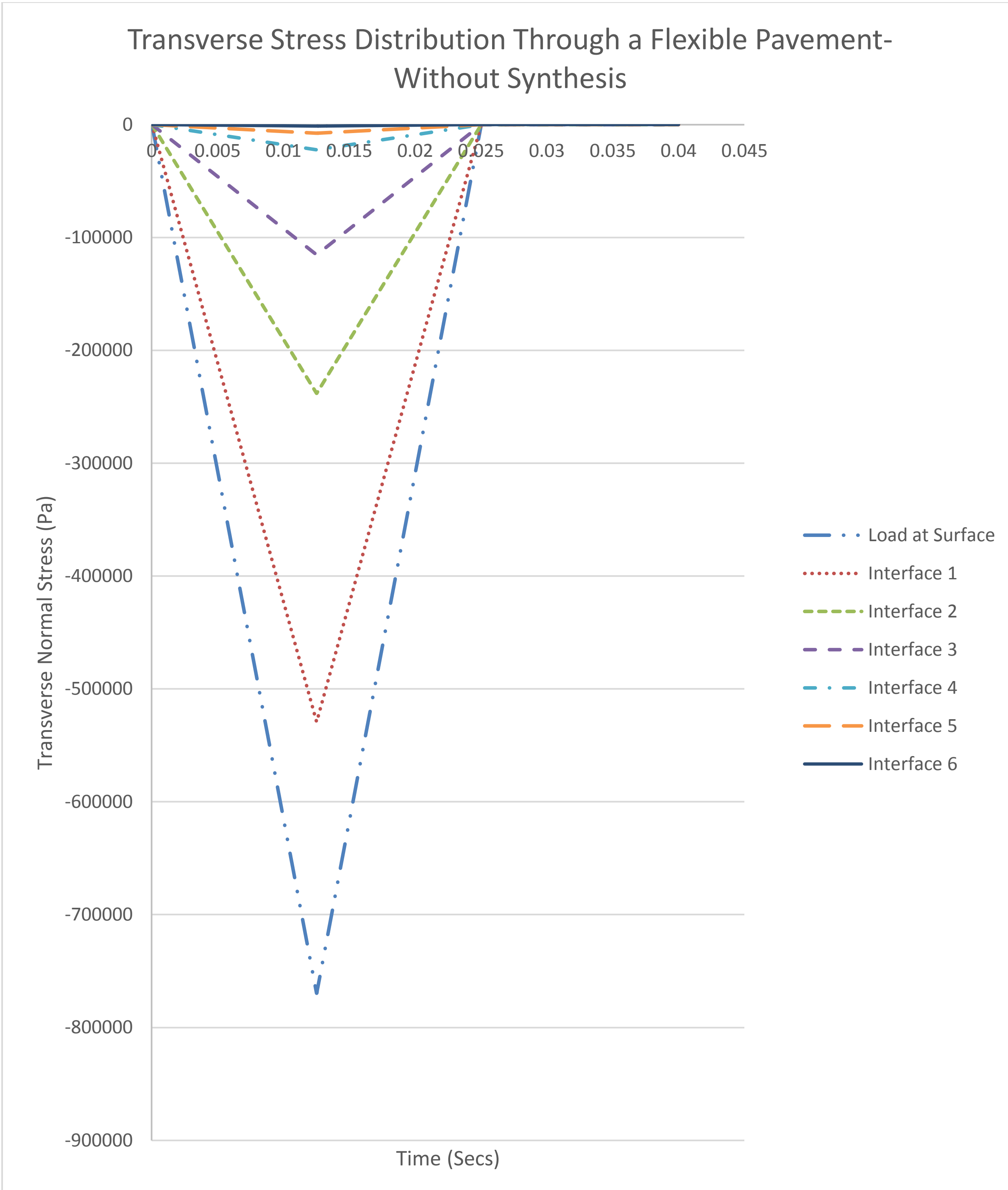

Figure 4.11 Transverse Stress distribution through depth of the pavement structure without Synthesis

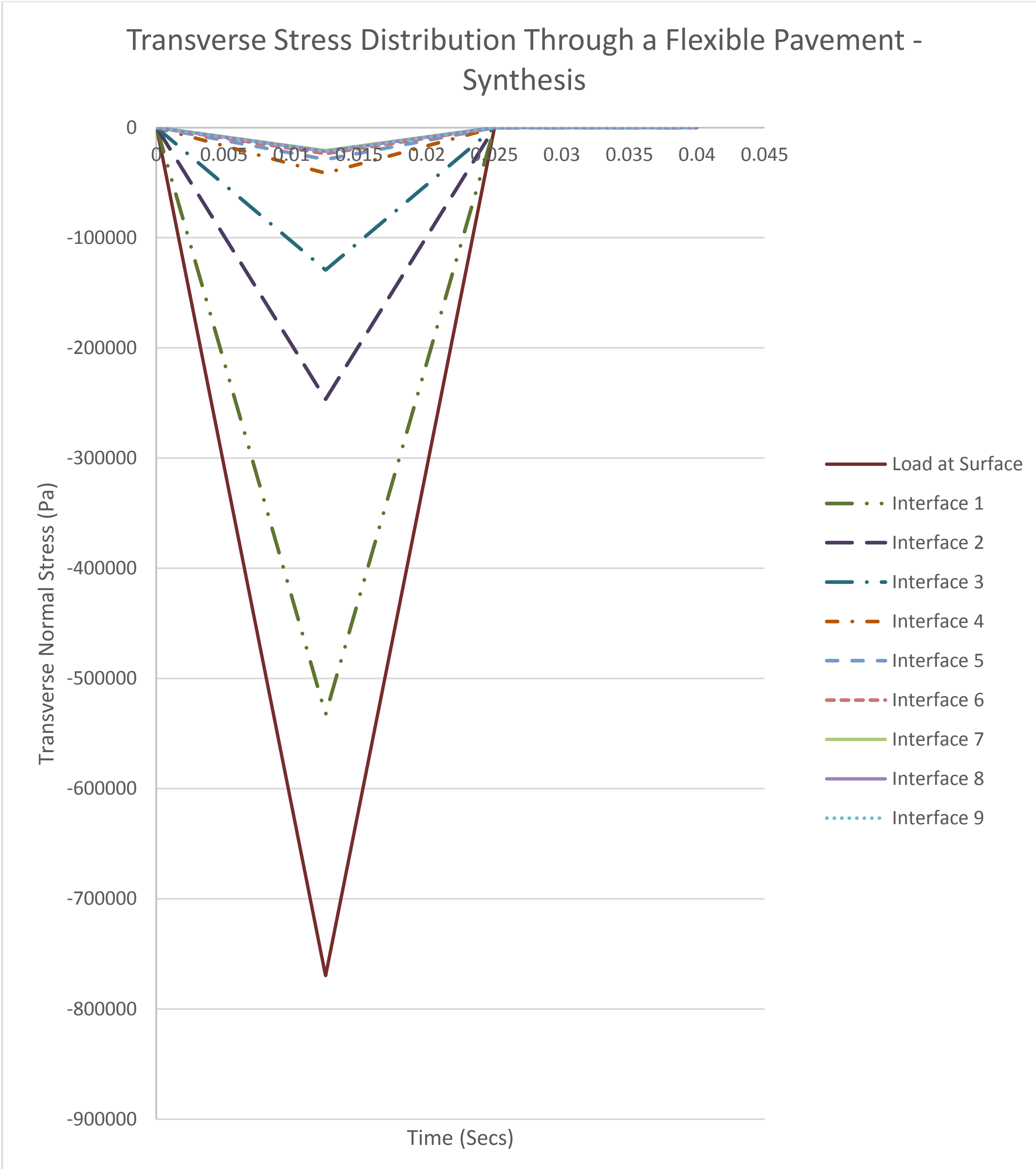

Figure 4.12 Transverse Stress distribution through depth of the pavement structure with Synthesis.

As previously stated, pavement layer debonding has proven to be a particularly destructive phenomenon as it relates to preserving the pavement asset. In addition the efforts aimed at providing a solid bond condition at the layer interfaces has been based primarily on engineering experience and is an emerging research interest which is of particular importance to pavement engineering practitioners. This synthesis has demonstrated promise in ensuring that the material characterization allows for more accurate response predictions and should be further coupled with an appropriate pavement prediction model to conduct a full design. Nonetheless, it clearly demonstrates adequate promise for use with flexible pavements on cohesive subgrades.

Chapter 5: Conclusions and Recommendations for Future Research

5.1 Conclusions

A challenge continues to exist in bringing the state of the practice in flexible pavement design to the current research developments in the state of the art. The use of the Mechanistic Empirical Pavement Design Guide has been avoided to some degree in favor of the more straightforward AASHTO 1993 Pavement Design Guide which continues to enjoy great popularity among pavement designers in developing countries. The designs developed on the use of the 1993 Guide tend to be conservative and as such results in significant monetary losses which developing countries cannot afford. In order to begin the shift to a more mechanistic approach, one of the key components is a robust pavement response model which includes the framework to assess stresses, strains and deflections based on tire loads exerted on the pavement as well as material characterization. In this study, the extension of a material characterization model introduced by Kim (2004) is extended to accommodate soils from Guyana. The pavement response formulation after Tu (2007) developed at Ohio State shows great promise in assessing the transverse stress distribution through the thickness of a flexible pavement system created by tire loads with more accuracy than displacement based models which are commonly used. These two separate but complimentary models are combined in a new synthesis to serve as the foundation for pursuing a more mechanistic approach that will save developing countries like Guyana, small municipalities and townships in the United States.

5.2. Recommendations for Future Research

As the structural responses in the flexible pavement design have been evaluated, it has been done using the principle of layered elastic systems. In the extension of this stress based model, the asphaltic concrete was assumed to be linear elastic in behavior. The reason for this assumption is that it allows for a simplification of the analysis without introducing greater complication. However, this simplification while convenient may not be as accurate. The asphaltic concrete is more visco-elastic in nature. This provides an opportunity for further research aimed at extending the Stress Based Finite Element Model to include constitutive equations which account for the visco-elasticity of the pavement material. Researchers have started to look at more robust viscoelastic response solutions for multilayered asphalt pavements which are worth exploring.

Another important component of the mechanistic approach is the pavement performance prediction model. An appropriate pavement performance model should be combined with the model extension presented in this research to further advance the attempts to develop a complete mechanistic-empirical pavement design guide. Salem et al (2013) propose that while performance models can be of a deterministic or probabilistic nature, there should be some caution in applying a deterministic model. This observation recognizes some of the current gaps in mechanistic pavement design research. There is a high level of subjectivity applied in the assessing pavement condition, the reliability of the pavement condition data, difficulty in fully quantifying parameters responsible for pavement deterioration and the effects of climate change.

The environmental conditions play a significant role in the behavior of a road pavement under given load conditions. The model in its current form does not allow for environmental conditions to be factored into the analysis. In the case of tropical countries, such as Guyana which is relatively close to the equator, not accounting for predominantly high temperatures may reduce the accuracy of the model. Further research into incorporating this factor into the model can assure greater accuracy of predictions.

One limitation of the Mr Prediction Model is that it is not as accurate when used in its general form versus the soil specific variations. As such for practical use, it can be quite cumbersome for practitioners to be required to use different models for greater levels of accuracy in prediction. In order to further improve the accuracy of the pavement response stress based model, it is necessary for further extension of the material model or the use of other prediction techniques. At The Ohio State University, a model is being developed which employs the joint capability of Artificial Neural Networks (ANN) and Genetic Algorithms (GA) (Montoya et al, 2013). This model and others of this ilk may be better suited for use in the stress based model since it is capable of application across different soil types and geographic boundaries.

References

AASHTO, *AASHTO Guide for Design of Pavement Structures*, American Association of State Highway and Transportation Officials, 1993.

Abrate, S., "Impact on Laminated Composite Materials", *Applied Mechanics Review*, Vol. 44, No. 4, pp. 155-190, 1991.

Acum, W. E. A. and L. Fox. "Computation of Load Stresses in a Three-Layer Elastic System", Geotechnique. Vol. 2, pp. 293-300, 1951.

ARA, Inc., ERES Consultants Division, Guide for Mechanistic-Empirical Design
Bathe, K.J., Finite Element Procedures, Prentice Hall, 1996.

ASCE, "2013 Report Card For America's Infrastructure," retrieved from internet source: http://www.infrastructurereportcard.org/a/#p/roads/conditions-and-capacity Accessed 07-06-2015, 2013.

Burmister, D. M., "The General Theory of Stresses and Displacements in Layered Soil Systems", Journal of Applied Physics. Vol. 16, pp. 89-94, 126-127, 296-302, 1945.

Burmister, D. M., "The Theory of Stresses and Displacement in Layered Systems and Application to the Design of Airport Runways." Proceedings of the Highway Research Board. Washington, DC. , pp. 126-148, 1943.

Butalia, T.S., Dynamic response of advanced composite plates subjected to low velocity impact, Ph.D. Dissertation, The Ohio State University, Columbus, Ohio, 1996.

Carmichael, R. F. III and Stuart, E., "Predicting Resilient Modulus: A Study to Determine the Mechanical Properties of Subgrade Soils," Transportation Research Record No 1043, Transportation Research Board, National Research Council, 1986, pp. 145-148.

Chyou, H.A., Variational Formulation and Implementation of Pagano's Theory of Laminated Plates, Ph.D. Dissertation, The Ohio State University, Columbus, Ohio, 1989.

Coastal Road Repair, Alligator/ Fatigue Cracking, retrieved from the internet source: http://www.coastalroadrepair.com/Knowledgebase/Alligator%28Fatigue%29Cracking.aspx, Last Accessed 07-06-2015, 2015.

Collins, H.J. and C.A. Hart, Principles of Road Engineering, Edward Arnold Publishers, Ltd., London, 1936.

Conchon, A., Road Construction in Eighteenth Century France, Proceedings of the Second International Congress on Construction History, Volume 1, pp. 791-797, 2006.

Cornell, Typical Values of Young's Elastic Modulus and Poisson's Ratio for Pavement Materials, Retrieved from internet source: Last accessed 07-06-2015, 2015.
ftp://www.clrp.cornell.edu/CDOT/.../4c%20%20Materials%20Table.pdf

Dokainish, M.A. and K. Subbaraj, "A Survey of Direct Time-Integration Methods in Computational Structure Dynamics – I. Explicit Methods", Computers and Structures, Vol. 32, No. 6, p. 1371-1386, 1989.

Drumm, E. C., Boateng-Poku, Y. and Pierce, T. J., "Estimation of Subgrade Resilient Modulus from Standard Tests," Journal of Geotechnical Engineering, ASCE, Vol. 116, No. 5, pp. 774-789, May, 1990.

Final Report, Illinois Cooperative Highway and Transportation Serial No. 160,
Ghaboussi, J. and E.L. Wilson, "Variational Formulation of Dynamics of Fluid-Saturated Porous Elastic Solids", Journal of the Enginering Mechanics Division, Proceedings of the American Society of Civil Engineers, Vol. 98, No. EM4, pp. 947-963, 1972.

Gurtin, M.E., "Variational Principles for Linear Elastodynamics", Archive for Rational Mechanics and Analysis, Vol. 16, pp. 34-50, 1964.

Gurtin, M.E., "Variational Principles in Linear Theory of Viscoelasticity", Archive for Rational Mechanics and Analysis, Vol. 13, pp. 179-191, 1963.

Hallin, J. P., Teng, T. P., Scofield, L. A. and Quintus, H. V., Pavement Design in the Post AASHO Road Test Era, Transportation Research Circular, E-C118, July, 2007.

Highway Research Board, The AASHO Road Test- History and Description of Project, Special Report 61, National Academy of Sciences – National Research Council, Publication NO. 816, 1961.

Hiremath, M.S., A Dynamic Theory of Wave Propagation in Fluid – Saturated Solids, Ph.D. Dissertation, The Ohio State University, Columbus, Ohio, 1987.

Hiremath, M.S., R.S. Sandhu, L.W. Morland, and W.E. Wolfe, "Analysis of One-Dimensional Wave Propagation in a Fluid-Saturated Finite Soil Column", International

Journal for Numerical and Analytical Methods in Geomechanics, Vol. 12, pp. 121-139, 1988.

Huang, Y. H. 1993. Pavement Analysis and Design. Prentice Hall. Englewood Cliffs, NJ.

Huang, Y. H., “Finite Element Analysis of Slabs on Elastic Solids”, Transportation Engineering Journal, ASCE, 100(TE2): pp. 403-415, 1974.

Huang, Y.H., Pavement Analysis and Design, Second Edition, Pearson Prentice Hall, 2004

Hughes, T.J.R. and M. Cohen, “The “Heterosis” Finite Element for Plate Bending”, Computers and Structures, Vol. 9, pp. 198-203, 1974.

Hughes, T.J.R., Finite Element Method, Prentice Hall, 1987.

IADB, Guyana Country Report, retrieved from the internet source: http://www.iadb.org/en/countries/guyana/guyana-and-the-idb,1056.html, Last Accessed 07-06-2015, 2015.

Jones, A., “Tables of Stresses in Three-Layer Elastic Systems”, Highway Research Board bulletin 342, pp. 176-214, 1962

Khweir, K. and Fordyce, D., “Influence of Layer Bonding on the Prediction of Pavement life”, Proceedings of the Institute of Civil Engineers, Transport 156, Paper 12814, pp. 73-83, 2003.

Kim, D. S. and Drabkin, S., “Accuracy Improvement of External Resilient Modulus Measurements Using Specimen Grouting to End Platens,” Transportation Research Record No 1462, Transportation Research Board, National Research Council, 1994, pp. 65-71.

Kim, D., Development of a Constitutive Model for Resilient Modulus of Cohesive Soils, Ph.D. Dissertation, The Ohio State University, Columbus, Ohio, 2004.

Kruntcheva, M.R., Collop, A.C., and Thom, N.H., “Effect of Bond Condition on Flexible Pavement Performance”, Journal of Transportation Engineering Vol. 131, No. 11, pp. 880-888, 2005.

Kruntcheva, M.R., Collop, A.C., and Thom, N.H., “Feasibility of Assessing Bond Condition of Asphalt Concrete Layers with Dynamic Nondestructive Testing”, Journal of Transportation Engineering Vol. 130, No. 4, pp. 510-518, 2004.

Lee, W. J., Bohra, N. C., Altschaeffl, A. G., and White, T. D., "Resilient Modulus of Cohesive Soils and the Effect of Freeze-Thaw," Canadian Geotechnical Journal, Vol. 32, 1995, pp. 559-568.

Montoya, C., Wolfe, W.E. and Butalia, T.S., "Novel Optimization Technique To Obtain Resilient Modulus Values For Pavement Design", The Ohio State University, Columbus, Ohio, July. 6 p. 2013.

Muench, S., retrieved from internet source:
http://www.pavementinteractive.org/article/pavement-typespavement-types/,
Last Accessed 07-06-2015, 2008.

National Asphalt Pavement Association, Engineering Overview, Retrieved from internet source:
http://www.asphaltpavement.org/index.php?option=com_content&view=article&id=14:asphalt-pavement-overview&catid=15:asphalt-pavement&Itemid=33,
Last Accessed 07-06-2015, 2015

National Cooperative Highway Research Program Transportation Research Board National Highway Institute (NHI) Course No. 131064, "Introduction to Mechanistic-Empirical Design of New and Rehabilitated Pavements", FHWA, April 2002.

National Highway Institute (NHI) Course No. 131064, "Introduction to Mechanistic-Empirical Design of New and Rehabilitated Pavements", FHWA, April 2002.

National Research Council, NCHRP Project 1-37A, retrieved from the internet source: NCHRP, "Guide for Mechanistic-Empirical Design of New and Rehabilitated Pavement Structures", Final Report for NCHRP project 1-37A, 2004. Last Accessed 07-06-2015, 2015.

NHI, Analysis of New and Rehabilitated Pavement Performance with Mechanistic-Empirical Design Guide Software, NHI Course No. 131109 Participant Workbook, June 2007.

Oglesby, C.H., Highway Engineering, 3rd Edition, John Wiley & Sons, 1975

Ohio Department of Transportation, Pavement Design Concepts, 1999

Pagano, N.J., "Free Edge Stress Fields in Composite Laminates", International Journal of Solids and Structures, Vol. 14, pp. 401-406, 1978b.

Pagano, N.J., "Stress Fields in Composite Laminates", International Journal of Solids and Structures, Vol. 14, pp. 385-400, 1978a.

Parris, K., Tu, W., Wolfe, W., and Butalia, T.S., Stress-Based Displacement Model For Realistic Analysis of Pavements." International Road Federation World Meeting 2013, Riyadh, Saudi Arabia, Conference Proceedings.

Pavement Interactive, retrieved from the internet source: http://www.pavementinteractive.org/article/pavement-history/, Last Accessed 07-06-2015, 2008

Peattie, K. R., "Stress and Strain Factors for Three-Layer Elastic Systems", Highway Research Board bulletin 342, pp. 215-253, 1962.

Pezo, R and Hudson, W. R., "Prediction Models of Resilient Modulus for Nongranular Materials," Geotechnical Testing Journal, GTJODJ, Vol. 17, No. 3, 1994, pp. 349 - 355.

Rada, G., and Witczak, M. W., "Comprehensive Evaluation of Laboratory Resilient Moduli Results for Granular Material," Transportation Research Record No. 810, Transportation Research Board, pp. 23-33, 1981

Reddy, J.N., Mechanics of Laminated Composite Plates and Shells: Theory and Analysis, Second edition, CRC Press, 2004.

Sandhu, R. S., & Salaam, U., Variational formulation of linear problems with nonhomogeneous boundary conditions and internal discontinuities. Computer Methods in Applied Mechanics and Engineering, pp. 75-91, 1976

Santha, B.L., "Resilient Modulus of Subgrade Soils: Comparison of Two Constitutive Equations," Transportation Research Record No 1462, Transportation Research Board, National Research Council, 1994, pp. 79-90.

Schiffman, R.L., "General Solution of Stresses and Displacements in Layered Elastic Systems", International Conference on the Structural Design of Asphalt Pavement, Proceedings, University of Michigan, Ann Arbor, Michigan, USA, 1962.

Schoeppner, G.A., A Stress Based Theory Describing the Dynamic Behavior of Laminated Plates, Ph.D. Dissertation, The Ohio State University, Columbus, Ohio, 1991.

Schwartz, W. and Carvalho, R.L., "Implementation of the NCHRP 1-37A Design Guide Final Report - Evaluation of Mechanistic-Empirical Design Procedure," University of Maryland, Volume 2, pp. 18-24, February 2007.

Secretaria de Comunicaciones y Transportes, Modulos De Resiliencia En Suelos Finos Y Materiales Granulares, Instituto Mexicano del Transporte, Publicacion Tecnica No. 142, pp. 43, 2001

Seed, H.B., Chan, C.K., and Lee, C.E., Resilience Characteristics of Subgrade Soils and Their Relation to Fatigue Failure in Asphalt Pavement, Proceedings, International Conference on Structural Design of Asphalt Pavement, University of Michigan, Ann Arbor, pp.611-636, 1962

Subbaraj, K., M.A. Dokainish, "A Survey of Direct Time-Integration Methods in Computational Structure Dynamics – II. Implicit Methods", Computers and Structures, Vol. 32, No. 6, p. 1387-1401, 1989.

Thomson, M. R., and Robnett, Q. L., (1976). "Resilient Properties of Subgrade Soils," Timm, D.H., Robbins, M.M., Tran, N. and Rodezno, C., Flexible Pavement Design-State of the Practice, National Center for Asphalt Technology, NCAT Report 14-04, August 2014.

Tschegg, E.K., Kroyer, G; Tan, D.M., Stanzl-Tschegg, S.E., Litzka, J., "Investigation of Bonding between Asphalt Layers on Road Construction", Journal of Transportation Engineering Vol. 121, No. 4, pp. 309-316, 1995.

Tu, W., Response Modeling of Pavement Subjected to Dynamic Surface Loading Based on Stress-Based Multi-Layered Plate Theory, Ph.D. Dissertation, The Ohio State University, Columbus, Ohio, 2007.

Wolfe, W.E., T.S. Butalia, H. Walker, W. Tu, B. Zand and S.H. Kim, Full Scale Testing of Coal Combustion Product (CCP) Pavement Sections Subjected to Repeated Wheel Loads, Final Report # CDO-D-00-5, The Ohio State University, Columbus Ohio, Aug 2006.

Works Service Group (WSG), Loan Contract LO2454-BL/GY East Bank Demerara Four Lane Extension, Between the Government of Guyana and the Inter-American Development Bank, Contract Appendices for Expansion of East Bank Demerara Public Road (Providence to Diamond) – Lot 1, Dipcon Engineering, May 2011

Works Service Group (WSG), RMMS Project Status Report, Ministry of Public Works and Communications, Guyana, 2008

Works Service Group, Evaluation Report – First Implementation of Routine Maintenance Program East Bank Public Road, Ministry of Public Works and Communications, Guyana, 2007

Yoder, E.J., Witczak, M.W., "Principles of Pavement Design", John Wiley & Sons Inc., Second Edition, pp. 24-125, 1975.

Zhao, Y., Liu, W., and Tan, Y., "Analysis of Critical Structure Responses for Flexible Pavements in NCHRP 1-37A Mechanistic-Empirical Pavement Design Guide." J. Transp. Eng., 138(8), 983–990, 2012.

Appendix A: Laboratory Test Results

A.1.1 Soil Classification Test

Sample Name	Location	Date Collected	Soil Type
STRATSPHEY GY1	East Coast Demerara, Guyana	JULY 2013	A-7-5
CANEVIEW GY22	Georgetown, Guyana	JULY 2013	A-7-5

Table A.1 Sample Location for the A-7-5 Soil Samples

A.1.2 Atterberg Limits Test

Soil Type AASHTO	Sample Name	Liquid Limit (%)	Plastic Limit (%)	Plasticity Index (%)
A-7-5	STRATSPHEY-G1	64.5	36.3	28.2
	CANEVIEW-G2	57.8	29.9	27.9

Table A.2 Summary of Atterberg Limit Test Results

A.1.3 Percentage Passing the #200 Sieve

Soil Type AASHTO	Sample Name	% Passing #200
A-7-5	STRATSPHEY-G1	97.64
	CANEVIEW-G2	87.58

Table A.3 Percentage Passing no. 200 Sieve for A-7-5 Soils

A.1.4 Standard Proctor Compaction

Soil Type	Sample Name	Optimum Moisture Content (%)	Maximum Dry Density (lbs./ft^3)
A-7-5	STRATSPHEY-G1	25.20	91.3
	CANEVIEW-G2	22.50	98.2

Table A.4 Optimum Moisture Content and Maximum Dry Density Results

A.1.5 Unconfined Compressive Strength

Soil Type	Sample Name	Optimum Moisture Content (%)	Maximum Dry Density (lbs./ft^3)	q_u (lbs./in^2)
A-7-5	STRATSPHEY-G1	25.20	91.3	36.90
	CANEVIEW-G2	22.50	98.2	32.70

Table A.5 Unconfined Compressive Strength Test Results

q_u: Stress vs. Strain Curves

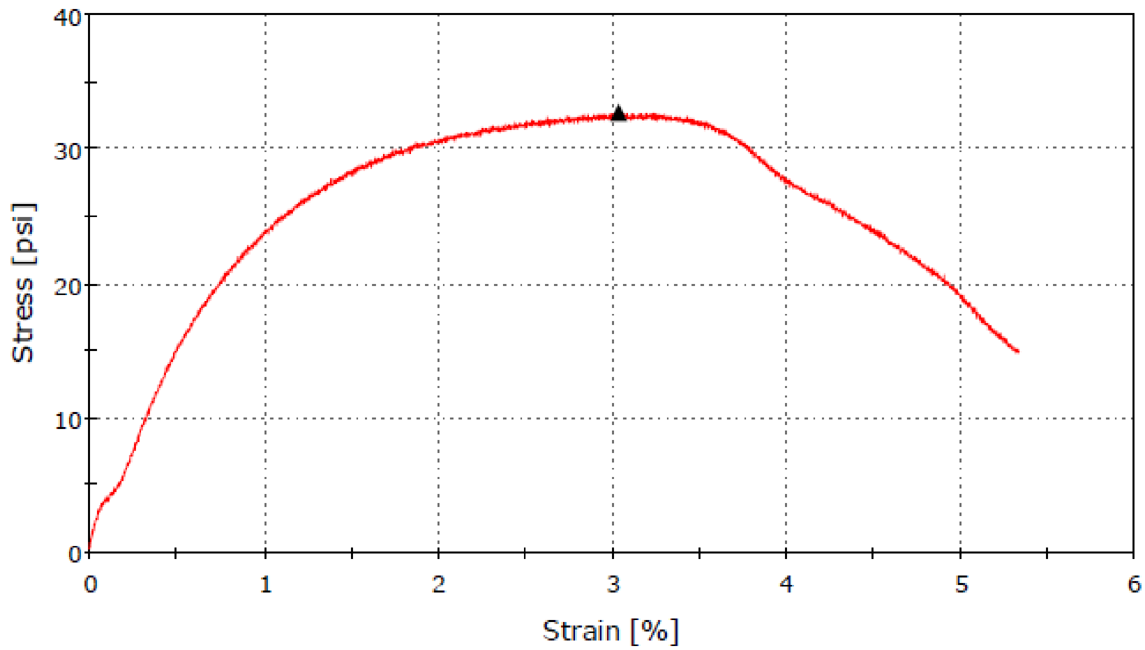

Figure A.1 Stress vs. Strain STRATSPHEY-G1: Specimen 1

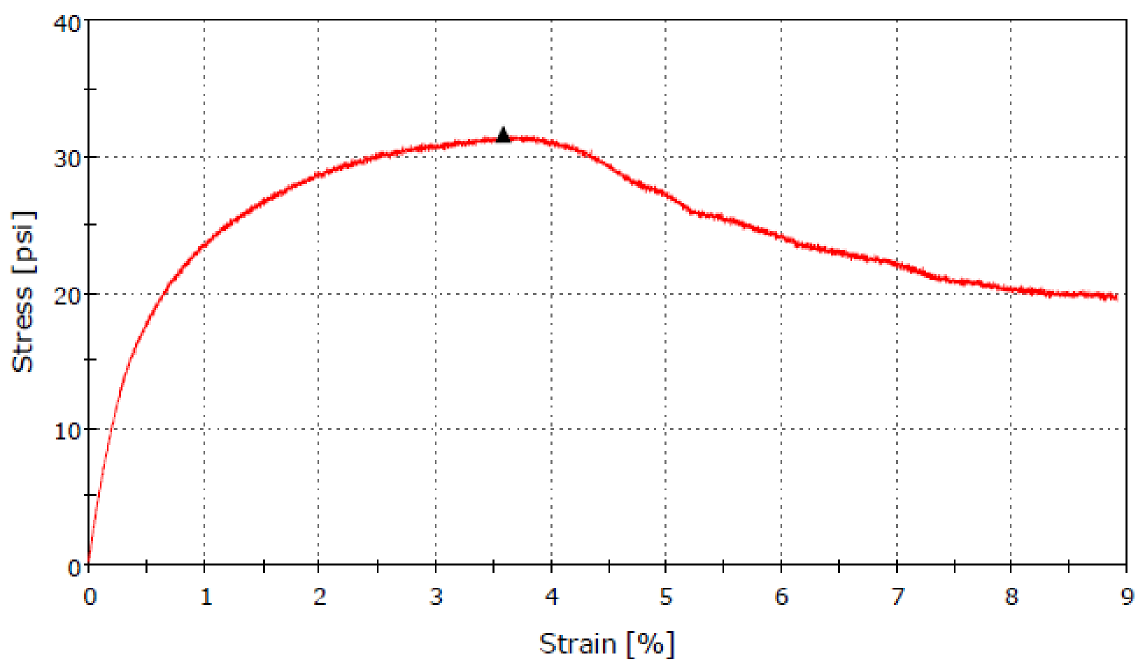

Figure A.2: Stress vs. Strain STRATSPHEY-G1: Specimen 2

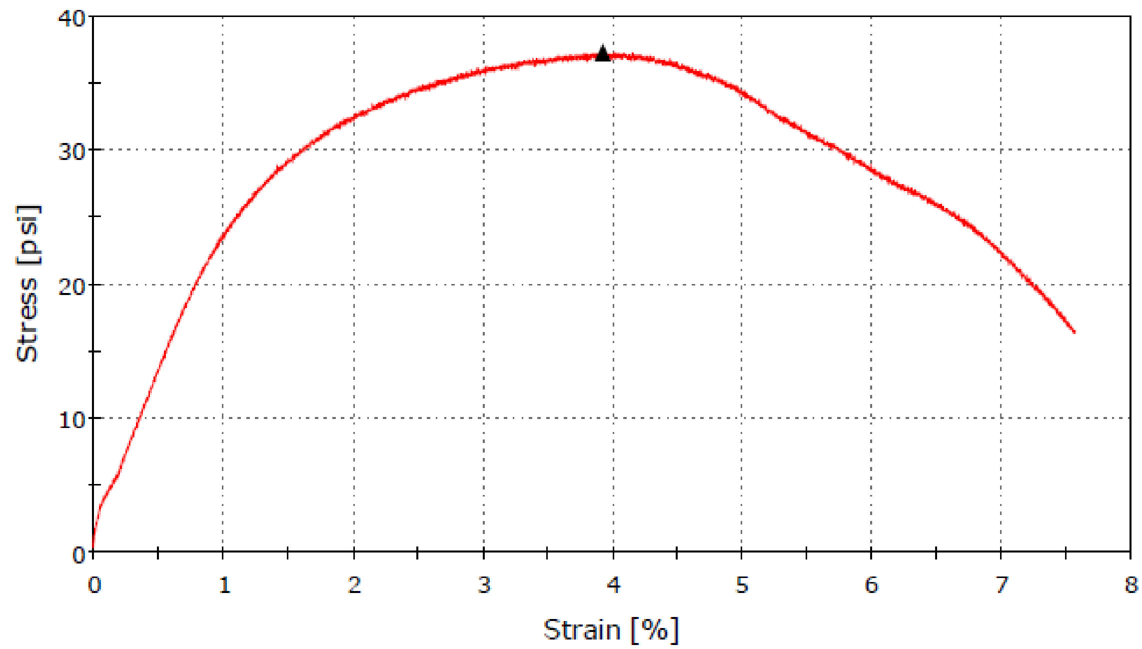

Figure A.3 Stress vs. Strain STARTSPHEY-G1: Specimen 3

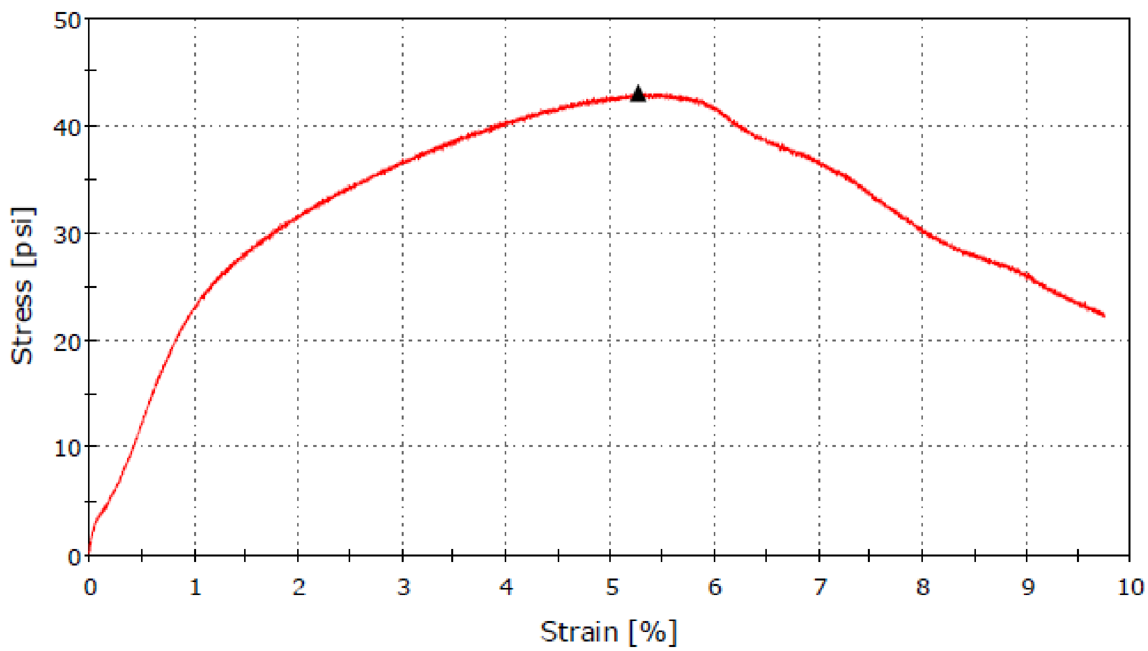

Figure A.4 Stress vs. Strain STRATSPHEY-G1: Specimen 4

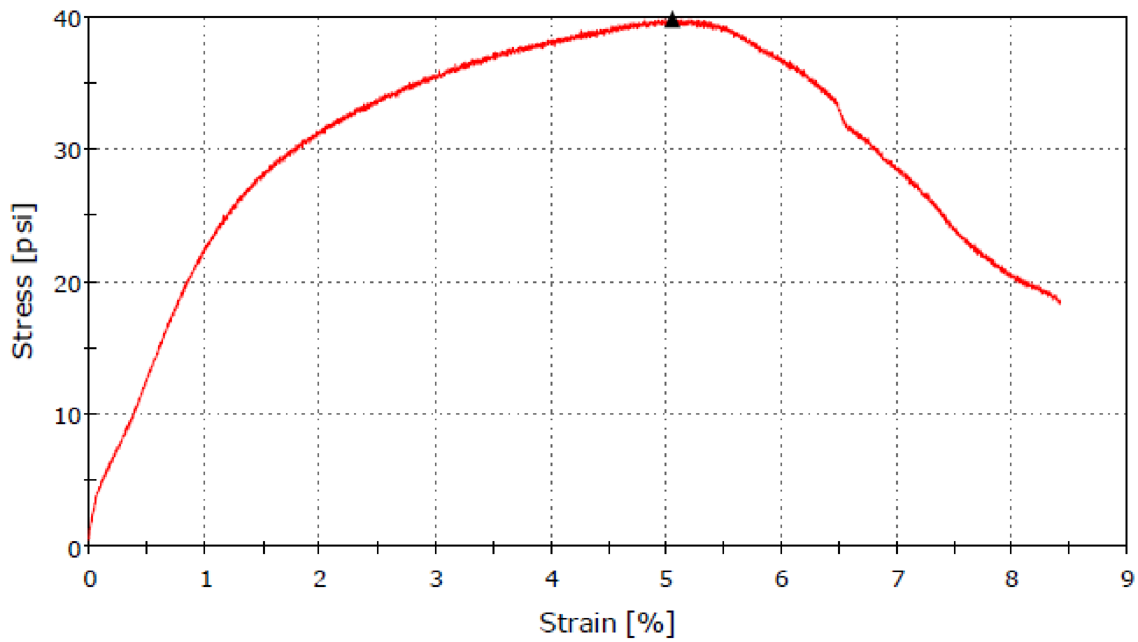

Figure A.5 Stress vs. Strain STRATSPHEY-G1: Specimen 5

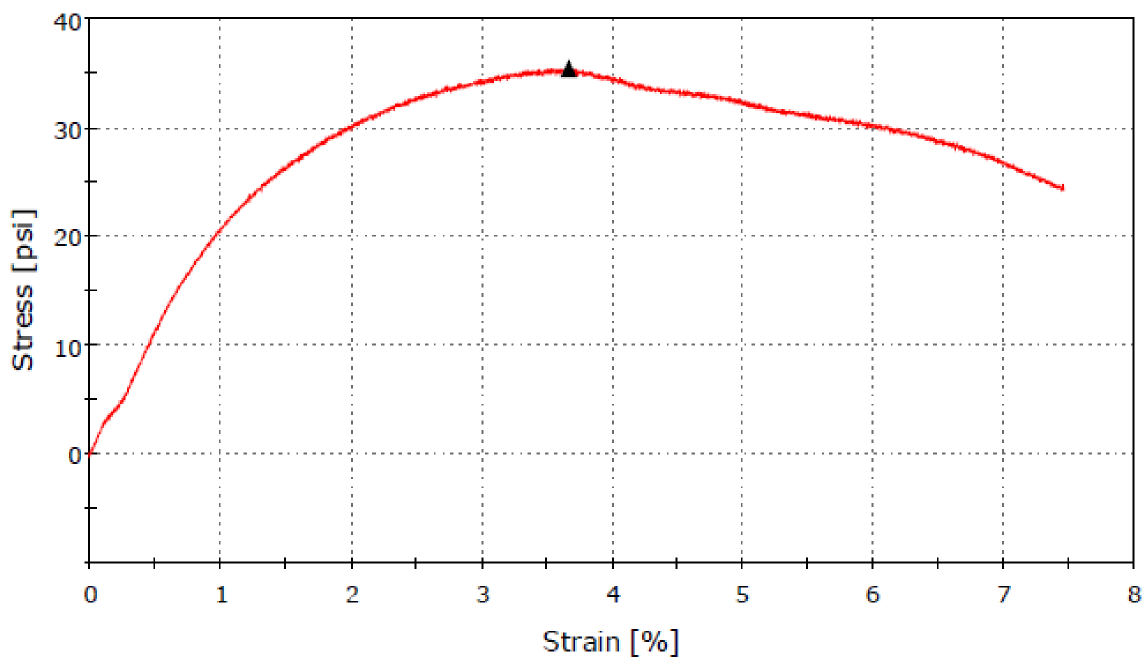

Figure A.6 Stress vs. Strain CANEVIEW-G2: Specimen 1

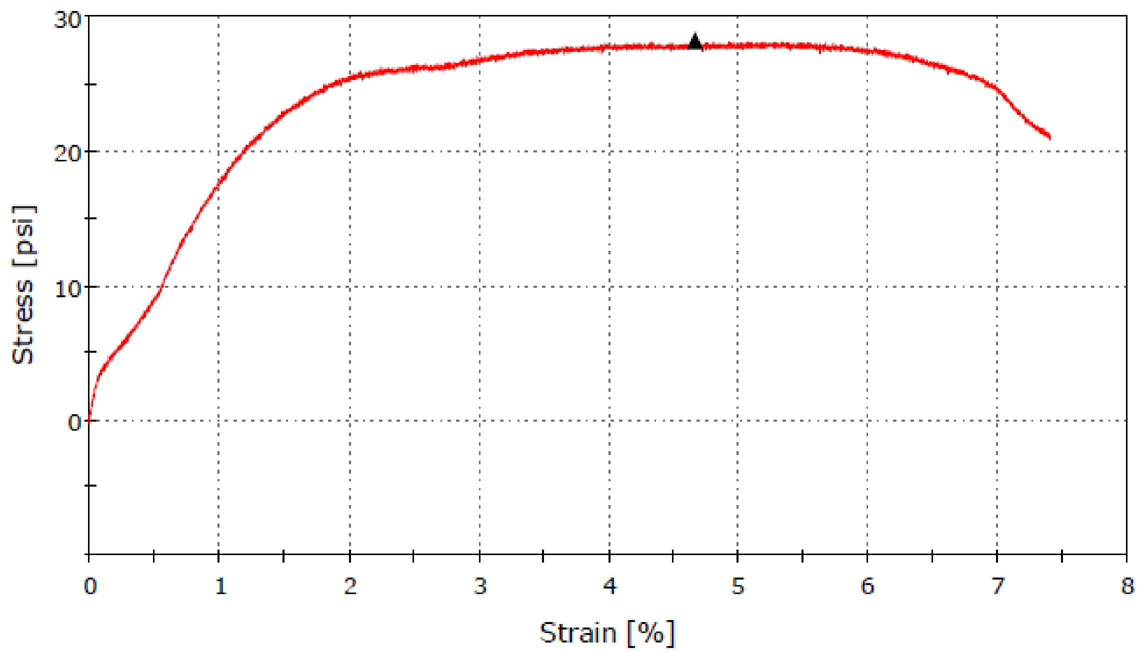

Figure A.7 Stress vs. Strain CANEVIEW-G2: Specimen 2

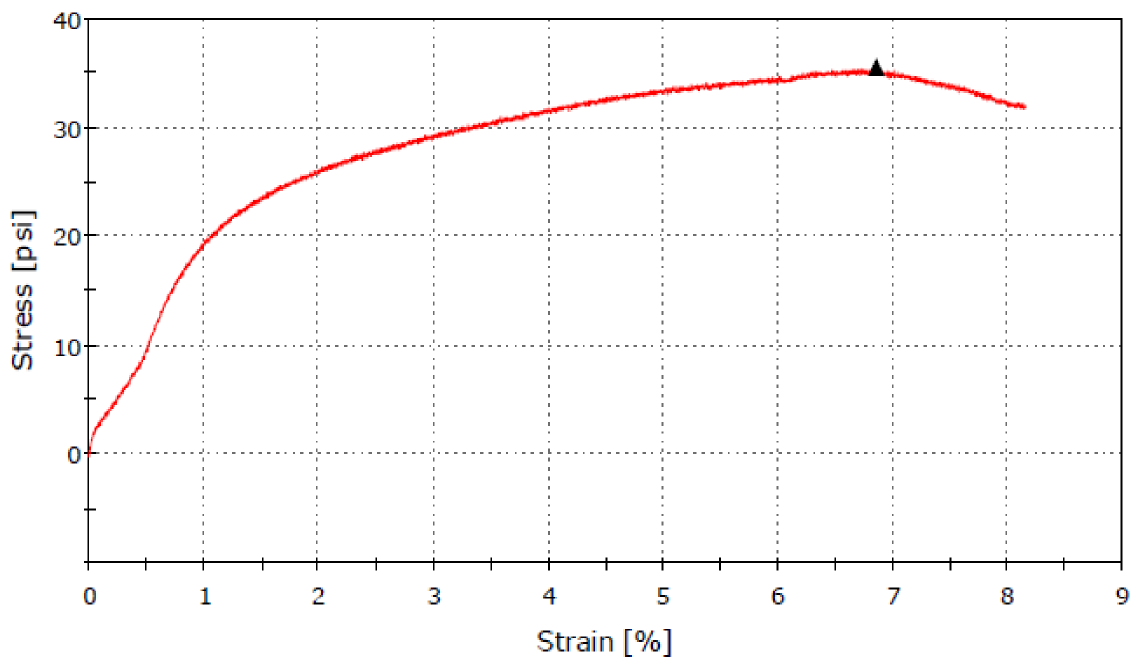

Figure A.8 Stress vs. Strain CANEVIEW-G2: Specimen 3

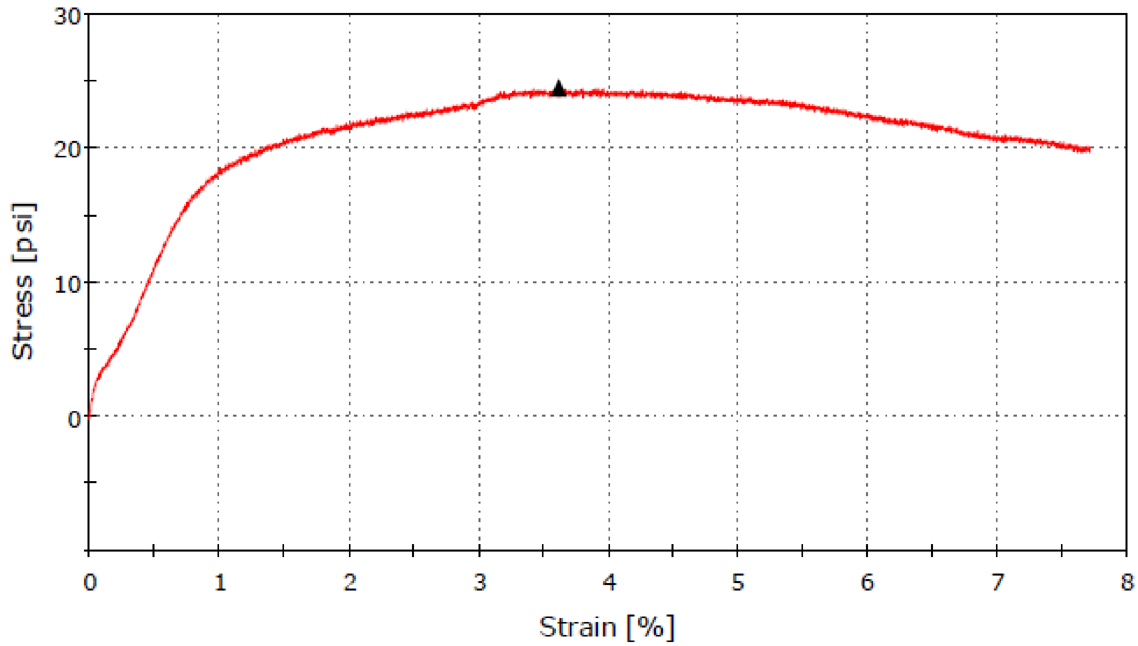

Figure A.9 Stress vs. Strain CANEVIEW-G2: Specimen 4

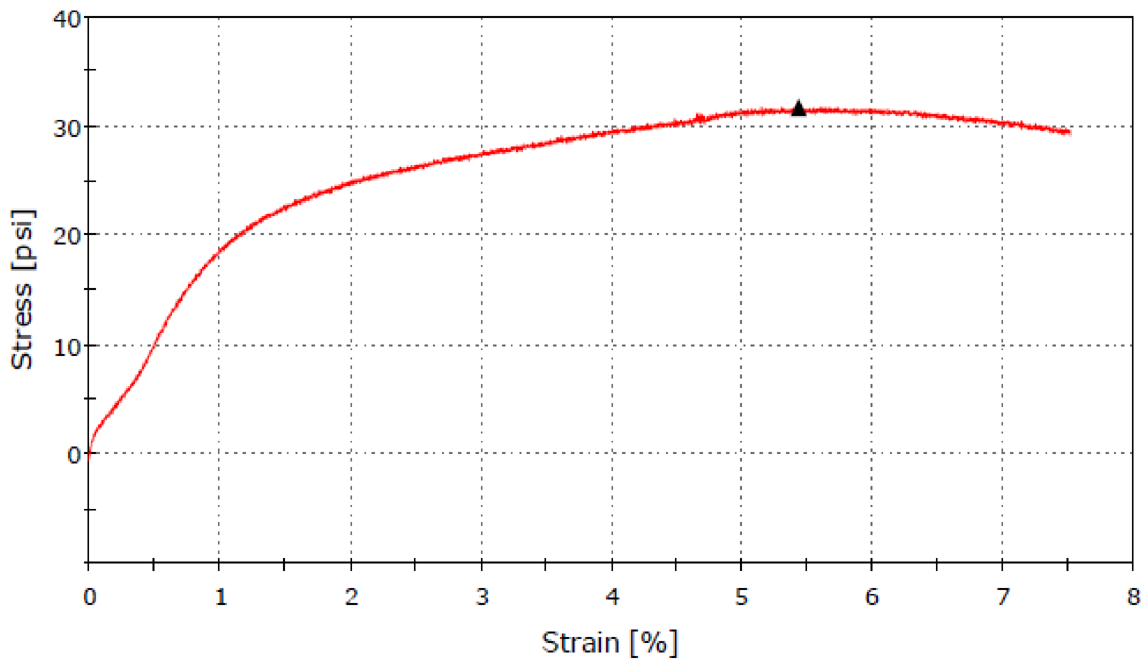

Figure A.10 Stress vs. Strain CANEVIEW-G2: Specimen 5

A.1.6 Atterberg Limits Data Sheets

Liquid Limit, Plastic Limit, and Plasticity Index

Location:	Stratsphey, East Coast Demerara, Guyana	Date:	9/11/2014
Depth:		Tested by:	K. Parris and C. Montoya
Description:			
Sample No.:	STRATSPHEY-G1		

Liquid Limit

Number of blows	29	25	19
Mass of can (g)	50.55	49.64	50.02
Mass wet soil + can (g)	63.77	70.20	70.70
Mass wet soil (g)	13.22	20.56	20.68
Mass dry soil + can (g)	58.64	62.20	62.39
Mass dry soil (g)	8.09	12.56	12.37
Mass water (g)	5.13	8.00	8.31
Moisture content (%)	63.41	63.69	67.18

Plastic Limit

Mass of can (g)	13.89	13.32
Mass wet soil + can (g)	23.63	22.06
Mass wet soil (g)	9.74	8.74
Mass dry soil + can (g)	21.15	19.63
Mass dry soil (g)	7.26	6.31
Mass water (g)	2.48	2.43
Moisture content (%)	34.16	38.51

Liquid Limit: **64.5%**

Plastic Limit: **36.3%**

Plasticity Index: **28.2%**

Table A.6 Atterberg Limits Data sheet for STRATSPHEY-G1 (A-7-5)

Liquid Limit, Plastic Limit, and Plasticity Index

Location:	Cane View Ave., Georgetown, Guyana	Date:	9/11/2014
Depth:		Tested by:	K. Parris and C. Montoya
Description:			
Sample No.:	CANEVIEW-G2		

Liquid Limit

Number of blows	33	30	23	17
Mass of can (g)	50.16	50.12	49.99	50.17
Mass wet soil + can (g)	62.40	72.86	67.28	62.42
Mass wet soil (g)	12.24	22.74	17.26	12.25
Mass dry soil + can (g)	58.06	64.54	60.86	57.88
Mass dry soil (g)	7.90	14.42	10.87	7.71
Mass water (g)	4.34	8.32	6.39	4.54
Moisture content (%)	54.94	57.70	59.06	58.88

Plastic Limit

Mass of can (g)	14.30	13.40	11.09
Mass wet soil + can (g)	19.41	18.88	16.40
Mass wet soil (g)	5.11	5.48	5.31
Mass dry soil + can (g)	18.23	17.61	15.19
Mass dry soil (g)	3.93	4.21	4.10
Mass water (g)	1.18	1.27	1.21
Moisture content (%)	30.03	30.17	29.51

Liquid Limit: **57.8%**

Plastic Limit: **29.9%**

Plasticity Index: **27.9%**

Table A.7 Atterberg Limits Data sheet for CANEVIEW-G2 (A-7-5)

Appendix B: Mr Laboratory Test Results and Model Predictions

B.1.1 Resilient Modulus Testing Results

	σ3 (kPa)	σd (kPa)	Measured Mr (MPa)	Predicted Mr (MPa)
DRY	41	14	42.0	98.0
	41	28	85.4	92.1
	41	41	97.0	89.1
	41	55	79.1	87.0
	41	69	80.1	85.4
	21	14	74.5	88.1
	21	28	91.3	83.2
	21	41	169.1	80.7
	21	55	199.0	79.0
	21	69	113.7	77.7
	0	14	335.0	69.5
	0	28	206.3	67.4
	0	41	182.1	66.3
	0	55	169.3	65.5
	0	69	164.8	64.8
OMC	41	14	21.5	86.9
	41	28	39.9	79.3
	41	41	47.9	75.5
	41	55	43.2	72.9
	41	69	42.4	70.9
	21	14	40.6	77.1
	21	28	52.2	71.4
	21	41	94.3	68.6
	21	55	98.4	66.7
	21	69	61.6	65.2
	0	14	112.3	60.6
	0	28	107.4	58.7
	0	41	100.3	57.8
	0	55	92.7	57.0
	0	69	88.5	56.5

Table B.1 MR Test Results and Predictions for Cane View (A-7-5)

	σ3 (kPa)	σd (kPa)	Measured	Predicted Mr (MPa)
DRY	41	14	51.4	101.6
	41	28	89.1	96.4
	41	41	106.2	93.7
	41	55	91.0	91.8
	41	69	86.5	90.3
	21	14	70.7	92.5
	21	28	98.0	88.0
	21	41	186.8	85.8
	21	55	215.7	84.2
	21	69	125.1	83.0
	0	14	367.0	75.0
	0	28	250.0	73.1
	0	41	184.2	72.0
	0	55	189.9	71.2
	0	69	180.2	70.6
WET	41	14	19.5	89.2
	41	28	40.3	81.4
	41	41	49.1	77.5
	41	55	42.8	74.8
	41	69	42.1	72.8
	21	14	30.8	79.5
	21	28	42.9	73.7
	21	41	78.5	70.9
	21	55	86.9	68.9
	21	69	55.8	67.5
	0	14	93.0	63.4
	0	28	81.8	61.7
	0	41	78.4	60.8
	0	55	74.7	60.1
	0	69	74.6	59.6
OMC	41	14	31.6	89.6
	41	28	63.2	81.8
	41	41	74.4	77.9
	41	55	60.2	75.2
	41	69	54.8	73.2
	21	14	56.5	79.9
	21	28	67.9	74.1
	21	41	137.0	71.3
	21	55	149.9	69.3
	21	69	83.3	67.9
	0	14	191.8	63.6
	0	28	144.5	62.0
	0	41	127.9	61.1
	0	55	134.8	60.4
	0	69	133.2	59.8

Table B.2 MR Test Results and Predictions for Stratsphey (A-7-5)